ATMOSPHERIC DENSITY CURRENTS: IMPACTS ON AVIATION OVER NSW AND ACT

[Shuang Wang]
[Master of Science and Master of Engineering]

[Supervisors: Tapan Rai, Lance Leslie, Yuriy Kuleshov]

Submitted in fulfilment of the requirements for the degree of
Doctor of Philosophy

School of Mathematical and Physical Science
University of Technology Sydney
[2019]

Statement of Original Authorship

CERTIFICATE OF ORIGINAL AUTHORSHIP

I, Shuang Wang declare that this thesis, is submitted in fulfilment of the requirements for the award of PhD, in the School of Mathematical and Physical Sciences at the University of Technology Sydney.

This thesis is wholly my own work unless otherwise reference or acknowledged. In addition, I certify that all information sources and literature used are indicated in the thesis.

This document has not been submitted for qualifications at any other academic institution.

This research is supported by the Australian Government Research Training Program.

Production Note:
Signature removed prior to publication.

Signature: Date: 06-Oct-2019

Keywords

ACT, Aviation, Canberra, climate, cooler, damaging winds, density current, down burst, microburst, NSW, observations, permutation testing, ranges, Rossby waves, satellite images, sort-lived gusty winds, southerly busters, squall lines, Sydney, thunderstorms, turbulence, warnings, wavelet analysis, wind shear (in alphabetical order)

Abstract

Three main types of density currents (DCs) which have significant impacts for aviation are investigated in detail over New South Wales (NSW) state of Australia and Australian capital Territory (ACT) in the research. The three types of density currents are southerly busters (SBs) along the coastal NSW, thunderstorm downbursts over north-western NSW and easterly DCs over Canberra.

The research take advantage of the recently available Himawari-8 high temporal- and spatial-resolution satellite data, Sydney wind profiler data, Doppler radar data, radiosonde data, half hourly METAR and SPECI aviation from observation data Bureau of Meteorology Climate zone, synoptic weather charts and other observational data. In addition, simply model for density currents, global data assimilation system (GDAS) meteorological model outputs, and the Australian Community Climate and Earth-System Simulator (ACCESS) operational model products are employed in the research.

Based on the impacts on aviation, for SBs and strong SBs (SSBs), when wind directions are between 160 degrees to 210 degrees, SBs are the average winds or gusty wind is >= 14.9 m/s (29 knots or 54 km/h), SSBs are the average winds or gusty winds more than 20.5 m/s (40 knots or 74 km/h). For easterly DCs, when wind directions are between 070 degrees to 150 degrees, the average winds or gusty wind is >= 7 m/s (13 knots or 23 km/h). For thunderstorms downbursts, damaging winds are the average winds or gusty winds more than 20.5 m/s (40 knots or 74 km/h) in any direction.

The results of this research show that the data analyses support the widespread view that the SB is a DC, coastally trapped by the Great Dividing Range. In addition, solitary waves develop ahead of SB in a shallow and stable prefrontal boundary layer.

A simplified density current model is applied to SBs, SSBs and easterly DCs. The model results have been verified by the observations. The results that are solely model based also suggest that the solitary waves travel at speeds about 20% faster than the DCs which is consistent with the high-resolution satellite data and shows the solitary waves moving increasingly ahead of the leading edge of the DCs.

The damaging winds caused by thunderstorm downbursts are DCs. The characteristics are presented, and forecast parameters and indices are discussed.

Finally, the climatological trends for SBs and SSBs at Sydney airport are examined statistically by using permutation testing and wavelet analysis. The results show that there is significant increase in SBs over last 49 years, however, the SSBs show no significant trend over the same period.

Table of Contents

Statement of Original Authorship ii
Keywords iii
Abstract iv
Table of Contents vi
List of Figures viii
List of Tables xi
List of Appendices xi
List of Abbreviations xii
Acknowledgements xiii
Chapter 1: Introduction 14
1.1 Background 14
1.2 Significance 3
1.3 Thesis Outline 7
Chapter 2: The Theory of Density Currents 8
2.1 Definition of Density Current 8
2.2 Density Current Speed 9
2.3 The Solitary Waves 10
2.4 Density Current in Thunderstorms 12
Chapter 3: Literature Review 15
3.1 Southerly Busters 15
3.2 Thunderstorm downdrafts 16
3.3 Climate 19
Chapter 4: Research Design 22
4.1 Data and Methodology 22
4.1.1 Observational data in SB 22
4.1.2 Parameters and Indices for the Damaging Winds 22
4.1.3 Density current event over NSW and ACT 26
4.1.4 Two SSBs 27
4.1.5 Data Selection and Methodology for SB/SSB Climatology 28
4.2 ICAO locations in NSW 30
4.3 Ethics and Limitations 31
Chapter 5: Experiments and Results 32
5.1 A Trapped Southerly Buster and Associated Solitary Waves 32
5.1.1 Introduction 33

5.1.2 Observations and Analysis 35
5.1.3 Synoptic Overview 39
5.1.4 Satellite Imagery 42
5.1.5 Radiosonde Data 48
5.1.6 Current Theory: Application to SBs. 50
5.1.7 Discussion and Conclusions 53

5.2 A Short-lived Gusty Wind Event Associated with a Squallline 56
5.2.1 Introduction 56
5.2.2 Synoptic Overview 59
5.2.3 Six Airports Observations 60
5.2.4 Satellite Imagery 65
5.2.5 Radiosonde Data 66
5.2.6 Trajectories for Air Parcels 67
5.2.7 Discussion and Conclusions 70

5.3 Easterly Density Current Events over NSW and ACT 71
5.3.1 Introduction 71
5.3.2 Data and Methodology 73
5.3.3 Observation and Analysis 75
5.3.4 Density Current Theory Application to Easterly Change 80
5.3.5 2018/2019 summer season analysis of easterly wind changes 82
5.3.6 Discussion and Conclusions 83

5.4 Analysis of Two Strong Southerly Busters 83
5.4.1 Introduction 83
5.4.2 Station observations 84
5.4.3 Synoptic Overview 90
5.4.4 Satellite Imagery 94
5.4.5 Sydney Airport Wind Profiler Data 99
5.4.6 Discussion of observations from January 30th to 31st from along the NSW ... 100
5.4.7 Radar Images 105
5.4.8 Density Current Theory: Application to two SSBs. 114
5.4.9 Discussion and Conclusions 116

5.5 Other Density Currents 118

Chapter 6: Climate Analysis for Southerly Busters 121

Chapter 7: Conclusions 126

Bibliography 130

Appendices 132

List of Figures

Figure 1: Photo taken from a SB.....2
Figure 2: A SB detected by satellite. 2
Figure 3: Idealized depiction of an aircraft taking off facing into a microburst. 5
Figure 4: Sydney Airport has three runways: 6
Figure 5: Schematic of a downburst development. 14
Figure 6: ICAO ID of Airports in New South Wales. 31
Figure 7: Topography of New South Wales. 35
Figure 8: Observations of wind change from 0000UTC to 2330UTC on October 6, 2015 at Nowra (YSNW). 37
Figure 9: As in Figure 8, except at Sydney (YSSY) from 0900UTC to 2400UTC on October 6, 2015. 37
Figure 10: Observations of wind, visibility and cloud change from 0900UTC to 2400UTC on October 6, 2015 at YSSY. 38
Figure 11: Synoptic weather charts October 6 to October 7. 41
Figure 12: Schematic representation deduced from wind temperature data, of the frontal structure in a vertical cross Section parallel to the coast. 43
Figure 13: Schematic of the cloud signatures of a Southerly Buster that can be detected using several sources of satellite imagery. 43
Figure 14: Himawari-8 satellite visible image at 2140UTC on October 6. 2015 over the New South Wales coast. 45
Figure 15: ASCAT winds at 2325UTC on October 6, 2015. 46
Figure 16: The Himawari-8 satellite visible images from 2020UTC to 2320UTC on October 6, 2015. 47
Figure 17: Radiosonde profile on October 6, 2015. 48
Figure 18: Map of North-western of NSW, Australia. 58
Figure 19: Synoptic weather charts for Australia at 0000 UTC (1000 AEDT) on December 13, 2018. 59
Figure 20: Observations of Bourke Airport (YBKE) from 0000UTC to 0600UTC on December 13, 2018. 60
Figure 21: Observations of Walgett Airport (YWLG) from 0000UTC to 0600UTC on December 13, 2018. 61
Figure 22: Observations of Coonamble Airport (YCNM) from 0000UTC to 0600UTC on December 13, 2018. 62
Figure 23: Observations of Narrabri Airport (YNBR) from 0000UTC to 0600UTC on December 13, 2018. 62

Figure 24: Observations of Moree Airport (YMOR) from 0000UTC to 0600UTC on December 13, 2018. 63

Figure 25: Observations of Gunnedah Airport (YGDH) from 0000UTC to 0600UTC on December 13, 2018. 63

Figure 26: Weather observations of wind gusts from 0000UTC to 0600UTC on December 13, at six airports. 64

Figure 27 Himawari-8 Satellite Visible Images on December 13, 2018 over NSW. 65

Figure 28: Radiosonde profile at 0531UTC on December 13, 2018 at Moree Airport (YMOR). 66

Figure 29: 24 hours forward trajectories for air parcels beginning 00 UTC 13/12/2018 and ending 00 UTC 14/12/2018. 68

Figure 30: 24 hours forward trajectories for air parcels beginning 00 UTC 13/12/2018 and ending 00 UTC 14/12/2018. 68

Figure 31: Canberra Airport Runways (From Google Map) 71

Figure 32: Map of South-eastern Australia. 74

Figure 33: Observations from 0000UTC to 1800UTC on December 18th, 2018 at Canberra Airport (YSCB). 75

Figure 34: Synoptic weather charts from 0000UTC to 1800UTC December 18, 2018 at Canberra Airport. 77

Figure 35: Topography of New South Wales Pacific Ocean coast with the Great Dividing Range west of Sydney in metres (m). 84

Figure 36: Observations from 0025UTC to 2355UTC on November 20, 1973 at Sydney (YSSY). 88

Figure 37: As Figure 36, except from 0005 to 2330UTC on January 31, 2019 at Sydney Airport. 90

Figure 38: Synoptic weather charts for 0200UTC November 20(a) and November 21 (b), 1973. 92

Figure 39: Synoptic weather charts from 1800UTC January 30 to 1200UTC January 31, 2019. 93

Figure 40: Himawari-8 satellite visible image at 0700UTC on January 31, 2019 over New South Wales coast. 95

Figure 41: Model cross Section for potential temperatures (°C) and winds below 800hPa (elevation in feet in the right) at 0700UTC on January 31, 2019 along the NSW coast. 96

Figure 42: Himawari-8 satellite RGB night microphysical image for low cloud and fog at 1200UTC on January 2019. 98

Figure 43: Sydney Wind Profiler from 0600UTC to 0900UTC on January 31, 2019. 100

Figure 44 Observations of wind change from January 30th to 31st from along the NSW coast from Gabo Island to Port Macquarie. 101

Figure 45: 0.5-degree elevation reflectivity, radar scans from Terry Hill radar for three locations in Sydney region.....107

Figure 46: 0.5-degree elevation reflectivity and velocity radar scans from Kurnell radar at 0640 UTC SSB at Sydney Airport.....109

Figure 47: 0.5-degree elevation reflectivity and velocity radar scans from Terry Hills radar at 0640 UTC SSB at Sydney Airport. 111

Figure 48: 0.5-degree elevation reflectivity and velocity radar scans from Wollongong radar at 0640 UTC SSB at Sydney Airport. 113

Figure 49: Himawari-8 satellite image at 2330UTC on 26th, January 2019. 119

Figure 50: Number of SBs and SSBs trend over Warm Season from 1970/1971 to 2018/2019 at Sydney Airport.....121

Figure 51: Difference in SSB Count (1995-2018 minus 1970-1994).....123

Figure 52: Difference in SB Count (1995-2018 minus 1970-1994).....124

Figure 53: Wavelets for SSB (1970-1994 and 1995-2018). 124

Figure 54: Wavelets for SB (1970-1994 and 1995-2018). 124

List of Tables

Table 1: The outputs of ACCESS NWP system for 3 stations when the damaging winds occurred on December 13, 2018. 25

Table 2: Details of the wind changes at YSNW and YSSY. 39

Table 3: The Nowra (YSNW) radiosonde data on 1700UTC October 6, 2015.....49

Table 4: Details of the low level structure of the inversion at Nowra (YSNW).....53

Table 5: Southerly Buster of 31 January 2019.....55

Table 6: Observations of Easterly Change at Canberra Airport on December 18, 201877

Table 7: Observations of winds directions (in degrees) from 0000 UTC to 0530 UTC on December 18, 2018 at six stations. 79

Table 8: Observations of temperatures (in °C) from 0400 UTC to 1030 UTC on December 18, 2018 at seven stations. 80

Table 9: Details of the density currents for the easterly change in Canberra on December 18th, 2018. 82

Table 10: All the easterly changes at Canberra Airport in 2018/2019 summer season.83

Table 11: Information in details on the two SSBs on November 20, 1973 and January 31, 2019. 87

Table 12: Locations and Aviation IDs 104

Table 13: Observations of wind change from January 30th to 31st. 104

Table 14: Details of the density currents for the two SSB....116

Table 15: Two Periods SBs and SSBs (25 years for each period)....122

List of Appendices

Appendix 1: ICAO ID of Airports mention in the Thesis 132

Appendix 2: The Observation of SSB at Sydney Airport on January 31, 2019 133

Appendix 3: Days of SBs and SSBs at Sydney Airport over last 49 years 134

Appendix 4: Details of SSBs for the 49 year period (1971-2019)....135

Appendix 5: Details of SBs for the 49 year period (1971-2019): 138

List of Abbreviations

ACCESS	Australian Community Climate and Earth-System Simulator
AEDT	Australian Eastern Daylight Time
AP	Airport
ATC	Air Traffic Control
AWS	Automatic Weather Station
CAPE	Convective Available Potential Energy
CAVOK	Sky and visibility OK
CDT	Coastal Trapped Disturbance
DC	Density Current
DMAPE	Downdraught Maximum Available Potential Energy (DMAPE)
GDR	Great Dividing Range
GDAS	Global Data Assimilation System
GPATS	Global Position and Tracking Systems
HAM	Highest Alternate Minina
ICAO	International Civil Aviation Organization.
MCS	Mesoscale Convective System
METAR	Routine weather report issued at hourly or half-hourly intervals.
NSW	New South Wales
NWP	Numerical Weather Prediction systems
QNH	A Q code indicating the atmospheric pressure adjusted to mean sea level. It is a pressure setting used by pilots, air traffic control (ATC).
SB	Southerly Buster
SC	Southerly Change
SIGMET	Significant Meteorological Information AIM 7-1-6
SPECI	Special weather report issued when there is significant deterioration or improvement in airport weather conditions
SSB	Strong Southerly Buster
TAF	Terminal Aerodrome Forecast
TTF	The Trend Forecast
UTC	Coordinated Universal Time

Acknowledgements

I thank the Australian Bureau of Meteorology for providing the data used and the work experience in this study. The study also was partially funded by the Australian Technology Network's Industry Doctoral Training Centre (IDTC). The PhD study was carried out at the School of Mathematical and Physical Sciences at the University of Technology Sydney, after originally starting at RMIT.

Firstly, I would like to express my sincere gratitude to my advisors' panel: Prof. Tapan Rai, Lance Leslie, Yuriy Kuleshov for the continuous support of my PhD study and related research, for their patience, motivation, and immense knowledge. Their guidance helped me in completing the research and writing of this thesis. I could not have imagined having better advisors and mentors for my PhD study. Particularly, I express my gratitude to Prof. Lance Leslie who always enlightens my interests on the research topic with his passion for research.

Besides my advisors, I would like to thank the rest of my thesis committee: Prof. Kefei Zhang Prof. Tim Langtry, Prof. Murray Cameron, A/Prof. Yakov Zinder, Dr. Milton Speer, Dr. Yan Ding, Dr. John Gear, Dr. Suqin Wu, Dr. Sally Cheng and PhD student Joshua Hartigan for their insightful comments and encouragement, but also for the hard questions which encouraged me to widen my research interests.

Also, I thank my colleagues in the Regional Forecasting Centre of Bureau of Meteorology for their stimulating discussions, for the sleepless nights we were working together and for enlightening me the first glance of research.

Last but not least, I would like to thank my family: my husband, my son and my parents for supporting me spiritually throughout writing this thesis and my life in general.

Chapter 1: Introduction

This chapter outlines the background (Section 1.1) and significance (Section 1.2) of the research. Finally, Section 1.3 includes an outline of the remaining chapters of the thesis.

1.1 BACKGROUND

In March 2019, the population of New South Wales (NSW) was over 8 million, making it Australia's most populous state (Australian Demographic Statistics, 2019). There are almost 100 airports across the state. The largest airports in NSW and the ACT are Sydney Airport, Canberra Airport and Williamtown Airports etc., among which Sydney Airport is one of the world longest continuously operated commercial airports and the busiest airport in Australia, handling 42.6 million passengers and 348,904 aircraft movements in 2016–17 (Domestic aviation activity, 2020). In 2018, the airport was rated in the top 5 worldwide for airports handling 40–50 million passengers annually and was voted the 20th best airport in the world at the Skytrax World Airport Awards. However, the flight activities depend on weather conditions a lot. The hazardous weather phenomena in NSW ACT are turbulence, wind shear, mountain waves, low cloud, fog, dust storms, thunderstorms, icing, heavy rain, damaging winds etc. All these hazardous phenomena are related to density currents. Pilots will benefit from understanding the characteristics of weather situations. They also benefit of obtaining the latest aviation products such as observations, forecasts, warnings etc. To provide better meteorology's aviation weather service with meteorological information necessary for safe and efficient civil aviation operations in NSW and ACT, it is necessary to first understand the

weather system in NSW and ACT. The significant weather systems are cold fronts, SBs (see Figure 1and Figure 2), easterly lows and other weather systems which can cause thunderstorms, wind shear, turbulence, mountain wave, low visibility and low cloud or fog. In this research, the several DCs especially the SBs in NSW and ACT, are investigated.

Southerly Buster at Turrimeta Beach, 26 December 1996. Photograph by John Grainger.

Figure 1: Photo taken from a SB.

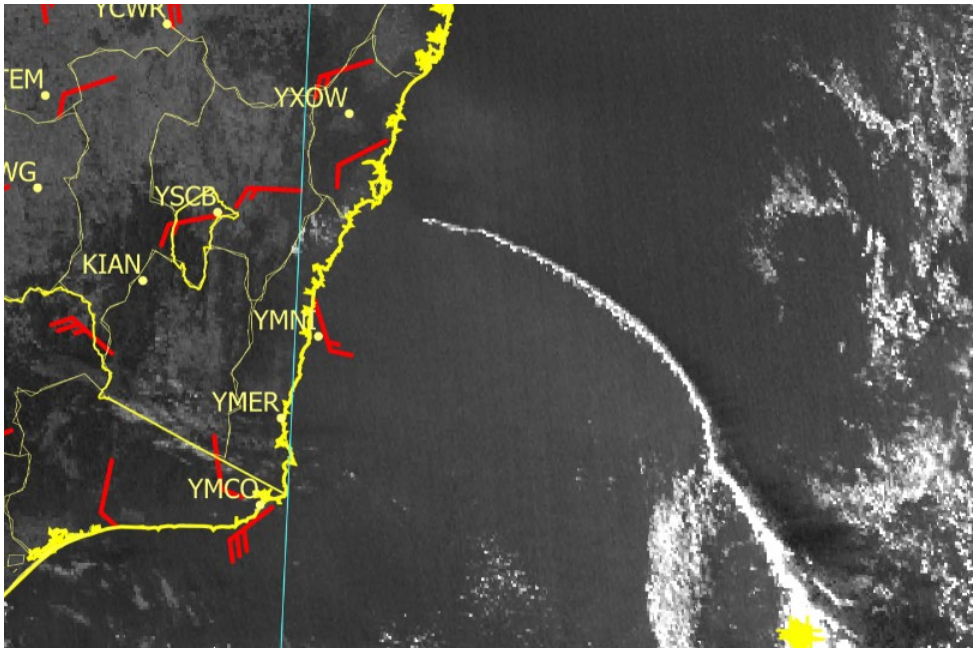

Figure 2: A SB detected by satellite.
Himawari-8 satellite at 7:50Z Wed, 14th February 2018

1.2 SIGNIFICANCE

There are common weather phenomena resulting from the DCs that are associated with rapid increases in surface pressure, winds and abrupt changes in other parameters such as temperature and moisture. Thus, density currents can result in some major hazards such as turbulence and wind shear. The turbulence is detrimental for safe aircraft operations. In-flight turbulence produces abrupt vertical and horizontal displacement of aircraft and is the main cause of injury to passengers and crew. In extreme cases it can produce loss of control and physical damage to the aircraft, causing passenger injury and fatalities. Wind shear is a hazard for aircraft, particularly larger jet aircraft, as their greater inertia causes them to maintain their speed relative to the ground when changing winds are encountered. This results in air speed and lift variations that can lead to disruptions to the flight. Higher approach speeds of modern aircraft increase the suddenness of wind shear effects, leaving pilots less time to interpret visual clues and respond.

It has been proposed that the SB, which affects coastal areas of NSW in spring and summer, is a density current trapped by the regional topography(Colquhoun et al., 1985); (McInnes and McBride, 1993; Reid and Leslie, 1999). The scale is about several hundred kilometres wide and 1km in depth. The southerly buster usually gives rise to a dramatic drop in temperature, and it tends to move northwards along the coast more rapidly than the wind speed behind the change. On occasions, the leading edge of a southerly buster is sometimes marked by a spectacular 'roll cloud' running perpendicular to the coast and this can be clearly identified on the satellite pictures. Figure 2 shows an image from the high temporal and spatial resolution of the Himawari-8 satellite at 7:50Z Wed, 14th February 2018. Owing to the rapid wind and temperate changes, SBs frequently are accompanied by low cloud, fog, thunderstorms and gusty winds. Consequently, SBs are potential threats for human health, lives and property. In the case of aviation, there are numerous aircraft hazards that often result from the low-level

wind shear associated with them, especially during take-off or landing. The main consequences of wind shear include turbulence, violent air movement (e.g., abrupt up- and down-draughts, and swirling, or rotating, air patterns), sudden increases or reductions of airspeed, and rapid increases or decreases of groundspeed and/or drift. A loss in airspeed requires the pilot to regain airspeed to avoid a stall and loss of control of the aircraft. In some cases, the pilots do not take the appropriate adjustments or do not have the time or altitude to make these maneuvers. The result is catastrophe. The strong winds and associated low level turbulence also are hazards for boating, especially as SBs occur along the populous southeast seaboard of Australia. For marine activities such as surfing, rock fishing and boating, each year marine rescue organizations respond to thousands of calls for assistance from NSW coastal waters (Bureau of Meteorology, 2020), and many are related to the passage of SBs, which can produce sudden strong to gale force coastal winds and generate dangerously high waves and choppy seas.

Density currents in thunderstorms are downdrafts, gust fronts and microbursts, which induce severe turbulence and wind shear in low levels. For example, 'On 15 April 2007, while landing, a Boeing 747 encountered wind shear and turbulence at Sydney Airport. The aircraft suffered a rapid loss of airspeed at 100 feet above the ground, touched down heavily, rebounded and touched down firmly again before it climbed to go around and make a successful landing several minutes later. The aircraft encountered a decaying dry microburst that developed over the approach end of the runway as a line of thunderstorms with cloud base of 10 000 feet moved over the airport with very little precipitation' (Potts et al. 2007). The aviation hazard posed by microbursts is illustrated by Figure 3. The danger lies not so much in the loss of altitude due to the downdraft itself, but in the sudden loss of lift that occurs in response to the rapid change in the horizontal velocity when the plane passes through the downdraft, during which time the wind speed relative to the plane may drop by 10 m/s or more in a matter of 20s (Hjelmfelt, 2007).

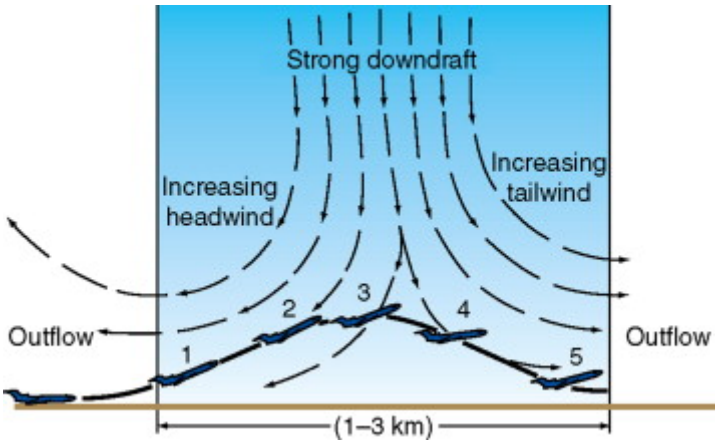

Figure 3: Idealized depiction of an aircraft taking off facing into a microburst.
In passing from 2 to 4, the aircraft loses its headwind and begins to experience a tailwind, causing a loss of lift, and consequently a sudden loss of altitude (Hjelmfelt, 2007) [From J. Clim. Appl. Meteorol., 25 (1986), p. 1399.] Copyright © 1986

Operating in strong tailwind and crosswind conditions can have adverse effects on aircraft performance during take-off, approach and landing. Aircraft take-off and land into the wind, or with minimal tail wind. Based on the wind direction, air traffic control will decide which runway is to be used at any given time. Larger airports tend to have more than one runway (e.g. 3 runways at Sydney Airport --see Figure 4), so that a runway is always available depending on the wind direction. Airports with just one runway are generally constructed so that the runway is aligned with the prevailing wind. Runway selection is always monitored, as weather conditions can quickly change. A loss in airspeed requires the pilot to regain airspeed to avoid a stall and loss of control of the aircraft. In some cases, the pilots do have little time or altitude to perform the appropriate aircraft adjustments.

The threshold to change runway when the runway is completely dry, is if the crosswind exceeds 20 knots including gusts and downwind exceeds 5 knots including gusts. When the runway is not completely dry, that threshold is that the crosswind exceeds 20 knots including gusts and there is any downwind component.

Figure 4: Sydney Airport has three runways:
16R/34L – Main north south runway (3,962m), 16L/34R – Parallel north south runway (2,438m), 07/25 – East west runway (2,530m)

Density currents play an important role in aviation both in flight or surface landing and taking off. Of significant importance is to investigate the weather system, and hazardous phenomena in NSW and ACT that are related to the density currents. The results and conclusions of this work will benefit aviation customers such as pilots, air traffic controllers and aviation forecasters.

1.3 THESIS OUTLINE

The topic of this thesis is Atmospheric Density Currents: Impacts on Aviation over NSW and ACT.

In the beginning of *Chapter 1* is the introduction of the research including the background and the significance of the research and the next is the thesis outline.

In *Chapter 2* is the theory of density currents including the definition, the simplified model for calculating the density currents speed, the solitary waves' speed, and downbursts (density currents in thunderstorms).

In *Chapter 3* is the literature review for density currents, southerly busters, thunderstorms and climate change over Australian, particularly over NSW. To implicate the research questions.

In *Chapter 4* is the research design, including data and methodology, procedure and timeline, and ethics and limitations.

Chapter 5 is the experiments and results. Five parts are included in this chapter, a trapped southerly buster and associated Poincare waves, a short-lived gusty winds event associated with a squall line, easterly density currents events over NSW and ACT, Analysis of two strong southerly busters, and finally other density currents in NSW and ACT.

Chapter 6 is focused on the climate analysis for the southerly busters over the last 49 years.

In *Chapter 7* is the conclusion.

Chapter 2: The Theory of Density Currents

2.1 DEFINITION OF DENSITY CURRENT

Any current in either a liquid or a gas that is kept in motion by the force of gravity acting on differences in density. A density difference can exist between two fluids or air masses because of a difference in temperature and a density current (DC) is a primarily horizontal flow in a gravitational field that is driven by a density difference; hence, density currents also sometimes are referred to as “gravity currents". In the atmosphere these currents involve flow (mass transport) of less dense air over denser air. The main force is downwards (due to gravity) but the flow is largely horizontal. Most of the pressure changes in the postfrontal air of cold fronts are attributable to the density difference between the pre- and post-frontal air masses, and the rate at which the cold air deepens. Propagation speeds also are strongly affected by changes in the density difference (Colquhoun et al., 1985). The dynamics of coastal ridging is well-described by the hydrostatic approximation and the shallow-water equations of motion are applicable (Gill, 1977; Reason and Steyn, 1992). The vertical structure of the coastal atmosphere consists of an inversion, separating a roughly constant density cool marine lower layer from a deep upper layer with weak winds. Note that CTDs do not require the presence of an ocean to exist; it is the presence of stable stratification beneath the crests of the mountain barrier that is essential. There are well-known trapped disturbances occurring over interior plains and confined against large continental mountain ranges elsewhere around the world including, for example, the Rocky Mountains and the Himalayas (Reason, 1994)

2.2 DENSITY CURRENT SPEED

The density of dry air is calculated from the ideal gas law, expressed as a function of temperature and pressure:

$$\boldsymbol{\rho = P/RT}\,, \qquad \textbf{(1)}$$

where: ρ = air density (kg/m³), P = absolute pressure (Pa), T = absolute temperature (K), and R = specific gas constant for dry air (287.058 J/(kg·K)).

In the atmosphere, density currents involve the flow (mass transport) of denser air moving into less dense air. For example, consider cold air separated from less dense air by a vertical wall, with the Coriolis force assumed to be negligible. When the wall is suddenly removed the denser air will spread out in the less dense air, as a density current, over a large horizontal area. All the initial potential energy will be converted to kinetic energy. Equating the loss of potential energy to the gain in kinetic energy, it can easily be shown that for a single layer, the density current flow speed is:

$$\mathbf{c} = \sqrt{\boldsymbol{gH}}. \qquad (2)$$

Where the velocity c (m/s), gravity g = 9.807 m/s^2 and height h (m). In a two-layer system such as cool air of density $\boldsymbol{\rho 1}$, moving into warm air of lower density $\boldsymbol{\rho 2}$, the density current flow speed now is:

$$\boldsymbol{c_{DC}} = \sqrt{\boldsymbol{g'H}}\,, \qquad (3)$$

Where the reduced gravity, $\boldsymbol{g'}$ (m/s^2) is:

$$g' = g\,(\rho 1 - \rho 2)/\rho 1\,, \quad (4)$$

2.3 THE SOLITARY WAVES

The solitary waves studied here are near-surface waves (not internal solitary waves) for which there are at least two possible explanations (Miles,1980). One is that trapped density currents can produce solitary waves that are nonlinear Kelvin waves (Reason, 1994) , which move faster than the density current speed (e.g., Ripa, 1982), so they propagate through and ahead of the leading edge of the density currents (Reason and Steyn, 1990; Reason et al., 1999). The presence of solitary waves accounts for some of the difficulties in interpreting the precise nature of the leading edge of CTD over coastal southeast Australia. However, there was insufficient observational data before data from the Himawari-8 satellite, a high spatial and temporal resolution satellite, became available. The Himawari-8 data shows clearly the solitary waves in the visible satellite imagery in the research in chapter 5.1 and 5.5. A second possibility is that the solitary waves are internal inertia-gravity waves, also known as Poincaré waves. These inertia-gravity waves are internal solitary waves that initially are generated on the interface between the density current and the warmer air above it. Their signature is sets of parallel, equally spaced bands of clouds in the sky which are visible under only certain conditions and ubiquitous in both the atmosphere and the ocean. In many dynamical systems, waves release excess energy in a fluid that is displaced from its energy-balanced state. Internal waves

extract and transport energy three dimensionally before releasing it to large-scale circulation. Like non-linear Kelvin waves, Poincaré waves also travel faster than the density current. For this thesis, it was decided to proceed with the assumption that the solitary waves are inertia-gravity waves, because non-linear Kelvin waves eventually break. However, there is no clear sign that the observed solitary waves do break; instead they appear to dissipate after they move well away from the cold front (Callum,2019). Hence, they lose both energy and moisture by increasingly moving well ahead of the forcing fontal system and by mixing with the environmental air. The dissipation process has a range of length and time scales depending on the strength of the cold front, but typically it has a time scale of 24-28 hours and a length scale of at least 1000km.

All waves have a dispersion relation, which quantifies the relationship between wavelength and frequency in terms of certain physical parameters. The two important parameters for internal waves are the Coriolis frequency and the buoyancy frequency. The Coriolis frequency f is the vertical component of Earth's rotation vector at a fixed point on its surface and depends on latitude. The value of f sets the minimum frequency for internal waves (Callum, 2019).

The formula for the calculation of the phase speed of inertia-gravity (Poincaré) waves is very well-known (e.g., Gill, 1982), and is given by:

$$\boldsymbol{c_{poincaré}} = \sqrt{\boldsymbol{g'H}}\left(\mathbf{1} + \frac{\boldsymbol{f_0^2}}{\boldsymbol{g'Hk^2}}\right)^{\mathbf{1/2}} = \mathbf{c_{DC}}\left(\mathbf{1} + \frac{\boldsymbol{f_0^2}}{\boldsymbol{g'Hk^2}}\right)^{\mathbf{1/2}} \qquad (5)$$

Where:

$\boldsymbol{c_{poincaré}}$ = Poincaré wave phase speed (m/s), and

c_{DC} = Density current speed (m/s)

g' = Reduced gravity(m/s^2)

f_0 =Coriolis parameter $f = 2\,\Omega \sin\varphi$),

Where the rotation rate of the Earth, $\Omega = 7.2921\times10^{-5}$rad/s, can be calculated as $2\pi/T$ radians per second, φ = latitude and H = the cold air depth (m), wave number k =2π/wavelength, where wavelength is the Rossby radius of deformation (L). Thus:

$$\mathbf{k^2} = (\frac{2\pi}{L})^2 \qquad (6)$$

Where the Rossby radius of deformation, $\mathbf{L} = \frac{\sqrt{g'\ H)}}{f}$

2.4 DENSITY CURRENT IN THUNDERSTORMS

Thunderstorms afford good examples of atmospheric density currents. The buoyant air which rises in the storm eventually meets the stable tropopause and spreads horizontally in an anvil. This anvil is a gravity current. Also, evaporation from falling rain and/or hail in a thunderstorm cools the air, resulting in a cool downdraught. The downdraught is forced to spread horizontally on reaching the ground, forming a gravity current. Such a gravity current is frequently turbulent and may raise large amount of dust as it advances over dry ground. The depth of such a cool, thunderstorm-induced gravity current tends to be of the order of several meters and can be as large as one kilometre. Gravity currents associated with the thunderstorms can be a major hazard to aircraft because of associated wind shear, turbulence and visibility drop. Downbursts are powerful winds that descend from a thunderstorm and spread out quickly and destructively once they hit the ground (Figure 5),forming either microbursts (covering areas approximately 4km in radius) or macrobursts (affecting areas larger than 4km in radius).

In the production of the downburst, that large core of rain and hail that the updraft had been holding in the upper parts of the storm falls rapidly towards the ground. It falls very quickly and drags a lot of air along with it, gaining speed as it plummets earthward. If the air beneath the base of the storm has low relative humidity, the downdraft's speed will increase further as some of the rain entering the dry air evaporates and cools the air, making the air "heavier." Then, if there is also a current of dry air coming into the storm aloft, cooling by evaporation can increase further and the downdraft becomes even stronger. When the downdraft hits the ground (Figure 5 (a)), much like a stream of water coming out of a faucet and hitting the sink, it spreads out rapidly in all directions (Figure 5 (b, c)) and becomes known as a downburst. Downbursts, particularly microbursts, are exceedingly dangerous to aircraft which are taking off or landing due to the strong vertical wind shear caused by these events (Figure 5 (d)). A few fatal crashes have been attributed to downbursts such as in New York in 1975, New Orleans in 1982 and Dallas-Fort Worth in 1985. About 500 fatalities and 200 injuries have resulted from windshear crashes involving at least 26 civil aircraft between 1964 and 1985. Windshear also has caused numerous near-accidents in which aircraft recovered just

before ground contact. (NASA Langley Air Force Base, Retrieved on 29 March 2010.)

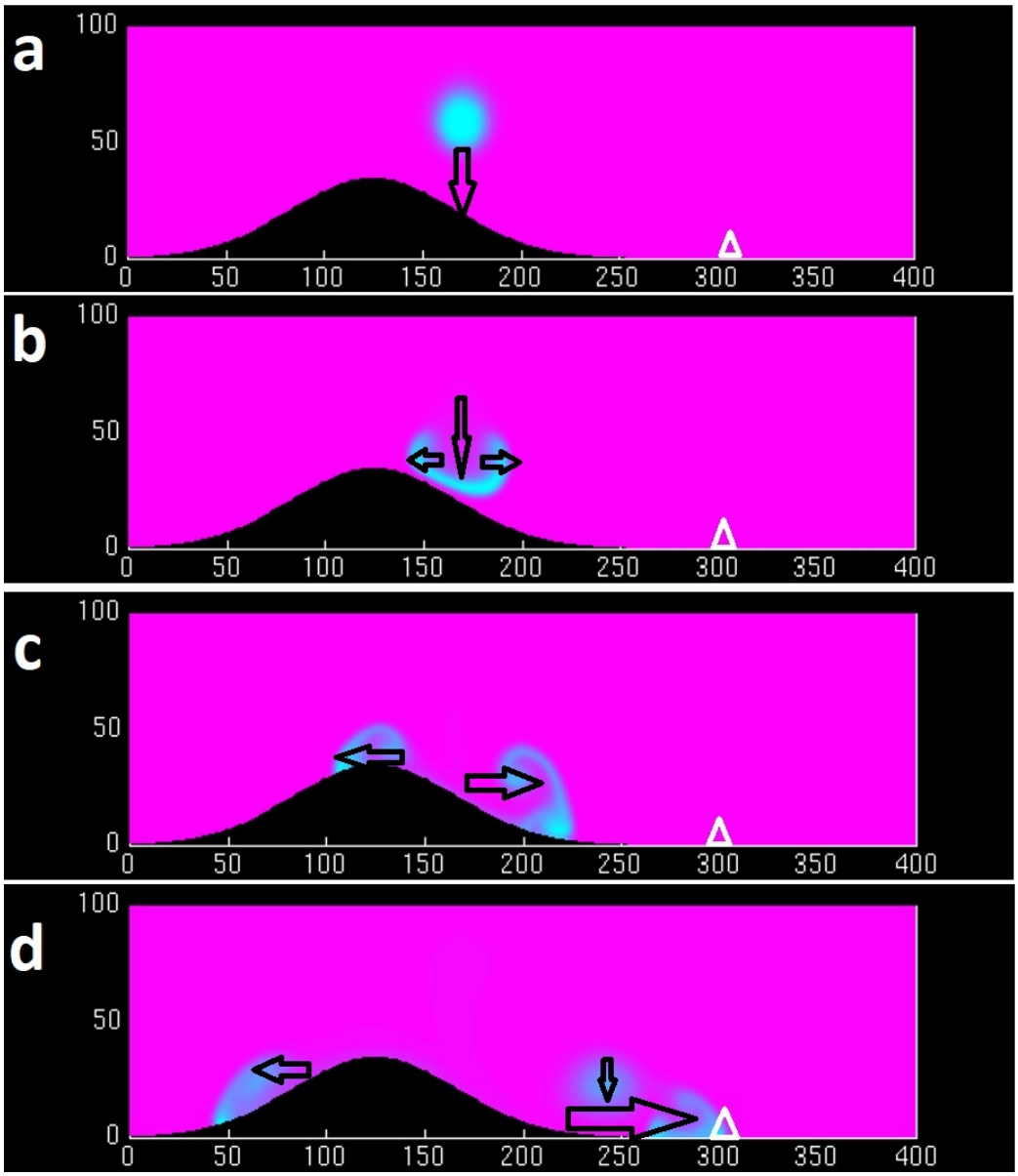

Figure 5: Schematic of a downburst development.

The blue represents a cool downdraught, the pink is the environmental air mass. The white triangle represents the location of the airport. The black arrows indicate the wind direction: (a): A cool heavier air beneath the base of the storm falling down. (b): The cool heavier air hitting the ground and spreading out. (c) The cool heavier air spreading out quickly. (d)Reaching the airport.

Chapter 3: Literature Review

3.1 SOUTHERLY BUSTERS

Southerly busters (SBs) occur during the spring and summer months in southeast Australia, to the east of the Great Dividing Range, along the coast of New South Wales (NSW) from about 38ºS to 30ºS (See location map in Chapter 4 and Appendix 1). They are strong, sudden and squally southerly wind surges (Colquhoun et al., 1985); (McInnes and McBride, 1993; Reid and Leslie, 1999). The depth of the surge is generally less than 1km, the horizontal spatial scale is about 1000-2000km. The SB passage is notable for the typical wind shift from north-westerly to southerly, and for the sudden temperature decreases of up to 20ºC within minutes (Gentilli, 1969). A wind gust is a sudden increase in the wind speed, typically for less than 20 seconds. More precisely, SBs are defined by as "squally wind change that produce strong southerly winds near the coast with gusts to at least 15m/s soon after their passages and which are not associated with a major depression over the Tasman Sea at New South Wales latitudes" (Colquhoun et al., 1985). Strong SBs (SSBs) are defined as those with wind gusts of at least 21m/s, which is the issuance criterion for airport warnings of expected damaging winds. SBs are particularly intense examples of thermally and orographically influenced cold fronts. They occur because inversions ahead of the cold front prevent the vertical escape of energy, and Coriolis effects trap the energy against the Great Dividing Range (GDR) (Colquhoun et al., 1985; Gill, 1977).

SBs also have been investigated under other names. These designations include ducted coastal ridging, which is an atmospheric surge over coastal southeast Australia, moving at a speed of about 20m/s at the leading edge of the ridge (Holland and Leslie, 1986). The coastal ridging is

initiated by a forced Kelvin-type edge wave which forms on the southwest end of the GDR, in coastal western Victoria, and is ducted, anticlockwise, around the coast. The ridge then is stabilized by inertial modification, and decays on a synoptic time scale of a few days along the NSW coast (Holland and Leslie, 1986). Another widely used term is coastally trapped disturbances (CTDs), following the study by Gill (1977) of the coastal lows observed moving anticlockwise around southern Africa. Coastal lows are similar in structure to coastally trapped waves in the ocean. As in the case of SBs, inversion conditions typical of the area prevent the escape of energy upwards, and Coriolis effects trap energy against the high escarpment that borders the southern African coast. Hence, CTDs are produced because low-level flow in the synoptic-scale systems cannot cross the escarpment (Gill, 1977). The term CTD also has been used frequently for south-eastern Australia SBs (Reason, 1994; Reason and Steyn, 1990; Reason and Steyn, 1992; Reason et al., 1999). Notably, the consensus is that the SB is a gravity current, also known as a density current, trapped against the coast by the Great Dividing Range (e.g., Baines, 1980, Mass and Albright, 1987; Egger and Hoinka, 1992; McInnes, 1993; Reid and Leslie, 1999). As such, it is initiated by a synoptic scale system and is generated by the density difference between the cooler southerly flow and the *in situ* warmer environment ahead of the surge.

3.2 THUNDERSTORM DOWNDRAFTS

A squall line is a non-frontal narrow band of active thunderstorm (FAA handbook, 1975). In the narrow band, the adjacent cells are so close together that they form a continuous line of thunderstorms accompanied by a continuous, and often strong, surface gust front along the line's leading edge. Squall lines can be too long for an aircraft to easily detour and too wide and severe for an aircraft to penetrate. They often contain severe steady-state thunderstorms

and therefore present a significant aviation hazard. Cloud bases can change rapidly and are often very low, adding additional hazards to aviation operations (FAA handbook, 1975). Issuing a warning for a squall line is very important as there is a high probability that an aircraft will encounter strong downdrafts, hail, rain, poor visibility, severe turbulence and low cloud while flying around or beneath such a system (ICAO, 2016).

Deep convection gusts due to lines of thunderstorms commonly occurs in a pre-frontal trough in South-eastern Australia (Kraus et al., 2000; Speer and Geerts, 1994).

These gusts are mainly the difluence of downbursts at the surface, but also density current propagation and vertical transfer of horizontal momentum. Almost all of the kinetic energy in a downdraft converts to horizontal kinetic energy so the maximum gust speed near the edge of the downburst, upon impact, should be about the same as the maximum downdraft; however, differences are possible depending on the depth of the outflow and the downdraft diameter (Geerts, 2001). Evaporative cooling, which would depend upon the thundertorm cloud base height and the precipitaion load with the cloud, dominates especially when the layer below cloud base is deep and well-mixed (Wakimoto 1985), and the incipient downdraft is rich in liquid/frozen water (Srivastava 1995). Entrainment below the downdraft base can further accelerate the downdraft if the ambient wet-bulb temperature is lower than that of the downdraft parcelhowever the entrainment rate generally decreases as the downburst approaches the ground (Wakimoto 1995).

Density current propagation and downward transfer of horizontal momentum are related to convective downdrafts, i.e. they are thunderstorm outflow phenomena. In most storm systems damaging winds result from outflow processes, but in case of supercell storms inflow winds may also be damagingly strong (Johns and Doswell 1992). In mesoscale convective systems/complexes, mesoscale circulations induced by horizontal surface pressure gradients may contribute to strong surface winds (Vescio and Johnson 1992, Schmidt and Cotton 1989).

Strong wind gusts associated with isolated deep convection in a weakly-sheared environment are almost always due to downbursts, especially microbursts (Fujita 1990, Atkins and Wakimoto 1991, Proctor and Bowles 1992). Based on the ideas of Proctor (1989) and Wolfson (1990), McCann (1994) developed a microburst-gust prediction index, which he named WINDEX (Wind Index). Downbursts may occur in close proximity to horizontal or vertical vortex circulations, and sometimes a divergent microburst wind pattern cannot be readily discriminated from sheared or rotating winds (Kessinger et al. 1988).

A wind gust is a sudden increase in the wind speed, typically for less than 20 seconds. Gusts are attributed to deep convection if either a thunderstorm is reported at the station with the anemometer ('locally' or 'in the vicinity') within an hour of the gust event, or, in the absence of hourly reports, if the strong winds are short-lived and marked by sudden, large, but unsustained changes in wind speed and/or direction. Rather than using objective criteria, events are selected manually, sometimes with the aid of corresponding surface charts, to exclude wind maxima associated with strong frontal disturbances without deep convection, but to include gusts due to lines of thunderstorms found in pre-frontal troughs. Commonly, deep convection occurs in a pre-frontal trough in South-eastern Australia (Speer and Geerts 1994, Kraus et al. 2000). During the warmer months (when most strong gust events occurred) cold fronts rarely penetrate inland NSW, but strong winds, sometimes exceeding 21 m/s, may affect the coastal strip in association with a 'southerly burster', and most events lasted less than 20 minutes, with a maximum of 33 minutes (Colquhoun et al. 1985). There was no strict duration limit of events used in the selection process, although most long-duration events were interpreted as frontal and therefore were excluded.

3.3 CLIMATE

Extensive climate change research on severe weather events in the Southern Hemisphere are being investigated. For example the climatology of hail occurrence from 1989 to 2013 in the Greater Metropolitan Severe Thunderstorm Warning Area (GMSTWA) of NSW indicates that the hail distribution patterns are neither temporally nor spatially uniform in magnitude throughout the study area. They are particularly common in spring and summer, reaching maximum frequency in November and December. There is an average of 14.3 events per year, but a significant decreasing trend in hail frequency and associated magnitude in the recent years has been identified. In turn, spatial analyses also established three main distribution patterns over the study area which include the Sydney metropolitan, the coastal and the most pronounced topographic effects. Based on the understanding of the favourable factors for thunderstorm development in the GMSTWA, the potential impacts from climate variability and future climate change have been briefly discussed (Rasuly et al., 2015; Allen et al.,2011)

The dominant feature of sea-level pressure (SLP) patterns over the coastal regions of south-eastern Australia is a meso-scale ridging that extends northwards along the coast. This ridging is particularly evident in the warmer months, October to March, when it is present on part or all approximately 65 per cent of days, usually occurring in sequences ranging from one to several days. Three distinct forms of coastal ridging are identified. Climatology of the three types are prepared for the 20-year

period 1974–1993 in the form of both monthly and annual frequencies of occurrence. (Speer and Leslie, 1997).

Information obtained from several studies has suggested that climate change trends over the high latitudes of the Southern Hemisphere are dominated by a strengthening of the circumpolar westerly flow that extends from the surface to the stratosphere. Findings suggests that anthropogenic emissions of ozone-depleting gases have had marked impacts on climate at the stratospheric level and at the surface of the Earth (Gillett and Thompson, 2003). Recent trends in the Southern Hemisphere tropospheric circulation can be interpreted as a bias toward the high-index polarity with stronger westerly flow encircling the polar cap. It is argued by Thompson and Solomon that the largest and most significant tropospheric trends can be traced to recent trends in the lower stratospheric polar vortex, which are due largely to photochemical ozone losses. The climate change signal has been identified from a variety of diagnostics, using near-surface temperatures, near-surface and upper-level winds, sea level pressure, storm tracks, and rainfall, among others (Bender et al. 2012; Fu et al. 2006; Fyfe et al. 2012; Solman and Orlanski 2014; Orlanski 2013; Gillett et al. 2013).

A narrow focus on traditional climate sensitivity alone might miss out on important features of the atmospheric circulation's response to increasing greenhouse gases, particularly in the extra-tropics. Hadley cell expansion is strongly linked to climate

sensitivity in all seasons Poleward dry zone and jet shift are not linked to climate sensitivity in winter. (Grise and Polvani, 2014)

During the summer-fall season, the trend toward stronger circumpolar flow has contributed substantially to the observed warming over the Antarctic Peninsula and Patagonia and to the cooling over eastern Antarctica and the Antarctic plateau (Thompson and Solomon, 2002).

Because the SBs and SSBs frequently create strong vertical wind shear, they are hazardous for aircraft, particularly larger jet aircraft, as their greater inertia causes them to maintain their speed relative to the ground when changing winds are encountered. Therefore, the study is relevant to the aviation industry. Over the last 49-year climatology for SBs and SSBs is present.

Chapter 4: Research Design

4.1 DATA AND METHODOLOGY

My research focuses on observational data analysis, in addition, model calculation and model guidance are used in the analysis. Climate data are used in the climatological investigation.

4.1.1 Observational data in SB

In Section 5.1, a trapped southerly buster and associated solitary waves is investigated. half hourly METAR and SPECI aviation observation data, synoptic chart, Himawari-8 high temporal- and spatial-resolution satellite data, radiosonde data are used for analysing the feature of the SB and the solitary waves. The simplified model is used for verification of the analysis.

4.1.2 Parameters and Indices for the Damaging Winds

In Section 5.2, a short gusty wind event associated with a squall line, half hourly METAR and SPECI aviation observation data, high-resolution temporal and spatial Himawari-8 satellite, upper air sounding, six station surface observational data, GDAS meteorological data and model outputs are used for analysis. The Hybrid Single Particle Lagrangian Integrated Trajectory Model (HYSPLIT) is a computer model that is used to compute air parcel trajectories and deposition or dispersion of atmospheric pollutants. It was developed by NOAA and Australia's Bureau of Meteorology. HYSPLIT is employed for output of meteorological variables along a trajectory (Draxler and Hess, 1998).

Several parameters and indices are taken into consideration in the study: Convective Available Potential Energy (CAPE), Downdraught Maximum Available Potential Energy (DMAPE), Deep Layer Mean (DLM) Wind (800-600hPa), Squall Line Potential, and Mesoscale Convective System (MCS) Maintenance Parameter. There are some other important parameters and indices such as shear in the shallow and deep layers, lapse rate between 750 and 500 hPa, dew point at the surface and cloud base height. Some of these are combined in the MCS maintenance parameter below but are more informative when viewed individually to allow better diagnosis of each case.

1. **Convective Available Potential Energy (CAPE)**

CAPE is the amount of work that the buoyancy force would perform on a given mass of air (called an air parcel) lifted a certain distance vertically through the atmosphere. CAPE is an indicator of atmospheric instability. The unit is J/kg. The equation is:

$$\mathrm{CAPE} = \int_{z_\mathrm{f}}^{z_\mathrm{n}} g \left(\frac{T_{\mathrm{v,parcel}} - T_{\mathrm{v,env}}}{T_{\mathrm{v,env}}} \right) dz$$

Where Z_f is the height of the level of free convection and Z_n is the height of the equilibrium level(Neutral buoyancy), where $T_{v,parcel}$ is the virtual temperature of the specific parcel, where $T_{v,env}$ is the virtual temperature of the environment (note that temperatures must be in the Kelvin scale), and where g is the acceleration due to gravity. This integral is the work done by the buyant force minus the work done against gravity, hence it's the excess energy that can become kinetic energy.

2. **Downdraught Maximum Available Potential Energy (DMAPE)**

The Downdraught Maximum Available Potential Energy is the negative buoyancy of the downdraught and assumes the saturated descent along a moist adiabat to the surface. DMAPE is a cold pool production and measures the evaporative potential of the atmosphere..

- For downdraughts that evaporate sufficiently such that a portion of its descent is along a dry

adiabat, the DMAPE is likely to be less than a downdraught that descents along a moist adiabat to the surface. The unit is unit J/kg.

3. **Deep Layer Mean (DLM) Wind (800-600hPa)**

   DLM wind calculated as the arithmetic average of the 800-600hPa (inclusive of all isobaric levels in between) winds. Mid-level steering wind of single cell thunderstorms and used as an alternative to storm motion. The unit is knot.

4. **Squall Line Potential**

A multiple ingredient composite index that identifies environments considered favourable for cold pool "driven" wind events (linear/squall line thunderstorm organisation) through four primary mechanisms:

- Cold pool production (*DMAPE*)
- Ability to sustain strong storms along the leading edge of a gust front *CAPE*
- Organization potential for any ensuing convection (approximate 0-6 km above ground level shear)
- Sufficient flow within the ambient environment to favour development along the downstream portion of the gust front (*Storm Motion, using DLM winds here*).

$$\text{Squall Line Potential} = \frac{\text{DMAPE}}{980\ \text{J kg}^{-1}} \cdot \frac{\text{CAPE}}{2000\ \text{J kg}^{-1}} \cdot \frac{\text{Bulk Shear}_{\text{SFC}-500\text{hPa}}}{20\ \text{kt}} \cdot \frac{|\bar{u}|_{\text{SFC}}^{500\text{hPa}}}{16\ \text{kt}}$$

Squall Line Potential is a dimensionless quantity, when the value is above 1, it means the good chance of a squall line.

5. **MCS Maintenance Parameter**

MCS Maintenance Parameter is used to determine whether a squall line will continue to be maintained by the favourable environmental conditions. It is important to note that, if a

MCS has developed, even if the *Squall Line Potential* forcing terms is no longer significant, if the MCS maintenance is high, the squall line may continue to occur. The output expressed as a probability of MCS maintenance with maximum value as 100.

Primary ingredients:

- Maximum bulk shear in the approximate 0-1 and 6-10 km layers
- Approximate 3-8 km lapse rate
- *CAPE*
- Approximate 3-12 km mean wind speed

	YBKE (00UTC)	YWLG (03 UTC)	YGDH (05 UTC)
CAPE(J/kg)	1683.2	1767.7	1994.7
DMAPE(J/kg)	611	804.6	684.7
Squall line Potential	1.5	1.43	1.16
MCS Maintenance Parameter (%)	96.9	96.3	97.2
DLM Winds (knot)	291/28	302/28	298/28

Table 1: The outputs of ACCESS NWP system for 3 stations when the damaging winds occurred on December 13, 2018.

There is a guidance for the convective damaging winds in Sydney regional office of Bureau of Meteorology. The threshold for winds above 40 knots is often to meet the criteria below but not necessarily to meet all of them:

- DMAPE>1000 J/kg

- The CAPE>1000 J/kg (CAPE climatology is a function of geographical area. It should be noted that places that get hotter at the surface often have higher CAPE values but without damaging winds.).
- Precipitable water is above 25mm
- DLM>40 knots
- High cloud base.

We can see from Table 1, the CAPE values of the 3 stations was well above the threshold, however, the DCAPE and DLM winds was below the threshold. The squall line potential indices were all well above 1 and MCS maintenance parameter was above 95% and close to 100%. The ACCESS NWP output in this case indicates that when the CAPE is well above the threshold the forecast guidance, even if the Strom motion and DMAPE are both below the thresholds, there is still a good chance for the damaging winds. The squall line potential and MCS Maintenance Parameter are both good elements for the chance of damaging winds.

4.1.3 Density current event over NSW and ACT

In Section 5.3, a density current event over NSW and ACT, Canberra Airport, half hourly METAR and SPECI aviation observation data are employed in 2018/2019 summer season for seasonal analysis of easterly wind changes. The wind directions are between 070 to 150 degrees inclusive.

- The average wind speeds are equal or great than 13 knots (7m/s or 25km/h) which may bring wind and low cloud to affect the operation in Canberra Airport, also which is the threshold for "small boat alert",
- The time between late afternoon and evening from 04 UTC to 13 UTC.

4.1.4 Two SSBs

Section 5.4 is an analysis of two strong southerly busters, using recently available on temporal and spatial satellite visible, inferred, and RGB night microphysical data, operational model outputs, Sydney wind profiler data, radar data and other observational data.

Section 5.5, other density currents over NSW and ACT, Himawari-8 images are used.

Chapter 6 contains a climate analysis for southerly busters, the data are from Bureau of Meteorology Climate zone. Sydney Airport is chosen as a representative station of wind change in the southern regions of New South Wales. As the southerly busters (SB) mostly occur in the warm season, the data are selected from October to next year March as one seasonal year. All the data include routine half hourly observation data and Special Observations data (see the criteria below).

Criteria for Special Observations and Reports at Any Time Element Criterion

Wind Mean Direction: When the mean surface wind direction changes by 30º or more, the mean wind speed before or after the change being 20 knots or more. Wind Mean Speed: When the mean wind speed changes by 10 knots or more, the mean speed before or after the change being 30 knots or more. Wind Gusts: When gusts vary from a mean speed of 15 knots or more by 10 knots or more. When the variation from the mean speed (gust) has increased by 10 knots or more above the previously reported gust, the mean speed then or now being 15 knots or more.

According the characteristics of the southerly buster, the definition of the SB in the research, the criteria of southerly wind were either average winds or gusty wind is equal or great than 14.9 m/s (29 knots or 54 km/h) between 160 degrees to 210 degrees. The strong southerly busters are either average winds or gusty winds more than 20.5 m/s (40 knots or 74 km/h) between 160 degrees to 210 degrees.

The following criteria must be met to indicate the presence of southerly buster event. A very rapid establishment of a strong coastal ridge which occurs when a Southern Ocean anticyclone approaches south-eastern Australia. This ridging is initiated by a high pressure surge which begins off southern Victoria, then moves quickly along the Great Dividing Range for almost the entire east coast of Australia, a distance of 2000-3000 km, while the parent anticyclone moves only a few hundred kilometres(Holland and Leslie, 1986). The count of SBs only includes the initiated southerly change by a high-pressure surge. If a ducted ridging already presented on the previous day, we only count it as one SB. If there is an east coast low, off coast low or trough, or if there is a Tasman Sea low, which also can result in strong southerly winds, we won't calculate these synoptic situations as SB.

4.1.5 Data Selection and Methodology for SB/SSB Climatology

In Chapter 6, a 49-year data set of Sydney Airport Half hourly METAR and SPECI aviation observation data are employed in the study.

According the characteristics of the southerly buster, the definition of the SB in the research, we adopt the criteria of southerly wind either average winds or gusty wind is equal or great than 14.9 m/s (29 knots or 54 km/h) between 160 degrees to 210 degrees. The strong southerly busters require either average winds or gusty winds of more than 20.5 m/s (40 knots or 74 km/h) between 160 degrees to 210 degrees.

Meanwhile, on a weather map of mean surface level pressure chart, a SB must meet the following criterion: A very rapid establishment of a strong coastal ridge which occurs when a Southern Ocean anticyclone approaches south-eastern Australia. This ridging is initiated by a high pressure surge that begins off southern Victoria, then moves quickly along the Great Dividing Range for almost the entire east coast of Australia, a distance of 2000-3000 km, while the parent anticyclone moves only a few hundred kilometres (Holland and Leslie, 1986). The

count of SBs only includes the initiated southerly change by a high-pressure surge. If a ducted ridging is already on the previous day or there is an east coast low, an offshore low and a Tasman Sea low, which also can result in strong southerly winds, SBs and SSBs are not are not counted.

Although an SB approaches from the southeast mainly on a hot day, bringing in cool, storm-laden conditions, and a dramatic temperature drop, thus ultimately replacing and relieving the prior hot conditions, the research doesn't take the change of temperatures in to consideration as one of SB selective criteria. There are two reasons behind, one is sea breeze, at Sydney Airport, it is easy to get sea breeze while the strong northwest wind keeps in the west, and there is a large difference between Sydney Airport and some observation station in the west such as Penrith. The other reason is that if the SB arrives at night or early in the morning, there are no large temperature drops from the maximum temperature on the previous day.

This study examines SBs and SSBs trends over the warm season (from October the March the following year in the study) at Sydney Airport, and determines potential climate drivers of SB and SSB. An overview of SBs and SSBs trends present in the time series was first gained by graphing the time series with their trend lines. Because the data are not Gaussian, and non-stationary, non-parametric statistical analysis was applied to the data. The data were grouped into 25-year periods with one year overlapped (1994-1995). Permutation testing was applied. Wavelet analysis was performed on the time series following the approach of Torrence and Compo (1998). Wavelets are well-suited to the study of non-stationary time series as they provide an understanding of the time evolution of the periodicity of signals. This is done by stretching and translating local base functions in both space and time. This study used the Morlet wavelet which is described by:

$$\psi_0(\eta) = \pi^{\frac{-1}{4}} e^{-i\omega_0\eta} e^{\frac{-\eta^{2\cdot}}{2}} \qquad (a)$$

Where η is a non-dimensional time parameter and ω_0 is the non-dimensional frequency. The continuous wavelet for a time series, x_n, is given by:

$$W_n(s) = \sum_{n'=0}^{N-1} x_{n'} \psi^* \left(\frac{(n'-n)\delta t}{s} \right) \qquad (b)$$

Where s is the wavelet scale, n is a localised time index, N is the number of data points in the time series and $*$ is the complex conjugate. The wavelet transform is more efficiently computed in Fourier space rather than directly computing (2). The discrete Fourier transform of x_n is

$$\hat{x}_k = \frac{1}{N} \sum_{n=0}^{N-1} x_n \, e^{-2\pi i k n / N} \qquad (c)$$

Where k = 0, 1, . . ., N − 1 is the frequency index, and the Fourier transform of ψ(t/s) is given by $\hat{\psi}(s\omega)$. By the convolution theorem, and taking the inverse Fourier transform, the wavelet transform is given by

$$W_n(s) = \sum_{k=0}^{N-1} \hat{x}_k \hat{\psi}^{*} (s \, \omega_k e^{-i\omega_k n \delta t}) \qquad (d)$$

Where

$$\omega_k = \begin{cases} \frac{2\pi k}{N\delta t}, & k <= \frac{N}{2} \\ \frac{-2\pi k}{N\delta t}, & k > \frac{N}{2} \end{cases} \qquad (e)$$

4.2 ICAO LOCATIONS IN NSW

In this thesis, the ICAO of NSW airports are mentioned in Figure 6, below. See Appendix 1.

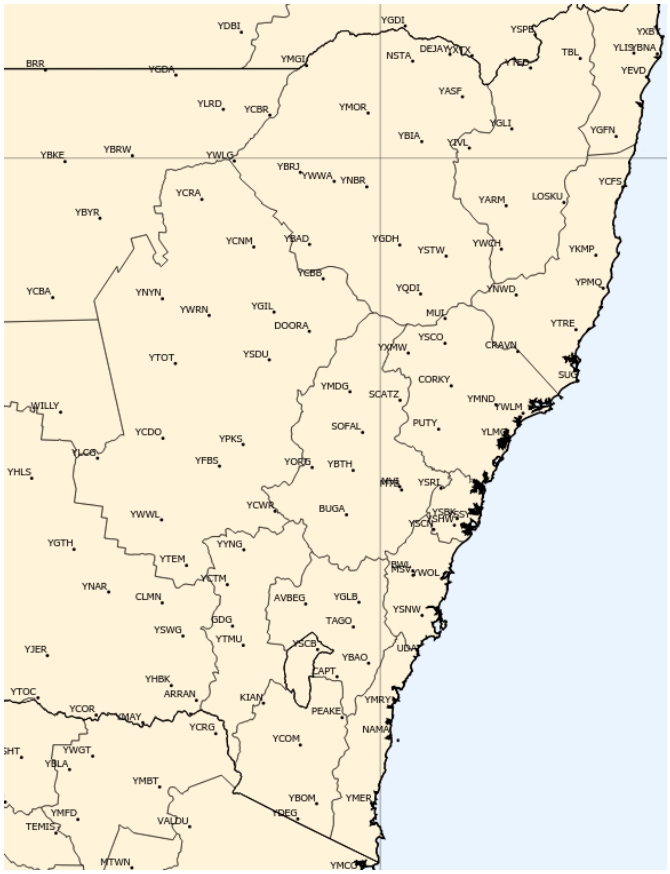

Figure 6: ICAO ID of Airports in New South Wales.

4.3 ETHICS AND LIMITATIONS

The research does not include any of the ethical considerations and does not have any health and safety issues.

Chapter 5: Experiments and Results

Chapter 5 details all the results of my study:

In Section 5.1, a trapped southerly buster and associated solitary waves.

In Section 5.2, a short gusty wind event associated with a squall line.

In Section 5.3, density current event over NSW and ACT.

In Section 5.4, analysis of two strong southerly busters.

In Section 5.5, other density currents over NSW and ACT, Himawari-8 images are used.

5.1 A TRAPPED SOUTHERLY BUSTER AND ASSOCIATED SOLITARY WAVES

This section is a detailed case study of the southerly buster of October 6-7, 2015, along the New South Wales coast. It takes advantage of recently available Himawari-8 high temporal- and spatial-resolution satellite data, and other observational data. The data analyses support the widespread view that the southerly buster is a density current, coastally trapped by the Great Dividing Range. In addition, it appears that solitary waves develop in this event because the prefrontal boundary layer is shallow and stable. A simplified density current model produced speeds matching well with observational southerly buster data, at both Nowra and Sydney airports. Extending the density current theory, to include inertia-gravity effects, suggests that the solitary waves travel at speeds approximately 20% faster than the density current. This speed difference is consistent with the high-resolution satellite data, which shows the solitary waves moving increasingly ahead of the leading edge of the density current.

5.1.1 Introduction

Southerly busters (SBs) occur during the spring and summer months in southeast Australia, to the east of the Great Dividing Range (Figure 7), along the coast of New South Wales (NSW) from about 38ºS to 30ºS. They are strong, sudden and squally southerly wind surges (Colquhoun et al., 1985); (McInnes and McBride, 1993; Reid and Leslie, 1999). The depth of the surge is generally less than 1km. The SB passage is notable for the typical wind shift from north-westerly to southerly, and for the sudden temperature decreases of up to 20ºC within minutes (Gentilli, 1969). More precisely, SBs are defined by as "squally wind change that produce strong southerly winds near the coast with gusts to at least 15m/s soon after their passages and which are not associated with a major depression over the Tasman Sea at New South Wales latitudes" (Colquhoun et al., 1985). Strong SBs (SSBs) are defined as those with wind gusts of at least 21m/s, which is the issuance criterion for airport warnings of expected damaging winds. SBs are particularly intense examples of thermally and orographically influenced cold fronts. They occur because inversions ahead of the cold front prevent the vertical escape of energy, and Coriolis effects trap the energy against the Great Dividing Range (GDR) (Colquhoun et al., 1985; Gill, 1977).

SBs also have been investigated under other names. These designations include ducted coastal ridging, which is an atmospheric surge over coastal southeast Australia, moving at a speed of about 20m/s at the leading edge of the ridge (Holland and Leslie, 1986). The coastal ridging is initiated by a forced Kelvin-type edge wave which forms on the southwest end of the GDR, in coastal western Victoria, and is ducted, anticlockwise, around the coast. The ridge then is stabilized by inertial modification, and decays on a synoptic time scale of a few days (Holland and Leslie, 1986). Another widely used term is coastally trapped disturbances (CTDs), following the study by Gill (1977) of the coastal lows observed moving anticlockwise around southern Africa. Coastal lows are similar in structure to coastally trapped waves in the ocean.

As in the case of SBs, inversion conditions typical of the area prevent the escape of energy upwards, and Coriolis effects trap energy against the high escarpment that borders the southern African coast. Hence, CTDs are produced because low-level flow in the synoptic-scale systems cannot cross the escarpment (Gill, 1977). The term CTD also has been used frequently for south-eastern Australia SBs (Reason, 1994; Reason and Steyn, 1990; Reason and Steyn, 1992; Reason et al., 1999). Notably, the consensus is that the SB is a gravity current, also known as a density current, trapped against the coast by the Great Dividing Range (e.g., Baines, 1980, Mass and Albright, 1987; Egger and Hoinka, 1992; McInnes, 1993; Reid and Leslie, 1999). As such, it is initiated by a synoptic scale system and is generated by the density difference between the cooler southerly flow and the *in situ* warmer environment ahead of the surge.

In this study, the SB event of October 6-7, 2015 is examined with the high temporal and spatial resolution observational data that was not available in the earlier studies mentioned above. As mentioned above, a SB is viewed as a density current advancing into a strongly stable *in situ* boundary layer which is comprised of warm summertime prefrontal continental air advection overlaying a cooler sea. Frequently a roll vortex is generated, which extends ahead of the cold front, in about half of observed SBs (Garratt,1988). The head of the density current breaks away from the feeder flow supplying it with cold air and the pre-frontal boundary layer commonly is between 100m and 200m deep and, if the pre-frontal stable layer is deep and strong, the roll vortex can evolve as a solitary wave, or as a bore wave, that propagates on the stable layer.

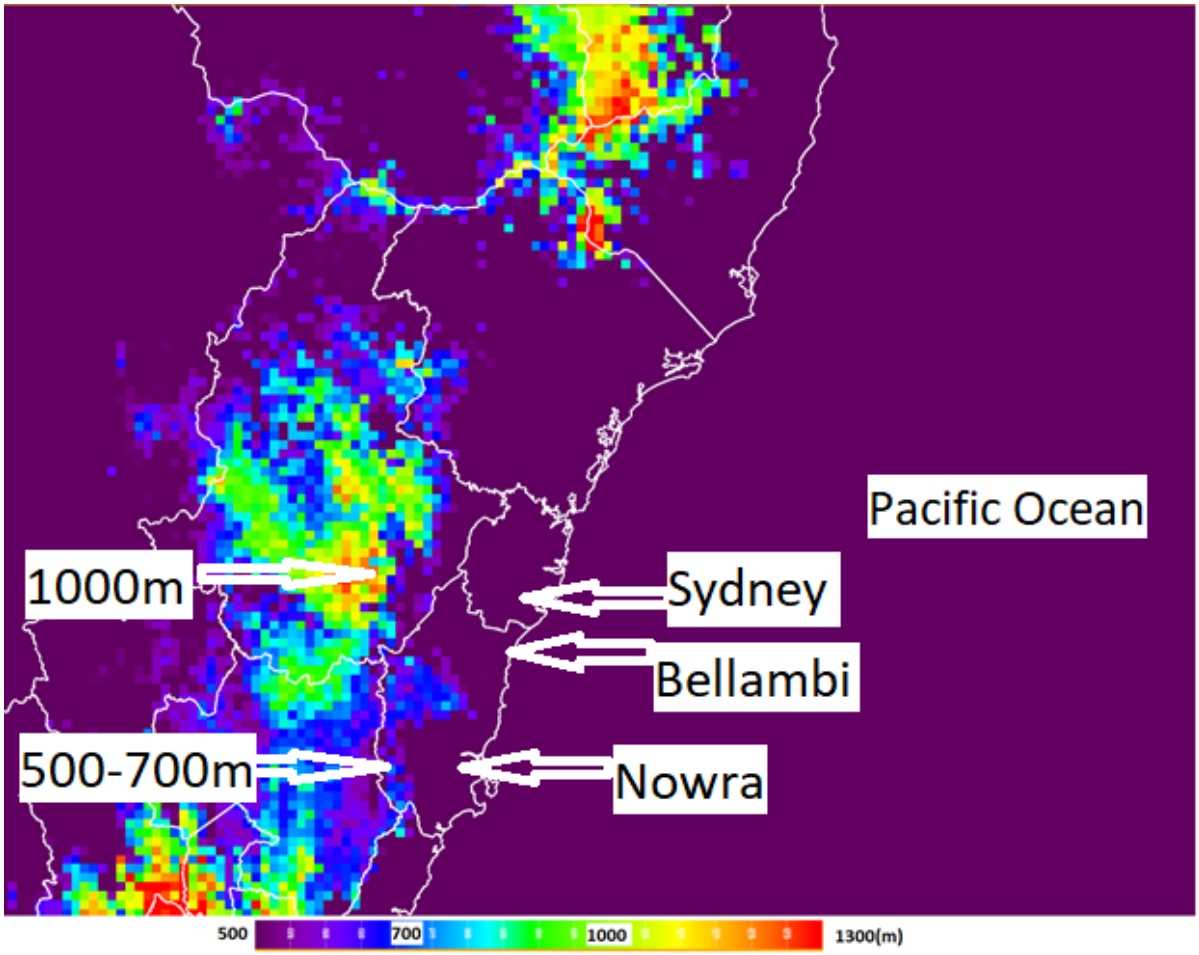

Figure 7: Topography of New South Wales.

From Pacific Ocean coast from Nowra to Sydney, with the Great Dividing Range to the west of Nowra, Bellambi and Sydney in metres (m). The map includes the regional district boundaries and the elevation bands are in metres. The heights just west of Nowra (YNSW) typically are ~500m and west of Sydney Airport (YSSY) are ~1000m.

5.1.2 Observations and Analysis

On October 6, 2015, a southerly wind change (SC) propagated along the southeast coast of Australia. At Nowra Airport (YSNW), the winds were moderate (5-10m/s) west to north-westerly during the day, from 0000UTC (Coordinated Universal Time) to 0730UTC, due to

the synoptic winds ahead of the trough. The winds became light and variable in the evening (0730UTC to 1200UTC), then trended to northwest drainage flow around or below 5 m/s before the SC occurred (Figure 8). At 1559UTC, the SC arrived at YSNW with southerly winds of 8m/s, gusting to 11m/s, at the automatic weather station (AWS) site which is 112km south of Sydney Airport (YSSY). At 1630UTC, the SC wind gusts touched 15m/s, thereby officially becoming a SB, then decreased over the following 90 minutes. The SC arrived at Sydney Airport (YSSY) at 1800UTC and became a SB just two minutes later. The wind gusts reached 21m/s which met the criterion for an airport warning at YSSY (Figure 9). At YSSY, ahead of the SC, there was light to moderate northwest drainage flow around 3-4m/s; at 1800UTC, the observations showed no significant cloud and the wind direction changed from northwest to south to southwest, the wind speeds picked up at 1802UTC with gusts to 15m/s, hence reaching SB levels. Approximately 16 minutes later, at 1816UTC, some low clouds developed at around 300m; at the same time, the visibility dropped to about 2300m, or 7000 feet (Figure 10). Another key signature was a sudden pressure rise of up to 6hPa after the SC, within three hours, at both YSNW and YSSY. This pressure rise had become noticeably steeper, starting at Mt Gambier and reached a maximum amplitude and steepness from Nowra (6.2hPa) to YSSY (6.4hPa). The rapid pressure rises associated with the coastal ridging that occur behind the SC

are a signature feature of the main CTD (Holland and Leslie, 1986).

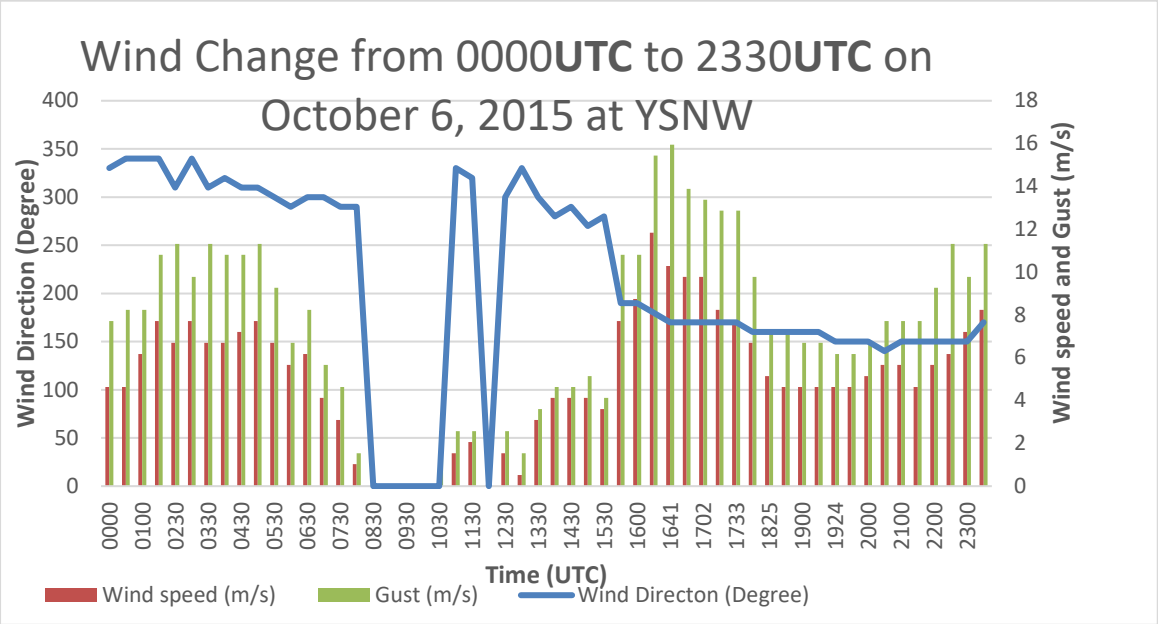

Figure 8: Observations of wind change from 0000UTC to 2330UTC on October 6, 2015 at Nowra (YSNW).

Time in UTC for horizontal axis, wind directions in degrees for primary vertical axis (left), wind speed gusts in m/s for secondary vertical axis (right). Wind speeds (orange clustered columns, m/s), Wind gusts (grey clustered columns, m/s), Wind directions (blue lines, degrees).

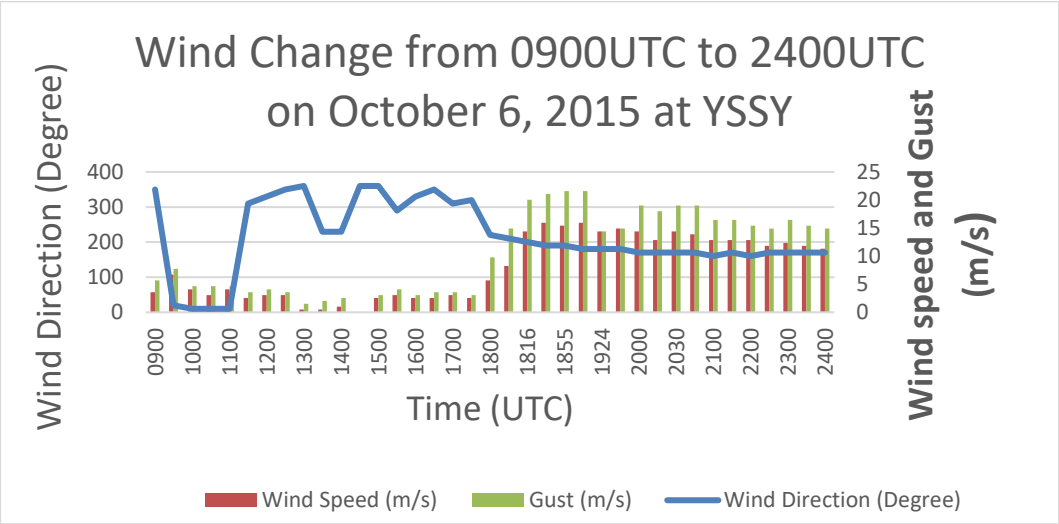

Figure 9: As in Figure 8, except at Sydney (YSSY) from 0900UTC to 2400UTC on October 6, 2015.

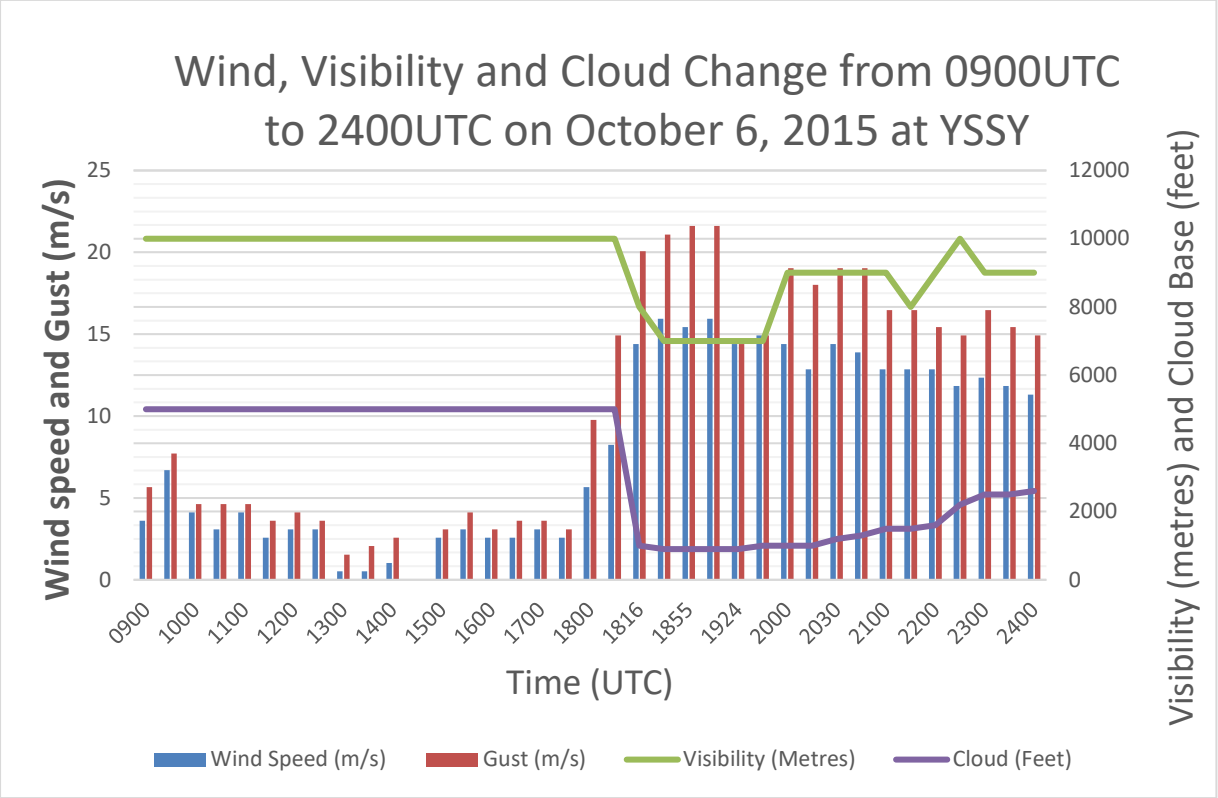

Figure 10: Observations of wind, visibility and cloud change from 0900UTC to 2400UTC on October 6, 2015 at YSSY.

Time in UTC for horizontal axis, wind speeds and wind gust in m/s for primary vertical axis (left), visibility in metres and cloud base in feet for secondary axis (right). Wind speeds (blue clustered columns in m/s), Wind gusts (orange clustered columns in m/s), Visibility (grey lines in metres), Cloud base (yellow lines in feet).

	SC time (UTC)	SC winds (m/s)	SB time (UTC)	SB winds (m/s)	Maximum SB time (UTC)	Maximum SB winds (m/s)
YSNW	1559	19008G11	1630	18012G17	1641	17010G16
YSSY	1800	22006G10	1802	21008G15	1900	18016G21

Table 2: Details of the wind changes at YSNW and YSSY.

The southerly change (SC) and southerly buster (SB) time and maximum SB occurring time and winds details including wind direction (degrees), speed and gust (m/s): e.g., 19008G11 means the wind direction is 190 degrees, the mean wind speed is 08 m/s and the gust wind speed is 11m/s.

5.1.3 Synoptic Overview

The synoptic situation is obtained from archived upper-level and mean surface level pressure (MSLP) charts. At 850hPa on 0000UTC October 5, 2015, a high pressure system dominated much of southeast Australia with warm temperatures up to 19°C, while a low pressure system with cooler temperatures extended a NW-SE orientated trough from southwest of Australia, crossing the Southern Ocean south of Tasmania. At 1200UTC October 5, the surface high pressure system moved slowly southwest while the trough moved northeast. By 0000UTC October 6, the surface high pressure system pressure centre had moved over the Tasman Sea, and the trough was situated further to the northeast.

A phenomenon well-known to Australian meteorologists is the rapid establishment of a strong coastal ridge, which occurs when a Southern Ocean anticyclone approaches south-eastern Australia. This ridging is initiated by a high pressure surge which begins off the coast of southern Victoria, then moves rapidly along the NSW coast, and often travels along most the entire east coast of Australia, a distance of 2000-3000km. In contrast, the parent anticyclone moves only several hundred kilometres (Holland and Leslie, 1986). The MSLP charts from 0600UTC October 6 to 1800UTC October 7, 2015 are shown in Figure 11. At 0600UTC October 6, coastal ridging was initiated at the south-western extremity of the GDR, between Mt Gambier and Cape Otway, associated with the northward movement of cold air behind a

nearly zonal Southern Ocean front. East of Mt Gambier the cold flow was blocked by the southern slopes of the GDR, thereby driving the ducted disturbance eastwards along the Victorian coast. At 1200UTC October 6, the coastal ridging had propagated around the southeast corner of Australia and was located on the NSW coast, north of Gabo Island. At 1800UTC October 6, a strong high-pressure centre (1036hPa) was situated in the Great Australian Bight, with an inland trough west of the ranges and a frontal zone off eastern Australia, further extending the coastal ridge along the southeast NSW coast. At 0000UTC October 7, the cold front had continued moving northeast while the surface high pressure system centre increased to 1039hPa, strengthening the ridge over southeast NSW. By 1200UTC and 1800UTC October 7, the original high pressure system had separated into two centres, with the parent high remaining over the Southern Ocean, and the second centre moving to the south of the Tasman Sea. The coastal ridging had extended along the entire NSW coast and entered southern Queensland.

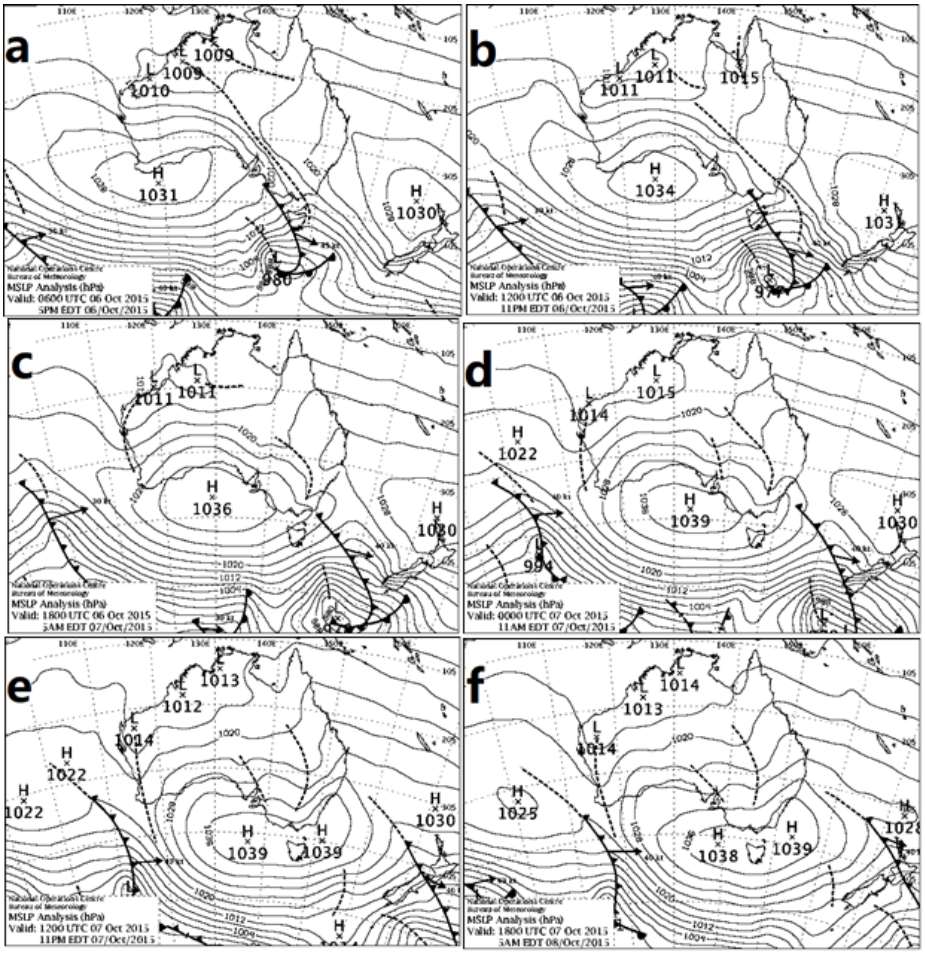

Figure 11: Synoptic weather charts October 6 to October 7.

a) 0600 UTC October 6, 2015. b) 1200UTC October 6. 2015, c) 1800UTC October 6, 2015. d) 0000UTC October 7, 2015. e) 1200UTC October 7, 2015. f) 1800UTC October 7, 2015. Shown are contours of Mean Sea Level Pressure (MSLP) in intervals of 4hPa, local maxima and minima of MSLP, manually analysed cold fronts (solid lines with triangular barbs), and low pressure troughs (dashed lines). (Charts are from http://www.bom.gov.au/australia/charts/).

5.1.4 Satellite Imagery

The Himawari-8 satellite image at 2140UTC on October 6 (Figure 14), reveals a possible roll cloud accompanying the SB offshore near Williamtown, extending to the southeast over the Tasman Sea. Ahead of the cold front cloud band, what appear to be shallow solitary waves are moving with the cold front cloud band. Clarke (1961) determined the mesoscale structure of the dry cold fronts using serial pilot balloon flights, radiosonde, and aircraft data. He found closed circulations (roll vortices) in the velocity field behind several fronts; in two cases, double circulations with the roll vortices were inferred (Clarke, 1961). A study of seventeen strong SBs over the period January 1972 to January 1978 was carried out by Colquhoun et al. (1985). Attempts were made to infer the structure of the 17 SBs from anemograph data and temperature profile measurements. The arrival of a clockwise rotating vortex (viewed from the west) was associated with an increase in wind speed and instability and a decrease in temperature; the highest wind speed occurred under the circulation centre of the vortex. Roll vortices were thought to be associated with more than 50% of SBs. The SB frontal structure, in cross Section parallel to the coast, is shown for the event of a SB passing Sydney Airport on December 11, 1972 (Figure 12. Streamlines represent airflow relative to the circulation centres of the roll vortices and straight arrows indicate wind direction. The first circulation cell corresponds with the 28 minute period following the first wind change and the second cell with the subsequent two-hour period (Colquhoun et al., 1985). A possibly similar structure appears in the visible satellite imagery on October 6, 2015 (within the green circle of Figure 13. The roll cloud in the lower atmosphere often exhibits a distinctive flow pattern. Winds near the surface in the horizontal propagating vortices exceed the speed of the propagation and can be a severe hazard to aircraft operating at low altitude (Christie, 1983).

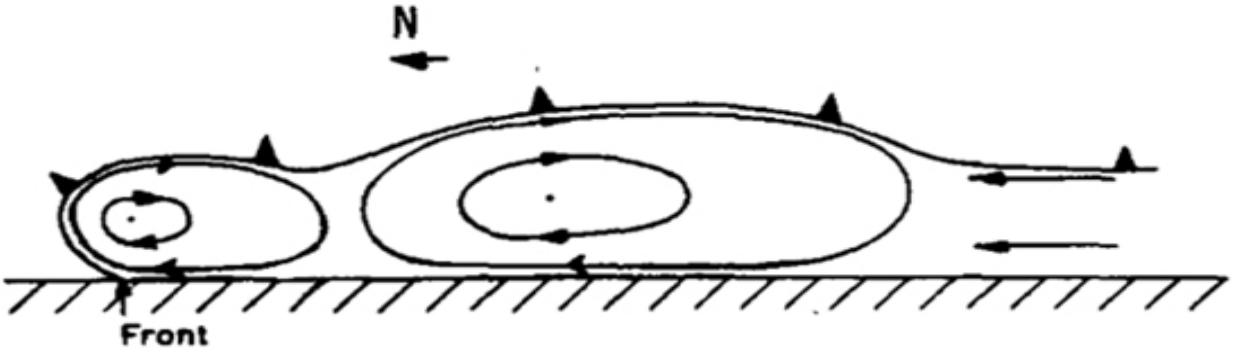

Figure 12: Schematic representation deduced from wind temperature data, of the frontal structure in a vertical cross Section parallel to the coast.

Streamlines are airflow relative to the circulation centres of roll vortices and straight arrows are wind directions (Colquhoun et al., 1985).

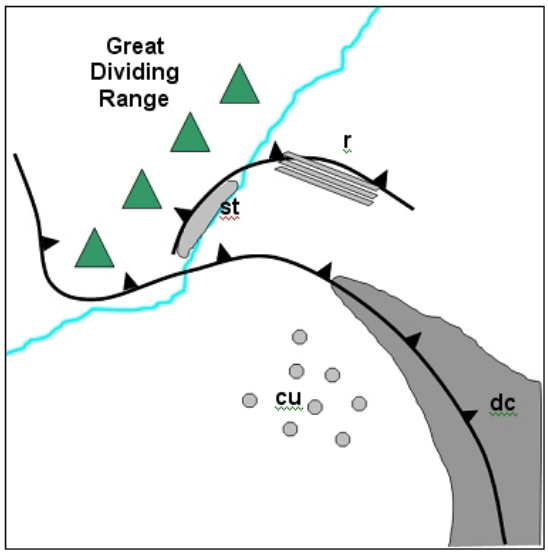

Figure 13: Schematic of the cloud signatures of a Southerly Buster that can be detected using several sources of satellite imagery.

From https://sites.google.com/site/cmsforsh/CoE-Australia/shallow-cold-fronts/cloud-structure-in-satellite-images.

Figure 13 is a schematic of SB cloud signatures detected by the satellite imagery. The acronym, dc, indicates deeper cloud associated with the cold front (seen in visible, infrared, and water

vapour images); st refers to low (stratus) cloud banking up against the escarpment of the range behind the SB (from visible and, sometimes, infrared images); r denotes roll clouds may be associated with the buster (from visible and, sometimes, infrared images). Finally, cu signifies open cell (speckled) cumulus cloud behind the cold front (from visible and infrared images)

Cloud features associated with the SB also were detected from the Himawari-8 visible imagery (Figure 14) at 2140UTC on October 6, 2015. The green arrow indicates the leading edge of the SB accompanied by a roll cloud. The roll cloud is consistent with the schematics of Figure 12 and Figure 13. The yellow arrow points to the low cloud banking up against the escarpment of the range behind the passage of the SB over eastern Great Dividing Ranges. The pink arrow provides the location of the parent cold front to the SB which is consistent with the schematic (Figure 13). The red arrow shows a wave train of solitary waves that propagated ahead of the roll cloud. Both the solitary waves and the single roll cloud may sometimes be seen at the head of the SB in the visible imagery although this is not clear in the corresponding infrared images. They can produce wind shear which is sufficiently strong enough to pose a hazard to aircraft operating at low altitudes (typically landing or taking off). Solitary waves in the lower atmosphere take the form of rows of isolated, single-crested gravity, or gravity-inertia waves, which propagate predominantly as clear-air disturbances in a boundary layer inversion waveguide. (Christie, 1983)

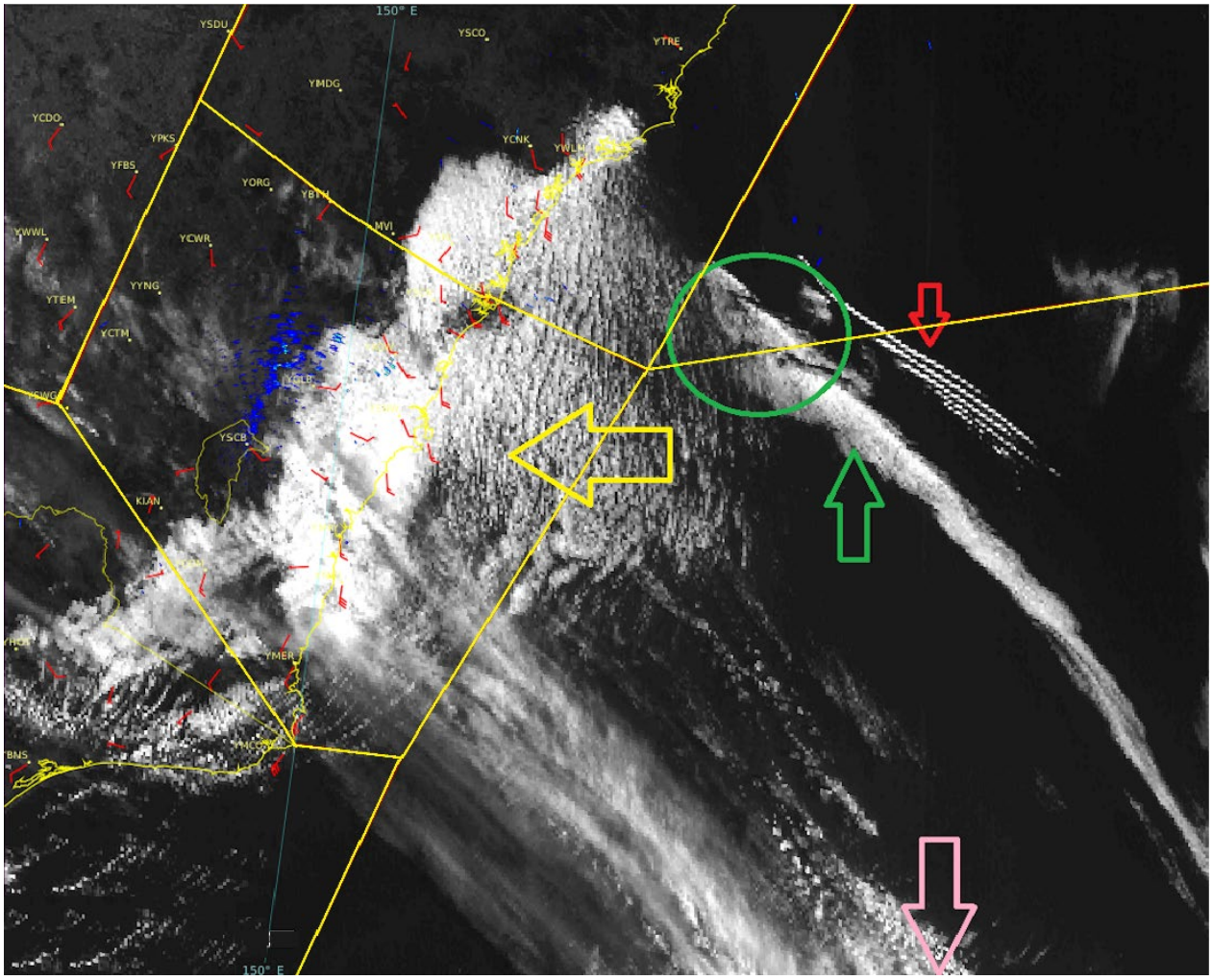

Figure 14: Himawari-8 satellite visible image at 2140UTC on October 6. 2015 over the New South Wales coast.

Image is shown with the permission of the Australian Bureau of Meteorology. The AWS wind barbs show wind direction and speed in knots (red barbs), and the overlain boundaries of the Australian aviation regions (yellow lines). The green arrow indicates the leading edge of the SB, accompanied by a roll cloud. The yellow arrow points to the low cloud banking up against the escarpment of the range behind the passage of the SB over the eastern Great Dividing Range. The pink arrow locates the parent cold front to the SB. The red arrow shows a possible train of solitary waves. The green circle shows a structure like the schematic representation in Figure 12.

Microwave scatterometer data, such as the winds from the advanced scatterometer (ASCAT) in Figure 14, also are useful for monitoring SBs, despite this polar orbiting satellite providing data of relatively limited temporal frequency. Fortunately, in this case, descending pass data were available at 2325UTC October 6 (Figure 14). The wind change zone propagated to the north of 32S, and also was detected by the Himawari-8 visible imagery from 2020UTC to 2320UTC (Figure 15). Using both red square boxes in Figure 14 and Figure 15, the SB was well represented for assessing the horizontal structures of the wind change, and for clouds. The transient wind horizontal wind shear in the red box of Figure 14 clearly is associated with the roll cloud in Figure 15. The wind speeds behind the change were about 10-15m/s, which were responsible for the stratus low clouds near the coast.

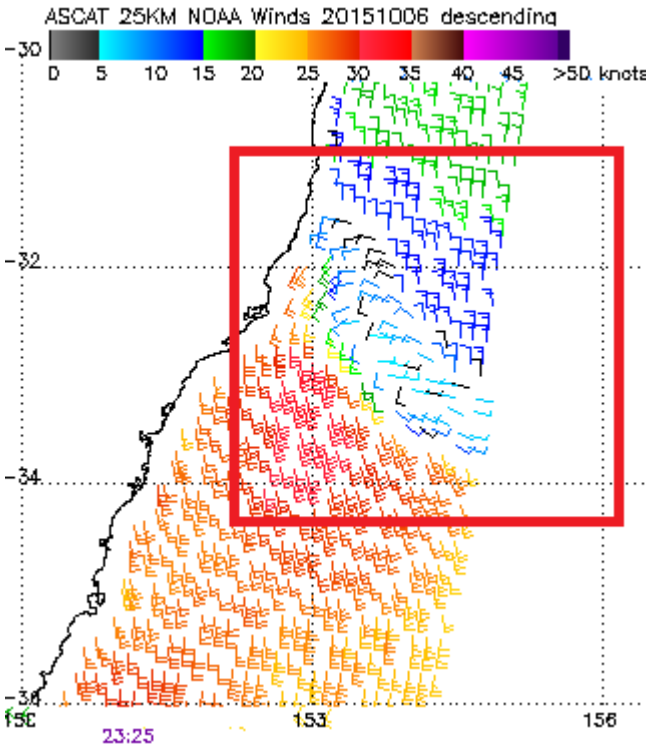

Figure 15: ASCAT winds at 2325UTC on October 6, 2015.

Note the detailed near-surface winds, associated with the passage of the SB, in the red square. Image from NOAA/NESDIS (https://manati.star.nesdis.noaa.gov/datasets/ASCATData.php)

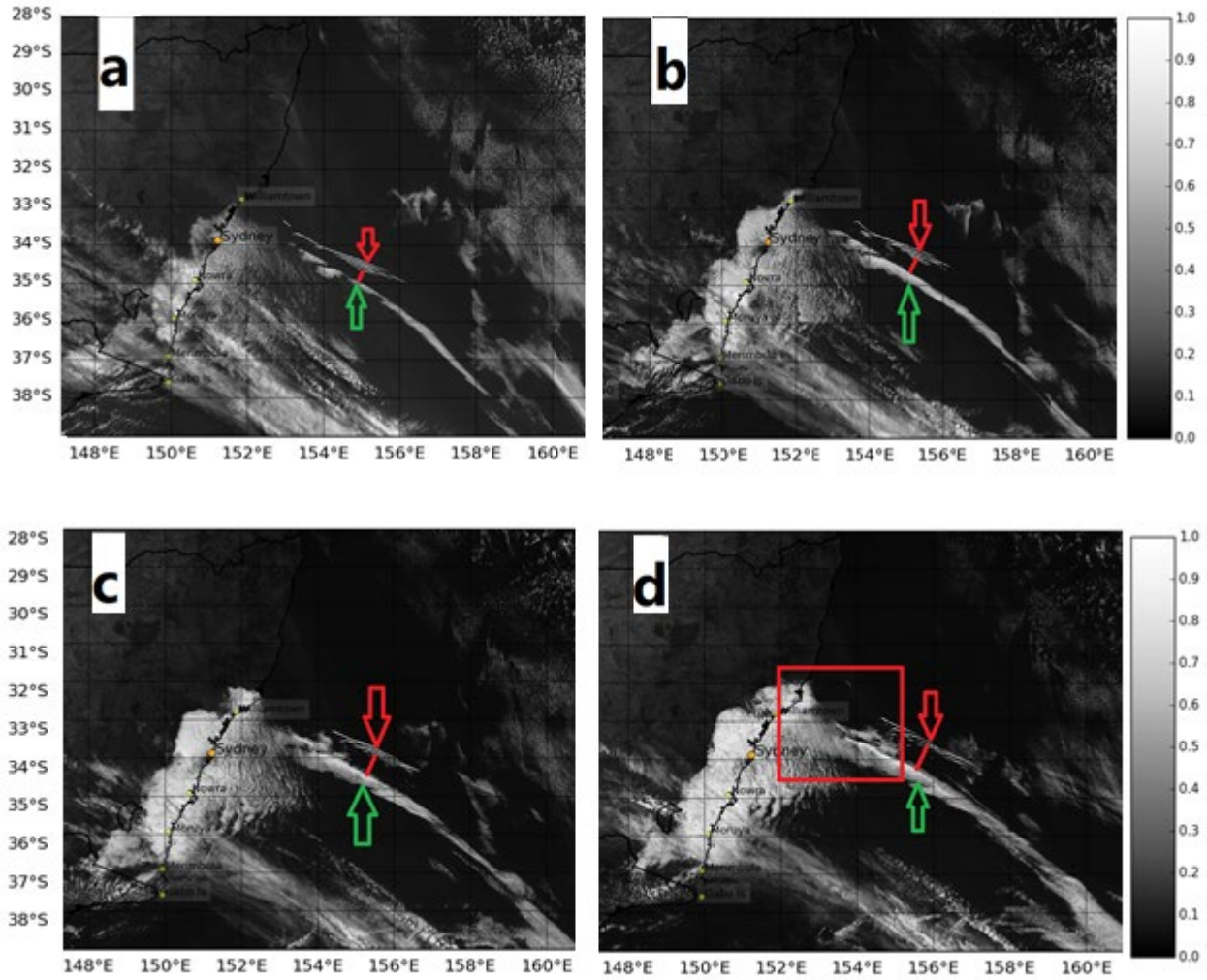

Figure 16: The Himawari-8 satellite visible images from 2020UTC to 2320UTC on October 6, 2015.

a) 2020UTC, b) 2120UTC, c) 2220UTC, d) 2320UTC. The green arrow indicates the leading edge of the SB, which is accompanied by a roll cloud. The red arrow shows a train of solitary waves. The solid red line is the distance between the roll cloud and the wave train. The red square in d) is consistent with the red square area in Figure 15.

5.1.5 Radiosonde Data

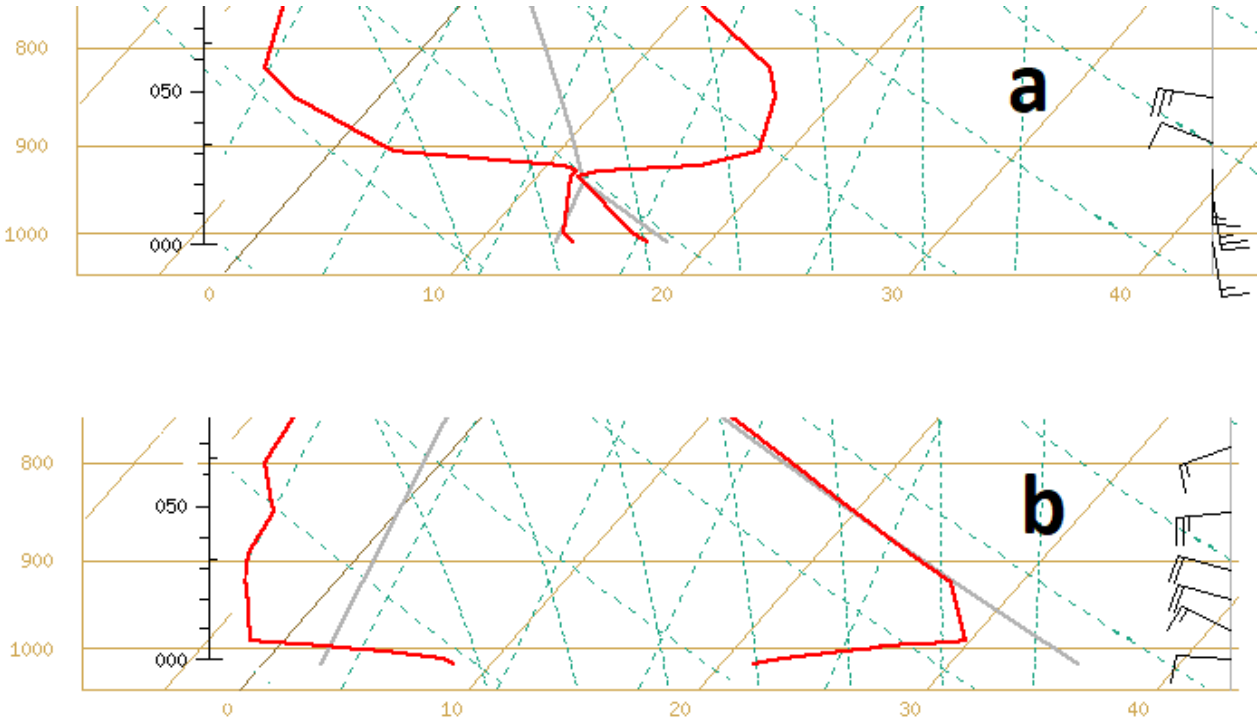

Figure 17: Radiosonde profile on October 6, 2015.

(Permission from the Australian Bureau of Meteorology) a) at 1700UTC at Nowra Airport (YSNW), b) at 1900UTC at Sydney Airport (YSSY). Light brown left vertical axis is pressure (hPa); left black vertical axis is height above sea surface in hundreds of feet. So, e.g., 050 means 5000ft (about 1600m) above the sea surface. Right vertical axis is wind profiler information. The red solid lines are the temperature profile (right), and the dew point profile (left). Wind speeds are in m/s; short bar = 2.5 m/s, long bar = 5 m/s.

The vertical structure of the atmosphere can be inferred from sounding data from Nowra (YSNW) in Figure 17 (a), and Sydney (YSSY) in Figure 17 (b). Solitary waves observed in the lower atmosphere typically take the form of rows of isolated, single-crested waves which

propagate predominantly as clear-air disturbances in a boundary layer inversion waveguide. The 1700 UTC sounding at YSNW (Figure 17(a)), which commenced one hour after the SB passage, shows a low-level stable layer to 900hPa overlain by a well-mixed, nearly isentropic layer (neutral layer) extending up to 820hPa. This configuration is attributed to the advection of the deep continental mixed layer eastwards across the GDR, and then lying over a lower stable marine layer maintained by sea breeze activity along the coast (Holland and Leslie, 1986). The low-level southerly winds indicate that the cold air extended to about 800m (934hPa) above mean sea level (MSL). This shallow, stable boundary layer was capped by a strong inversion extending to 1000m (907hPa) above MSL. The corresponding temperatures were 11.8°C (at 934hPa) and 18.8°C (at 907hPa). The dewpoints were 10.8°C and 14.2°C, respectively, significantly higher than those above the inversion (Table 3). The dewpoint depressions were no more than 5° below the inversion, then increased abruptly to 20°C at 850hPa. The winds were moderate to strong southerly below the inversion, and moderate to strong west to north-westerly above the inversion.

Pressure (hPa)	**Temperature (°C)**	**Dew point temperature (°C)**	**Wind Direction (degrees)**	**Wind Speed (knots) and m/s**
1023.6	17.5	14.2	170	19 (9.6m/s)
1011	17.4	14.1	170	17.4 (8.5m/s)
1000	16.4	13.4	170	22.6 (11.4m/s)
957	Nil	Nil	170	26.8 (13.7m/s)
934	11.8	11.5	nil	Nil
929	12.6	11.6	nil	Nil
926	Nil	Nil	180	14.4 (7.4m/s)
923	16.8	10.8	nil	Nil
907	18.8	2.8	nil	Nil
896	Nil	Nil	290	10.2 (5.2m/s)
850	17.4	-3.6	280	24.6 (12.5m/s)

Table 3: The Nowra (YSNW) radiosonde data on 1700UTC October 6, 2015.

After the SB passage. Nil means no data is available. Note the near-surface stable layer, topped by a neutral layer.

At 1900UTC at Sydney, just ahead of the southerly change, the sounding revealed a strong, shallow inversion from the surface to 50m above MSL (1000hPa). Hence, the southerly change is very shallow with an overlying deep inversion. Fronts with a north-west/south-east orientation can experience blocking by the coastal mountain ranges (Figure 7) of southeast Australia and progressively increase propagation speed on the eastern (coastal) side of the ranges while moving more slowly on the western side of the ranges. The effect is more pronounced for shallow cold fronts than those with the cold-air layer exceeding the height of the ranges (Coulman, 1985).

5.1.6 Current Theory: Application to SBs.

5.1.6.1 Density Current Speed

The theory of density currents is in detail in Chapter 2:, to verify the density current theory, the SB observation data are employed to the equations (1) to (4) in Chapter 2:

$$\rho\rho = P/RT\,, \qquad (1)$$

$$c = \sqrt{gH}. \qquad (2)$$

$$c_{DC} = \sqrt{g'H}\,, \qquad (3)$$

$$\boldsymbol{g}\,(\rho 1\text{-}\rho 2)/\rho 1\,, \qquad (4)$$

In this case, the density current speed can be estimated, using radio sounding data from the YSNW station.

From Equation (1) and Table 3, for a cooler, denser lower layer overlain by a warmer, less dense upper layer:

$\boldsymbol{\rho_1 = P1/RT1}$ = 934/(287.058*284.8)= 0.0115,

$\boldsymbol{\rho_2 = P2/RT2}$ = 907/(287.058*291.8) = 0.0108.

Hence, $\mathbf{c} = \sqrt{\boldsymbol{g'H}}$, the density current speed

Where $\boldsymbol{g'} = \boldsymbol{g(\rho_1 - \rho_2) / \rho_1}$= 0.597, (7)

and, H, the cold air depth (m) at YSNW, is approximately 500m, from Figure 7.

So, the density current speed, $\mathbf{c_{DC}} = \sqrt{\boldsymbol{g'\ H}}$ ~17m/s (~ 33knots). (8)

The estimated speed in (8) is consistent with the observational data from both the YSNW station observations and also the satellite wind data in Figure 16, in which the winds in the red square behind the change are approximately 15m/s (~29knots). However, it is important to note that the calculation of $\mathbf{c_{DC}}$ is highly dependent on the value of $\boldsymbol{H}$, so care was taken in selecting the value of H from detailed orographic maps.

5.1.6.2 The Solitary Waves Speed

It is likely that the parallel cloud lines in the red arrow area solitary waves (Figure 14 and Figure 16), ahead of the SB roll cloud. They are moving slightly faster than the roll cloud (DC). The formula for the calculation of the phase speed of inertia-gravity (Poincaré) waves is very well-known (e.g., Gill, 1982), and is given by in detail in Chapter 2:, to verify the density current theory, the SB observation data are employed to the equations (5) to (6) in Chapter 2:

$$c_{poincaré} = \sqrt{g'H}(1 + \frac{f_0^2}{g'Hk^2})^{1/2} = c_{DC}(1 + \frac{f_0^2}{g'Hk^2})^{1/2} \quad (5)$$

$$k^2 = (\frac{2\pi}{L})^2 \qquad (6)$$

Where:

$c_{poincaré}$ = Poincaré wave phase speed (m/s), and

c_{DC} = Density current speed (m/s)

g' = Reduced gravity(m/s^2)

f_0 =Coriolis parameter （$f = 2\,\Omega\,\sin\varphi$),

Where the rotation rate of the Earth, $\Omega = 7.2921\times10^{-5}$rad/s, can be calculated as $2\pi/T$ radians per second, φ = latitude (Nowra is 34.93°S), and H = the cold air depth (m), at Nowra (500m)

The Rossby radius of deformation, $\mathbf{L} = \frac{\sqrt{g'\ H)}}{f} = \frac{\sqrt{0.597*500}}{8.35\times 10^{-5}}$ = 204km, where

$$f_0 = 2\,\Omega\,\sin\varphi\ =\ 2 * 7.2921\ \times\ 10^{-5} * \sin(34.93\ ) = 8.35 \times\ 10^{-5}$$

g' = $(g(\rho_{lower} - \rho_{upper}))\ /\ \rho_{lower}$= 0.597

Rossby radius of deformation L = $\frac{\sqrt{g'\ H)}}{f_0} = \frac{\sqrt{0.597*500}}{8.35\times 10^{-5}}$ = 204km

Wave number k =2π/wavelength, where wavelength is the Rossby radius of deformation. Thus:

$$\mathbf{k^2} = (\frac{2\pi}{L})^2 = (\frac{2\pi}{2.04 * 10^5})^2$$

Hence, $c_{poincaré} = c_{DC}(1 + \frac{f_0^2}{g'\ Hk^2})^{1/2} = 1.197 * c_{DC}$ = ~$1.2\ * c_{DC}$ (9)

From Equation (9), the inertia-gravity waves move ~20% faster than the density current. This difference can explain how, in Figure 14 and Figure 16, the waves move increasingly ahead of the main southerly change, because they are propagating faster than the southerly change.

Pressure (hPa)	Temperature (°C)	Absolute temperature (°K)
934	11.8	284.8
907	18.8	291.8

Table 4: Details of the low level structure of the inversion at Nowra (YSNW).

5.1.7 Discussion and Conclusions

This study was intended primarily to be a detailed analysis of the southern buster (SB) event of October 6-7, 2015. The parallel cloud lines, revealed by the high-resolution imagery, appear to be solitary waves, and are travelling ahead of the SB along the New South Wales coast. This study has a major advantage over earlier SB studies, due to the access to the much higher temporal and spatial resolution of the Himawari-8 satellite imagery, and other data. The study supported the concept of a SB as a coastal trapped density current, from both the observations, and from the accuracy of the results obtained from the simple density current model. A simple density current model was used to estimate the propagation speed of the SB density current. The estimate of 17m/s for the density current speed was close to the observed wind speed of about 15m/s at Nowra airport. The calculated phase speed of the solitary waves, when assumed to be inertia-gravity (Poincaré) waves was about 20% greater than the speed of the density current. Again, this difference was consistent with the satellite imagery, which showed the solitary waves increasingly moving away from the leading edge of the SB. Observations at YSNW and YSSY both exhibit the common characteristics of a classical SB, with an abrupt change in winds, temperatures and pressure. The corresponding synoptic weather charts illustrate that, during the SB event a high pressure ridge, also referred to as a coastally trapped disturbance, and generated the SB along the south eastern Australian coast. Meanwhile, the main high-pressure cell had moved only a few hundred kilometres to the east.

Some interesting questions were raised during the study and will be addressed in future work. Questions raised include the following, and some speculation is made concerning possible

answers to these questions. Moreover, answers will be sought from a planned series of very high-resolution numerical modelling simulations of the October 6-7, 2015 SB event.

One key question is to determine why was the SB stronger and longer lasting at Sydney airport than at Nowra airport? Possible hypotheses include the influence of the differences in orography, differential continental heating and differential friction between land and sea. Each of these possible explanations was suggested by (Garratt, 1986), but supporting observational and modelling evidence was not available at that time. Also, there is related speculation on the effects of coastal irregularities, changes in coastal alignment, and land-sea temperature gradients (Holland and Leslie, 1986); some of these influences possibly affect the speed and duration of the SB. One factor is the greater distance of Nowra airport from the coast, about 20km; whereas the runways of Sydney Airport are adjacent to the water. The Nowra airport location will experience larger frictional effects from the land, which could decouple the motion towards to the north and reduce the propagation speed. Another factor is the possible effects of station elevation: the elevation of Nowra Airport is 109m, while Sydney Airport is only about 6m. As stated above, the southerly change is shallow cold air travelling along the coast under the warmer air. From Section 3, the speed of the SB depends on the depth of the cold air according to the formula $c = (g'H)^{1/2}$, where g' is the reduced gravity, and H is the depth of the SB. So, as the cold air depth at Nowra Airport is less than at Sydney Airport, the wind speeds in Nowra Airport can be expected to be weaker than at Sydney Airport. An additional possibility is due to the impact of the Illawarra escarpment, west of the Illawarra coastal plain, south of Sydney, with escarpment heights ranging from 300 to 803 meters. When the southerly winds travel from Nowra, past Kiama and Wollongong to Sydney, they are blocked from spreading westwards, so cold air mass accumulates along the escarpment and its depth must increase. When they move away from the escarpment, the deeper cold air trapped against the escarpment is released, thereby progressively increasing its propagation speed towards the

Sydney Basin, producing stronger southerly winds. A very recent example of the influence on a SB of the Illawarra escarpment and of the station height above sea level, is that of 31 January 2019, as shown in Table 5.

AWS station	Max. wind gust (km h^{-1}) & direction	Time (Local)	Station height above sea level (m)
YSSY	S 91 (25.3 ms^{-1})	18:17	6
Kurnell	S 87 (24.2 ms^{-1})	17:07	4
Wattamolla	SSE 107 (29.7 ms^{-1})	16:16	44
Bellambi	SSW 85 (23.6 ms^{-1})	16:20	10
YSNW	S 81 (22.5 ms^{-1})	14:30	109

Table 5: Southerly Buster of 31 January 2019.
Illustrating differences in maximum gust speed and times at locations Bellambi and Wattamolla adjacent to the Illawarra escarpment and YSNW in the south to Kurnell/YSSY in the Sydney basin to the north.

Table 5 indicates how the maximum wind gusts increase from 22.5 m/s at Nowra airport to 23.6 m/s Bellambi and 29.7 m/s at Wattamolla, then decrease to 24.2 m/s at Kurnell and 25.3 m/s at Sydney airport, after entering wider Sydney basin. Note also the differences in height above sea level of Nowra airport and Wattamolla compared to the other stations. Other interesting questions include why the maximum gust at Sydney airport was about 50 minutes after the maximum gust at Kurnell, when the distance between those two locations is only about 10 km; and was the height difference above sea level between Bellambi and Wattamolla the reason the maximum gust occurred at Wattamolla before Bellambi. As mentioned above, a series of planned high resolution numerical modelling studies hopefully will provide further insight into the questions raised.

Finally, it is noteworthy that the solitary waves extend east as far as 157^0 E on the Himawari-8 satellite visible image (Figure 16), which raises the question of how far east they can travel, and has possible safety implications for landing/take-off at Lord Howe Island airport. Again,

this question can best be answered with a combination of observations and high-resolution numerical modelling.

5.2 A SHORT-LIVED GUSTY WIND EVENT ASSOCIATED WITH A SQUALLLINE

5.2.1 Introduction

A squall line is a line of thunderstorms forming along or ahead of a cold front. Bluestein and Jain (1985) and Klimowski et al. (2003) squall lines were determined based on the following criteria:

• Length of 50 km or greater

• Length to width ratio of at least 5: 1

• Persist for 30 min or more

• Squall line initiation based on first occurrence of necessary length and length to width ratio

• Squall line termination occurred when any criteria failed

It contains heavy precipitation, hail, frequent lightning, strong straight-line winds, and possibly tornadoes and waterspouts. The short lived gusty winds are usually associated with the thunderstorm downdrafts or outflows of a squall line. Density current propagation and downward transfer of horizontal momentum are related to the thunderstorm downdrafts. The strong gusty winds, causing turbulence and windshear is a potential hazard to any aircraft operating at any level, especially in the landing or taking off phase of flight.

According to ICAO Annex3, when a squall line is forecast, observed or encountered:

- Special aircraft observations shall be made by all.
- Severe squall lines should be included in SIGWX forecasts High-level and medium-level significant weather (SIGWX) forecast charts.
- SPECI should be issued when the onset or cessation of a squall line.

- In local routine and special reports and in METAR and SPECI, the following types of present weather phenomena should be reported.
- The criteria used for the inclusion of change groups in TAF or for the amendment of Terminal aerodrome forecast (TAF) should be based on when the onset or cessation of a squall line is forecast to begin or end.
- The trend forecast (TTF) shall indicate the expected onset or cessation of a squall line.
- SIGMET or AIRMET should be issued when the onset or cessation of a squall line is forecast or observe to begin or end which should indicate a thunderstorm along a line with little or no space between individual clouds.
- Aerodrome warnings should relate to the occurrence or expected occurrence of a squall line.

The extreme wind gusts are difficult to forecast and there is a dearth of operational methods that reliably forecast the magnitude of thunderstorm wind speeds. In this chapter, a short-lived gusty wind event associated with a long-lived squall line on the northwest of New South Wales (NSW) on 13th December 2018 is presented. The conditions that led to the damaging winds are analysed by taking advantage of the recently available high-resolution temporal and spatial Himawari-8 satellite, upper air sounding, six station surface observational data, GDAS meteorological data and model outputs.

Figure 18: Map of North-western of NSW, Australia.

Showing six locations mentioned in the chapter, ICAO locations for airports: YBKE (Bourke), YWLG (Walgett), YCNM (Coonamble), YNBR (Narrabri), YMOR (Moree), YGDH (Gunnedah). (From google map)

5.2.2 Synoptic Overview

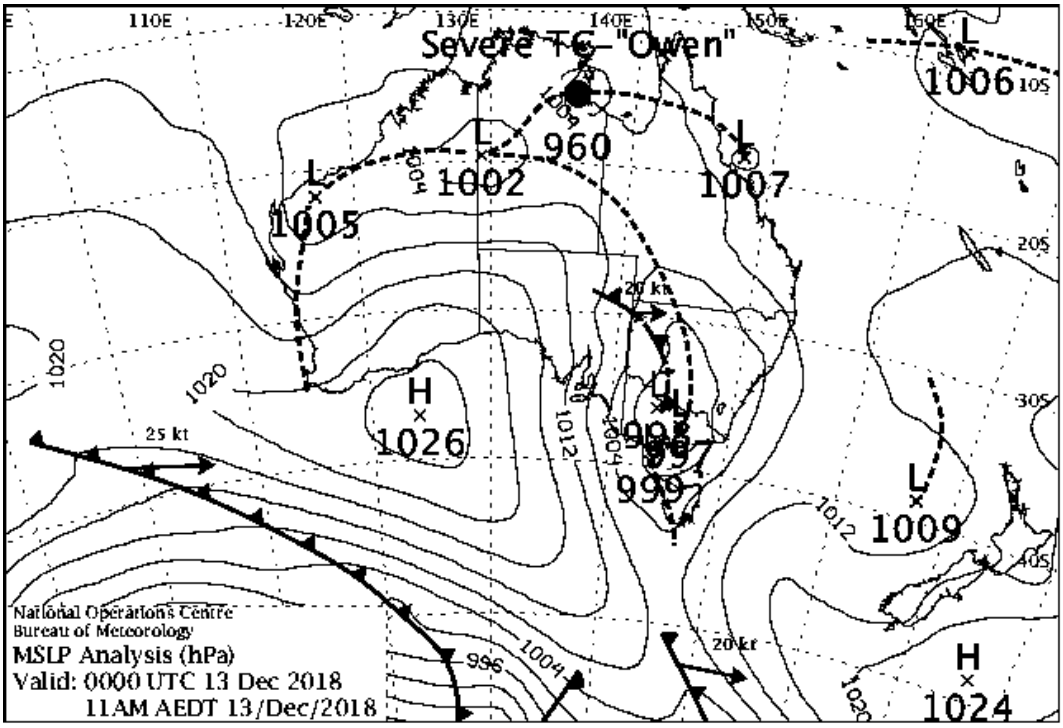

Figure 19: Synoptic weather charts for Australia at 0000 UTC (1000 AEDT) on December 13, 2018.

Shown are contours of Mean Sea Level Pressure (MSLP) in intervals of 4hPa, local maxima and minima of MSLP, manually analysed cold fronts (solid lines with triangular barbs), and low pressure troughs (dashed lines). (From http://www.bom.gov.au/australia/charts/).

At 0000 UTC (1000 AEDT) on December 13, 2018, A low pressure centre was near the state boundary between the southwest of NSW and the northwest of Victoria. A cold front extended from the low centre through the northwest of NSW to the east of South Australia and a pre-frontal trough extended to further northwest, as shown in Figure 19. A squall line thunderstorm associated with the pre-frontal trough moved towards to the east, from 0000 UTC (1000 AEDT) to 0900 UTC (1900 AEDT), the gusty winds excessed 41 knots (21 m/s) were more than 20 stations, which met the criterion for issuing airport warnings of expected gales (see annex 3).

5.2.3 Six Airports Observations

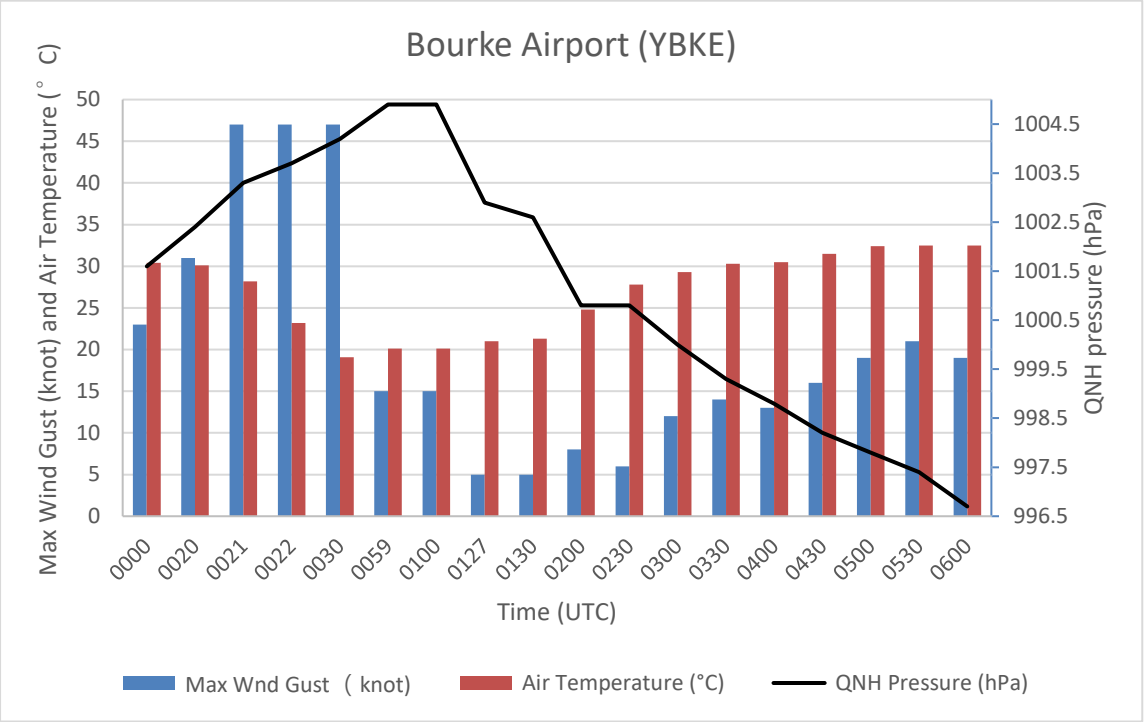

Figure 20: Observations of Bourke Airport (YBKE) from 0000UTC to 0600UTC on December 13, 2018.

Time is in UTC for horizontal axis, wind gust and temperature for primary vertical axis (left), QNH pressure for secondary vertical axis (right). Max wind gusts (blue clustered columns), air temperatures (red clustered columns). QNH pressure (black lines), the colours of data labels are consistent with the legends.

From Figure 20, at 0000UTC at Bourke airport, the maximum gust was 23 knot, from 0021UTC to 0030UTC, the maximum gusts were 47knots, which was in excess of the aerodrome warning criteria (Above 41 knots see annex 3), Simultaneously, the QNH was increasing significantly (more than 3hPa) and the temperatures were dramatically decreasing (more than 10 °C) which both met the criteria for amending a TAF. From Figure 19, the low pressure trough was approaching to Bourke, the QNH should have decreased according the synoptic chart, however, due to the thunderstorm squall line, and the small scale downdrafts density currents hit the ground and spread horizontally, inducing the short lived gusts. Similar

mechanism for the other 5 stations from Figure 20 to Figure 24 for Walgett, Coonamble, Narrabri, Moree and Gunnedah respectively.

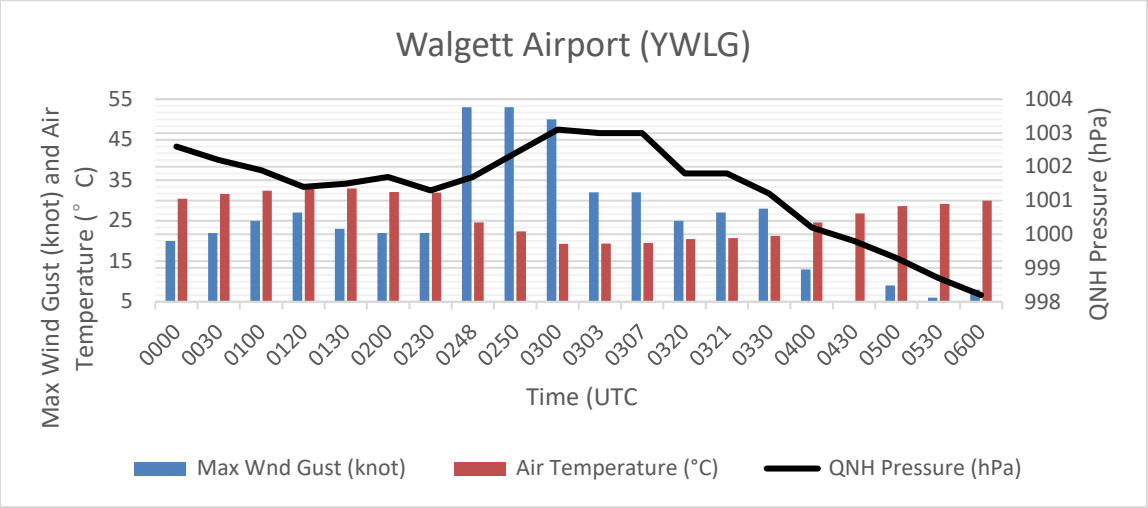

Figure 21: Observations of Walgett Airport (YWLG) from 0000UTC to 0600UTC on December 13, 2018.

As in Figure 20, except at Walgett Airport (YWLG).

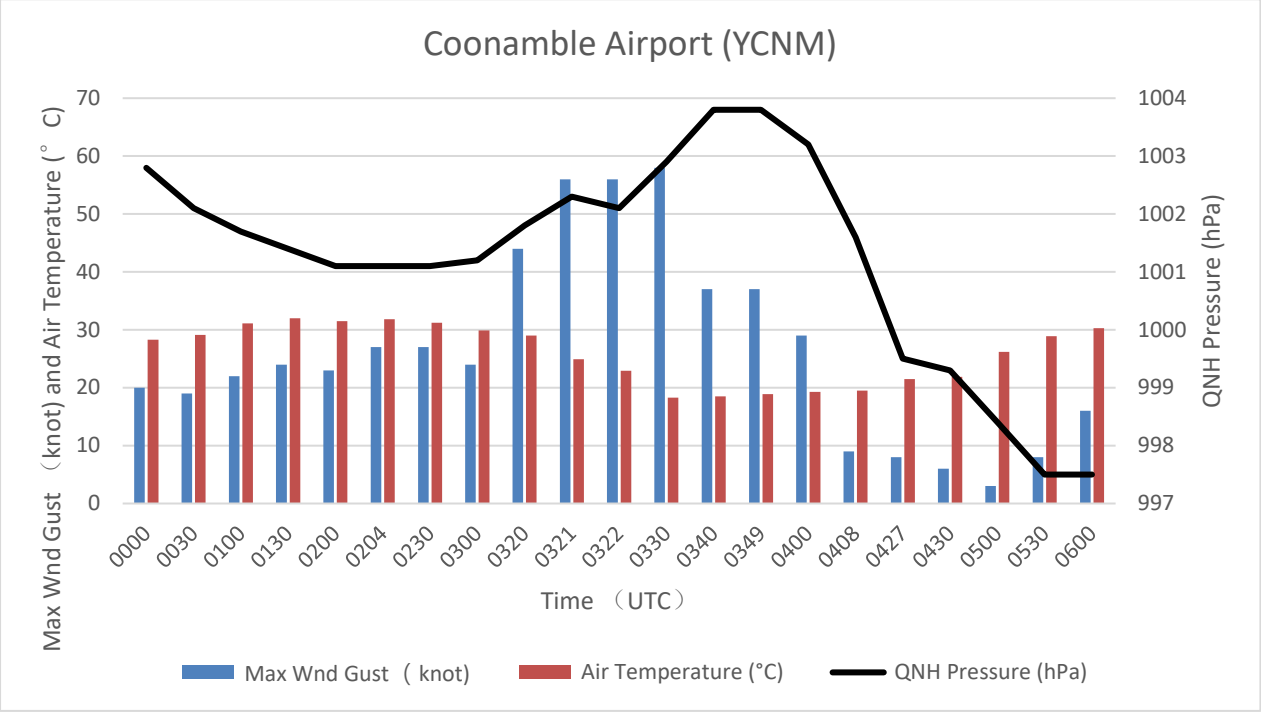

Figure 22: Observations of Coonamble Airport (YCNM) from 0000UTC to 0600UTC on December 13, 2018.

As in Figure 20, except at Coonamble Airport (YCNM).

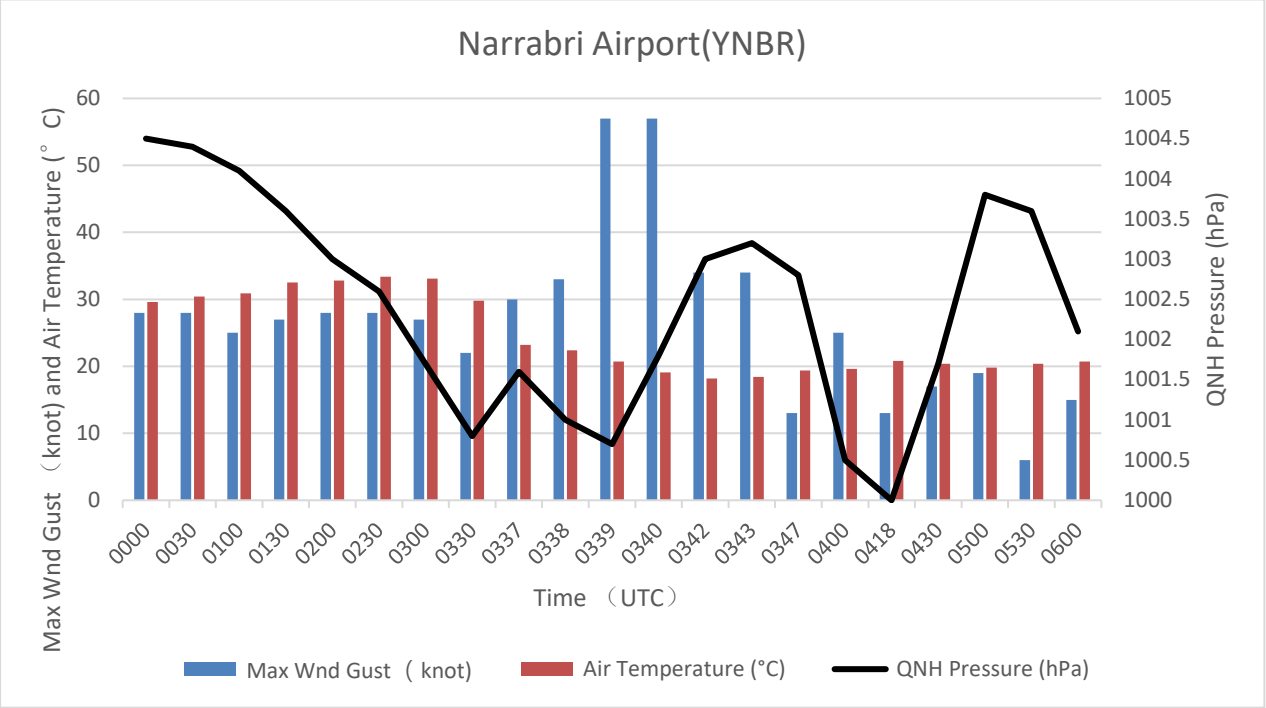

Figure 23: Observations of Narrabri Airport (YNBR) from 0000UTC to 0600UTC on December 13, 2018.

As in Figure 20, except at Narrabri Airport (YNBR).

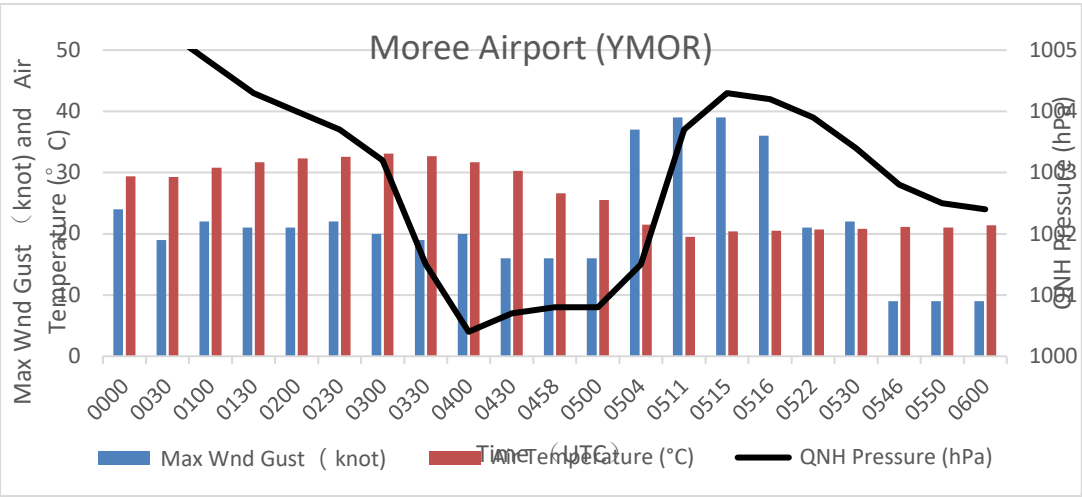

Figure 24: Observations of Moree Airport (YMOR) from 0000UTC to 0600UTC on December 13, 2018.

As in Figure 20, except at Moree Airport (YMOR).

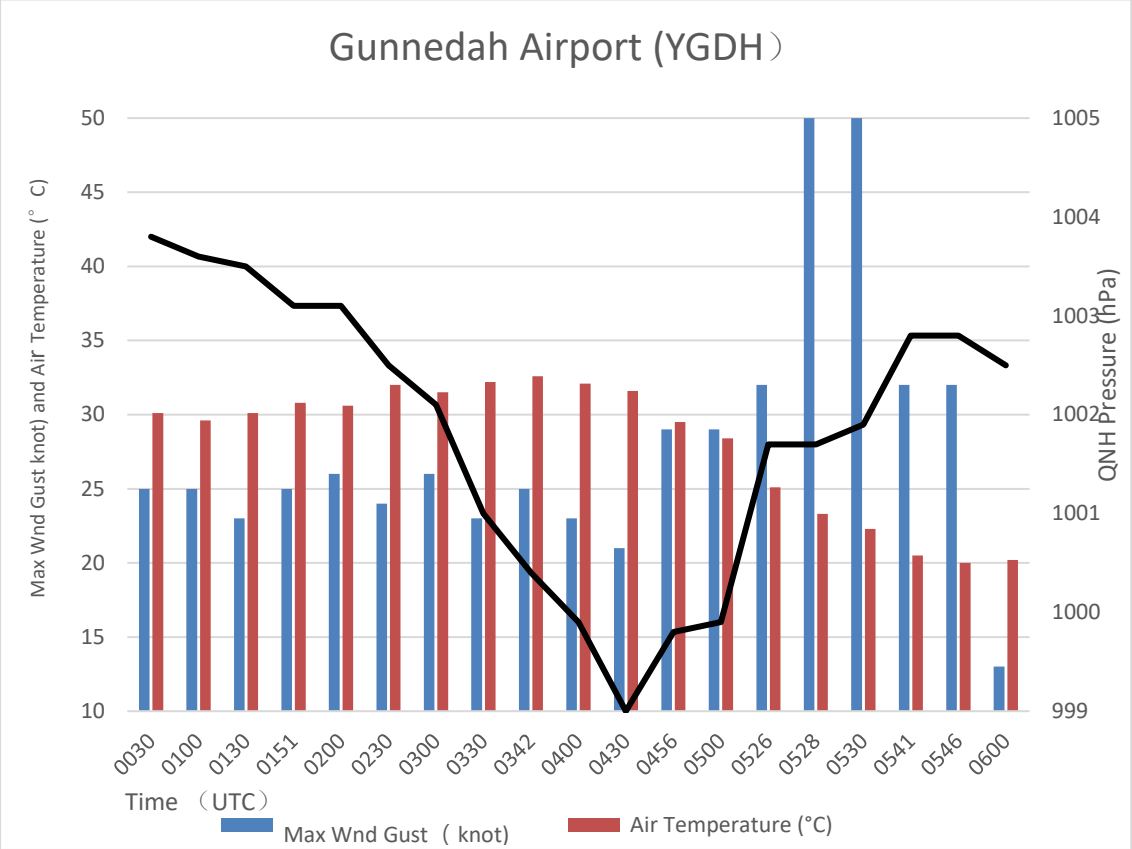

Figure 25: Observations of Gunnedah Airport (YGDH) from 0000UTC to 0600UTC on December 13, 2018.

As in Figure 20, except at Gunnedah Airport (YGDH).

Downbursts are caused by convective storms and are physically related to precipitation processes within these storms. The simplest case of isolated microburst is driven by the weight of precipitation causing a downdraft and evaporation and melting cooling of the descending air, which further accelerates the downdraft. As the descending heavier cooler current impinges on the ground, an outburst of diverging winds is produced. Squall lines can cause larger-scale downbursts , however, the most intense winds associated with these larger downburst-producing storms appear to be associated with small-scale low-level rotation centres (mesocyclones or mesoanticyclones) (Hjelmfelt, 2007). According to Professor T. Fujita's

definition: Dow*nburst*—an area of strong winds produced by a downdraft over an area from < 1 to 10 km in horizontal dimension.

Macroburst—A downburst that occurs over an area > 4 km in dimension and is typically 5–30 min in duration.

Microburst—A downburst that covers an area < 4 km in dimension and lasts 2–5 min. Differential velocity across the divergence centre is > 10 m/s (Hjelmfelt, 2007). In this case, It is noticed that the maximum gusts at the six stations were occurred in the order of west to east as the synoptic trough and the cold front headed towards the east. The gusts were well above the aerodrome warning criteria, however, they all last only short period, the maximum period was 12 minutes at Walgett and Moree, then Coonamble for 10 minutes, Bourke for 9 minutes, Gunnedah only for 3 minutes and Narrabri only for two minutes. The maximum gusts at each station ranged from 39 knot to 58 knots. It can be seen the synoptic situation provided a large mesoscale development environment, the squall line caused a large-scale downburst including macroburts and microburst.

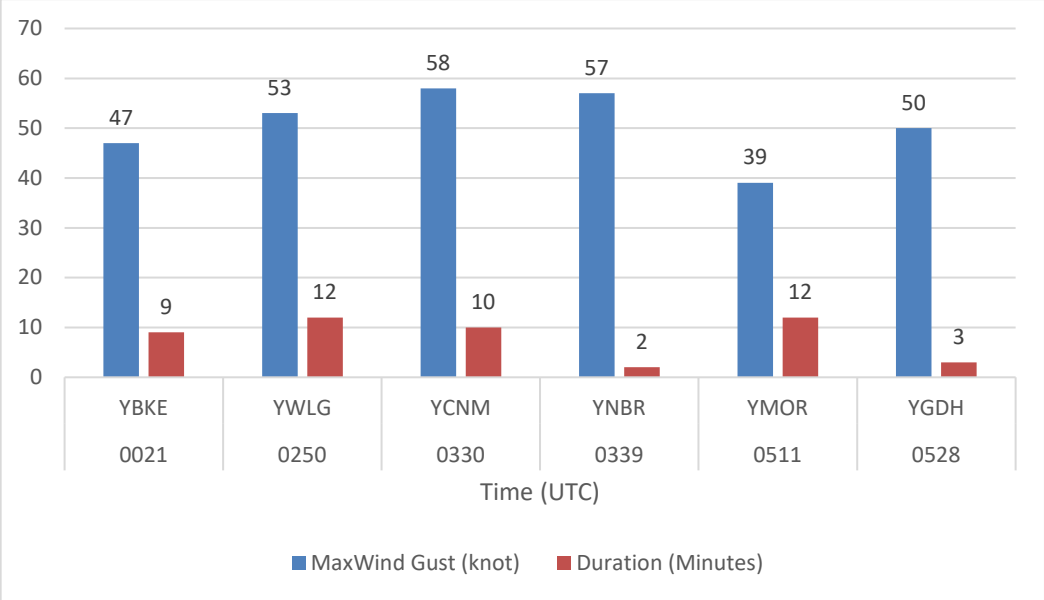

Figure 26: Weather observations of wind gusts from 0000UTC to 0600UTC on December 13, at six airports.

Time and airports for horizontal axis, Max wind gusts in knots and wind gust last time in minutes for vertical axis. Max wind gusts (blue clustered columns in knot), Wind gust last time (orange clustered columns in minute). ICAO locations for airports: YBKE (Bourke), YWLG (Walgett), YCNM (Coonamble), YNBR (Narrabri), YMOR (Moree), YGDH (Gunnedah)

5.2.4 Satellite Imagery

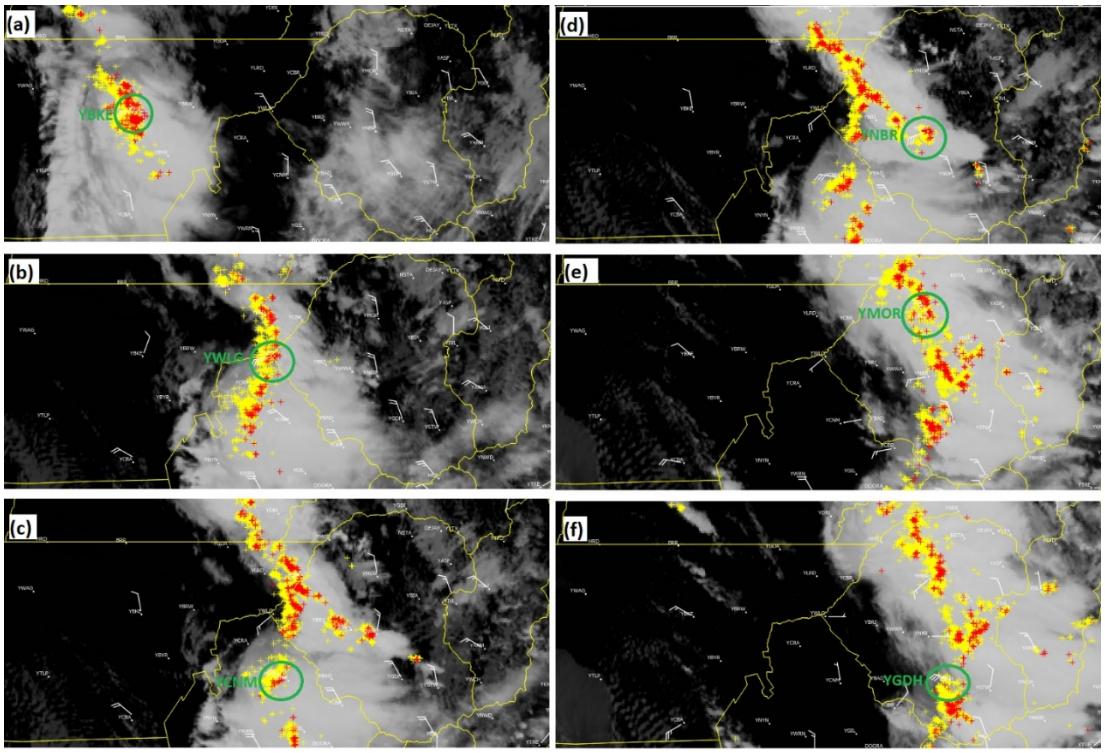

Figure 27 Himawari-8 Satellite Visible Images on December 13, 2018 over NSW. Overlain by the Australian GPATS (Global Position and Tracking Systems) network lightning strike data, red (within 30 seconds), yellow (0.5 to 10 minutes). AWS wind barbs show wind direction and speed in knots (white wind bards), and the boundary of the NSW districts (yellow line). The green circles show the locations of the six airports when the maximum gusty winds appeared and the ICAO names in green in the left. (a) 0021 UTC at YBKE (Bourke), (b) 0248 UTC at YWLG(Walgett), (c) 0326 UTC at YCNM (Coonamble), (d) 0339 UTC at YNBR (Narrabri), (e) 0505 UTC YMOR (Moree), (f) 0528 UTC at YGDH (Gunnedah).Images shown with the permission of the Australian Bureau of Meteorology.

Himawari-8 Satellite Visible Images are available every 8 minutes, Figure 27 displays the satellite images of the six stations when the maximum gusts occurred or the nearest time. From the GPAT over the last 10 minutes, it is clear that a squall line propagated from the west to the east in a cloud band which represented a trough from the low-pressure system that was the

same location as the synoptic chart shown. The time when the maximum gusts were observed were consistent with the time when the GPATS were detected.

5.2.5 Radiosonde Data

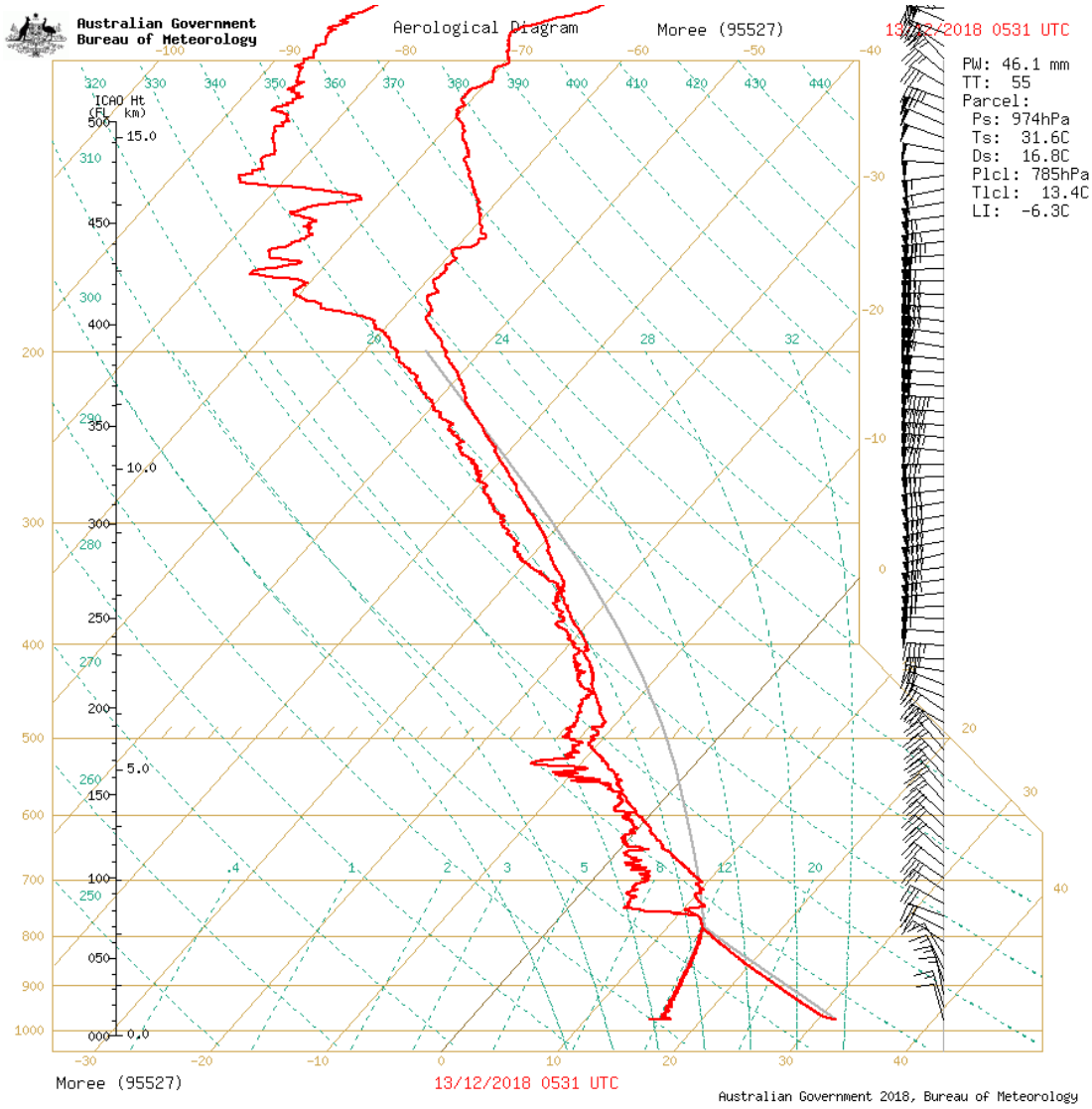

Figure 28: Radiosonde profile at 0531UTC on December 13, 2018 at Moree Airport (YMOR). Shown with the permission of the Australian Bureau of Meteorology. The light brown vertical axis in the left is the pressure (hPa), the left black vertical axis is height above the sea surface level in hundreds of feet. So, e.g., 050 means 5000ft (about 1600m) above the sea surface level; the right black vertical axis is height above the sea surface level in km. The right vertical axis

is the wind profiler information. The red solid line on the right is the temperature profiler, and the dew point profiler is on the left.

The observation of the atmosphere soundings was 0531 UTC (Figure 28); this time was close to the maximum gusty winds' appearance, showing that the potential for a strong downdraft which occurred at YMOR. A notable deep dry adiabatic layer exists below the cloud base ("inverted V" trace) from surface to around 780hPa, a typical feature of storms that produce damaging wind gusts. Another apparent feature was a dry slot in the middle level above the Lifting Condensation Level (LCL) between 750hPa and 620hPa. The dryness of the atmosphere is a key measure incorporated into the indices for predicting downdraft potential (Grundstein et al., 2017; Pryor, 2015). The precipitable water content is 46.1mm and the base height of the thunderstorms is about 2km (Plcl = 785hPa).

5.2.6 Trajectories for Air Parcels

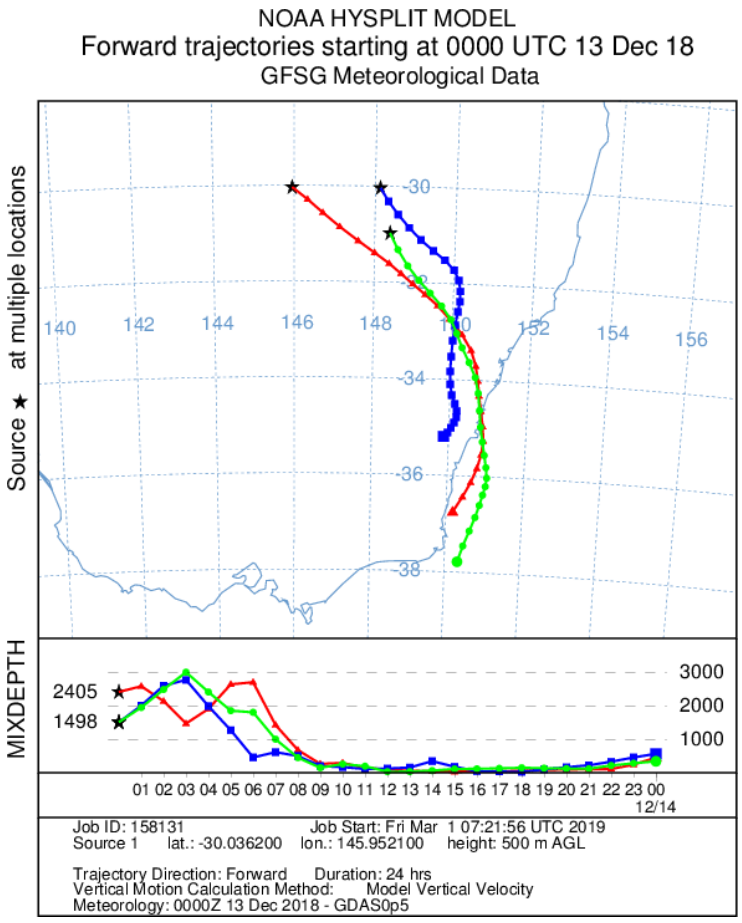

Figure 29: 24 hours forward trajectories for air parcels beginning 00 UTC 13/12/2018 and ending 00 UTC 14/12/2018.

At YBKE (Bourke, red line with triangles marked at one hour intervals), YWLG (Walgett, blue line with squares marked at one hour intervals), YCNM (Coonamble, green line with dots marked at one hour intervals). Shown are horizontal trajectories (upper panel) and vertical trajectories of mix depth (lower panel). Trajectories calculated using NOAA HYSPLIT model using GDAS meteorological data, with vertical motion from model vertical velocity and initial source elevation of 500 m above ground level.

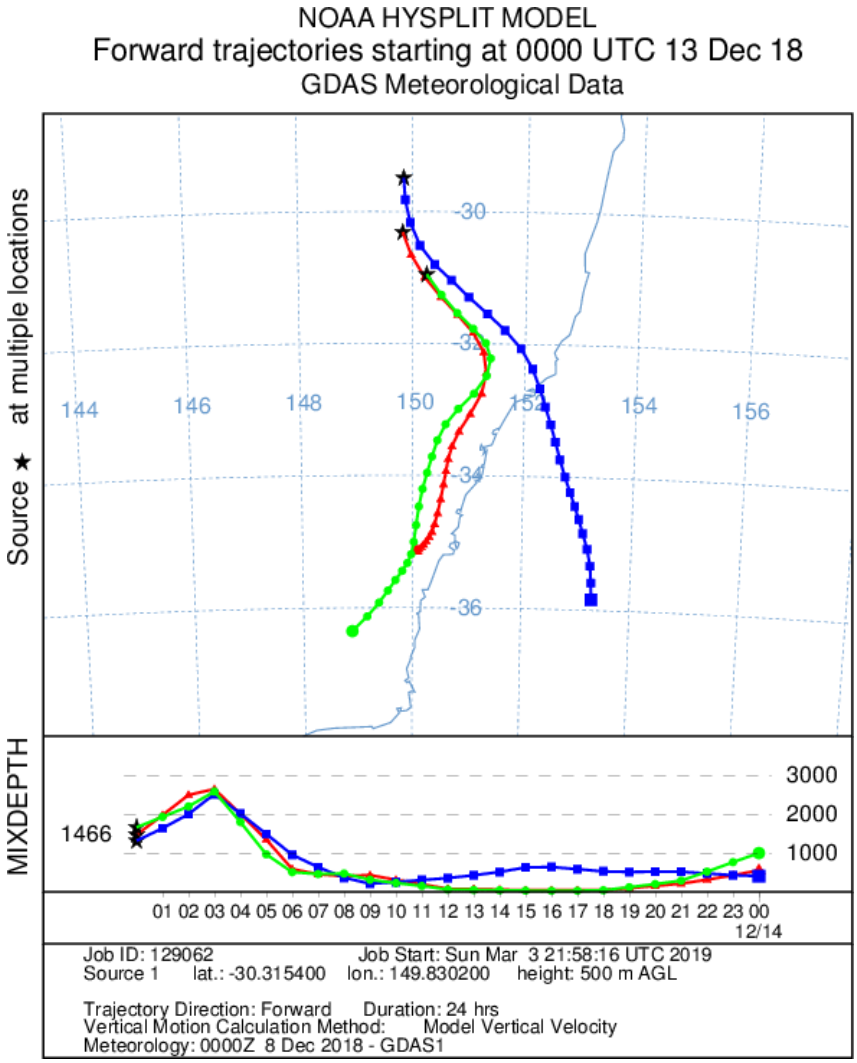

Figure 30: 24 hours forward trajectories for air parcels beginning 00 UTC 13/12/2018 and ending 00 UTC 14/12/2018.

At YNBR (Narrabri, red line with triangles marked at one-hour intervals), YMOR(Moree, blue line with squares marked at one hour intervals), YGDH(Gunnedah, green line with dots marked at one hour intervals). Shown are horizontal trajectories (upper panel) and vertical trajectories of mix depth (lower panel). Trajectories calculated using NOAA HYSPLIT model using GDAS

meteorological data, with vertical motion from model vertical velocity and initial source elevation of 500 m above ground level.

A grid of forward trajectory from air parcels was calculated using the HYSPLIT dispersion model and NCEP Global Data Assimilation System (GDAS). It includes the six locations of the squall line from 0000UTC to 2400UTC on December 13. The six trajectories of the parcels 500 m above ground level (AGL) were moving slowly towards the southeast, consistent with the 24-hour movement of the pre-frontal trough.

In strongly unstable conditions driven by surface heating, the outer region of the boundary layer is dominated by convective motions and is often referred to as the mixed layer. The top of the boundary layer in convective conditions is often well defined by the existence of a stable layer (capping inversion) into which turbulent motions from beneath are generally unable to penetrate very far, though they may continually erode it, particularly where latent heat is released in rising elements of air. Meanwhile the capping inversion can be broken when a change is in upper level conditions, such as a passing trough. The height of this elevated stable layer is quite variable but is generally below 2 to 3 km (Garratt, 1994). There are three ways of breaking the inversion: increasing the temperature, increasing the dewpoints and lifting the condensation level. Typically capping inversion can be broken from lower levels, but also can be broken by changes in upper levels. From the vertical trajectories of mix depth (lower panel) in Figure 29 and Figure 30, the depth of the six locations were from 1466 meters (YMOR) to 2405 meters (YBKE) at 0000UTC on December 13, during the daytime, the mix depth increased up to 3km, occurred around 0300 UTC at YCNM. The period was consistent with the gusty winds' appearance from 0320 to 0330 UTC (Figure 26). The other locations showed the similar phenomena, the time of the maximum wind gusts were consistent with the maximum mix depth. In stable conditions, in contrast to the above, the boundary layer is not so readily identified, turbulence is much weaker than in the unstable case, and consequently

the depth no more than a few hundred metres at most (Garratt, 1994). After 0600 UTC, the mix depth stared to decrease, by 0800 UTC, the mix depth of all the six locations decreased to below 1000 meters.

5.2.7 Discussion and Conclusions

This chapter presents a detailed analysis of a short-lived gusty wind event associated with a long-lived squall line on the northwest of New South Wales (NSW) on 13th December 2019. The damaging winds were generated by density current propagation and downward transfer of horizontal momentum from the thunderstorm downdrafts of a squall line.

The low pressure system and the prefrontal trough provided a synoptic environment for a squall line development.

The observation of the six stations over the northwest region of NSW showed that the winds caused by a squall line are extremely strong and the duration are from 2 minutes to 12 minutes.

The satellite images disclosed the damaging winds were associated with the GPATS over last 10 minutes, further confirmed the damaging winds were caused by the thunderstorms.

The sounding data from Moree airport showed a deep dry adiabatic layer below the cloud base, a deep layer moisture, a dry slot in the middle level, strong westerly steering winds and large value of CAPE which are all the favourite conditions for causing damaging winds. The trajectories for air parcels were consistent with the maximum mix depth.

The convective parameters and indices showed some of the parameters and indices met the threshold of the operational guidance for thunderstorm damaging winds, but some of them did not. However, some cases where the indices were below the threshold still resulting in severe convection. In such cases, the operational forecasters must use additional data to decide to predict severe convection.

5.3 EASTERLY DENSITY CURRENT EVENTS OVER NSW AND ACT

5.3.1 Introduction

Canberra Airport (ICAO ID: YSCB) is a major airport in the ACT. It's location is Latitude: 35.28389°S and Longitude: 149.16389°E, the elevation is 1888ft (575m), the highest alternate minima (HAM) for weather condition is: 2334ft for cloud base and 7000m for visibility. There are two runways, the long one is north to south orientation (17/35) and the short one is west to east orientation (12/30) (Figure 30). The wind speeds and directions are important for the airport operations. Meanwhile, the HAM is another key point for the airport operations.

Figure 31: Canberra Airport Runways (From Google Map)

Canberra is located west of the GDR. The winds present in a diurnal variation under a certain large-scale background with the interaction with the topography. Cool gusty easterly wind changes often arrive Canberra late on summer afternoon and evening, but occasionally can occur mid to late afternoon. The change is an important feature both locally and in the region to the east because, generally, they bring significant cooling and an increase in moisture. There is a marked change to easterly winds and a sudden drop in temperature, with an onset time generally in the late afternoon or early evening. Each change is abrupt and sharp with wind direction, temperature change and pressure increase, clearly this easterly wind change (and associated weather phenomena) is also "frontal" in character (Taylor et al., 2005). The easterly change is a density current. It occurs sometimes because of the sea-breeze penetrating inland, but sometimes a southerly change will move up the coast and penetrate inland as an E/SE change. The front moving over the ranges usually brings gusty southeast to easterly winds. Frontal passages in summer will generally bring a cooler wind change from the southeast 24 hours after the passage of the front (Temperatures will plummet to 18-22C with the change i.e. SST). During summer months, an easterly wind can often penetrate during the afternoon and evening, reaching Canberra and producing low clouds.

For the aviation industry, the timing of an easterly and easterly wind change is important for airport operations because of the runway orientations, the wind shift will cause low level turbulence and wind shear, which are hazardous for the aircraft taking off and landing. Additionally, low stratus cloud will often develop associated with the arrival of the easterly change. One possibility is that initially the low clouds form on the eastern slopes (the east of GDR) in the late afternoon, then advect inland over the tablelands (on and the west of GDR) to reach YSCB in the evening with the easterly. The other possibility is that stratus may form quickly after the easterly arrives when temperature and dewpoint are close enough to allow stratus to form. Climatologically, east is the most common direction from which stratus

advects, as there are no mountains high enough to block low cloud coming in from that direction. The low stratus often falls below the airport's alternate conditions (below 2334ft) and persists into the following morning. The low cloud usually remains a problem for small aircrafts. Moreover, timing of easterly change and wind speed are also used as a guidance to the local recreational activities, such as for wind surfers, gliders and boats.

In this chapter, an easterly density current event of December 18th, 2018 over south eastern inland of Australia is examined by the observation data and synoptic chart analysis. The density current theory is applied to the wind speed calculation and is verified by the observations. A seasonal analysis of 2018/2019 summertime is presented in this chapter too.

5.3.2 Data and Methodology

Canberra Airport half-hourly METAR and SPECI aviation observational data are employed in the 2018/2019 summer season for the analysis of easterly wind changes:

- The wind directions are between 070 to 150 degrees inclusive
- The average wind speeds are equal or great than 13 knots (7m/s or 25km/h) which may bring wind and low cloud to affect the operation in Canberra Airport.
- The time between late afternoon and evening from 04 UTC to 13 UTC.
- Winds meeting the above criteria but without the wind change are removed.

Half hourly METAR and SPECI aviation observation data at 7 stations are used for an easterly change case study at Canberra Airport and Young Airport over south eastern inland of Australia on December 18th, 2018. The 7 stations are Canberra (YSCB), Braidwood (BBDX), Ulladulla (UDAX), Nowra (YSNW), Moruya (YMRY), Merimbula (YMER) and Young (YYNG).

Figure 32: Map of South-eastern Australia.

Showing seven locations mentioned in the chapter, Canberra (YSCB), Braidwood (BBDX), Ulladulla (UDAX), Nowra (YSNW), Moruya (YMRY), Merimbula (YMER)and Young (YYNG), here YYNG is out of the map, the actual location should be further northwest. (Obtained from Google map)

5.3.3 Observation and Analysis

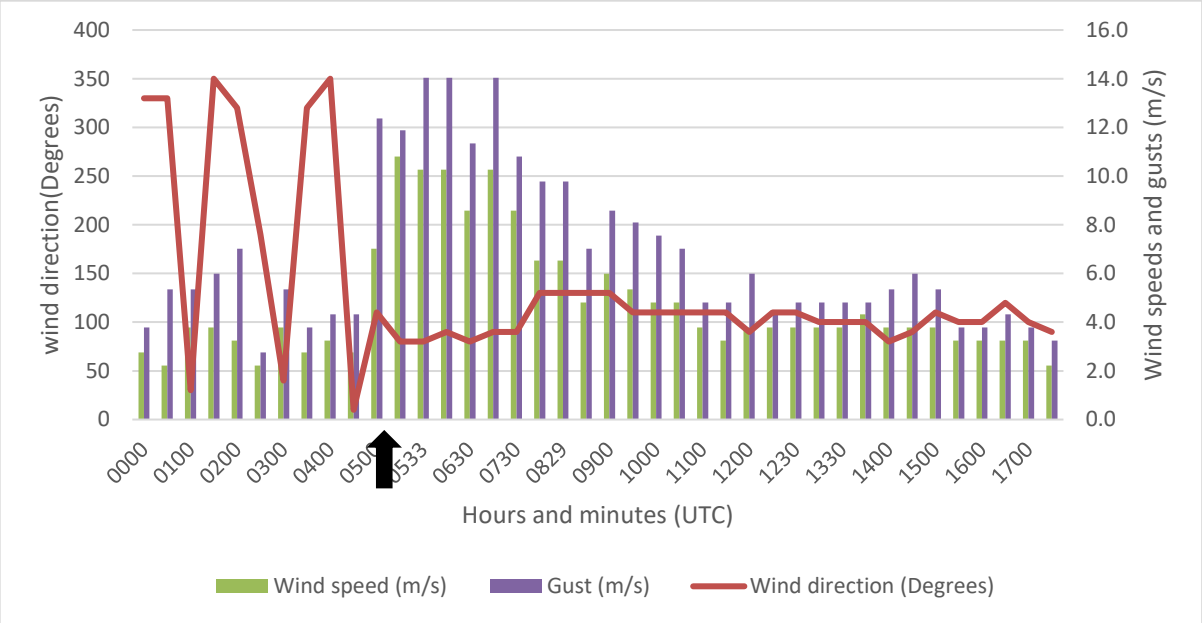

Figure 33: Observations from 0000UTC to 1800UTC on December 18th, 2018 at Canberra Airport (YSCB).

Wind speed, gust and direction change. Time in UTC for horizontal, the black arrow under the horizontal axis indicates the wind change time. Wind directions in degrees for vertical axis (left), Wind speeds and gusts in m/s for primary secondary vertical axis (right). Wind speeds (green clustered columns, m/s), Wind gusts (purple clustered columns, m/s), Wind directions (red lines, degrees).

From Figure 33 and Table 6, on December 18, 2018 at Canberra Airport (YSCB), the wind directions were light northerly winds less than 4m/s (both north-easterly and north-westerly) for most of period apart from at 0300 UTC, which were light southerly at 2.2 m/s. At 0530 UTC, the wind shifted from northerly to easterly at 110 degrees, with the average wind speed at 7m/s and gust at 12.4 m/s. From 0530 UTC to 1100 UTC, the wind directions remained easterlies, were between 80 to 130 degrees and the average wind speeds or gusts were above

7m/s. After the easterly change, the winds directions stayed easterly overnight. The average wind speeds were up to 10.8 m/s and gusts up to 14 m/s. These fresh easterly winds could induce cross winds for the Runways 17/35 and down winds for Runway 12 in excess of the threshold. The low cloud below the alternate (2334 feet) started to develop 3 hours after the easterly change. The cloud bases were initially around 2000ft and further dropped to 1500ft later that night. The low cloud persisted overnight and into the next afternoon (not shown after 1800 UTC). Temperatures were 24°C at 0000 UTC, kept increasing during the day, reaching 29.9°C before the change and dropped to around 19°C after the change.

Hours and Minutes (UTC)	Wind direction (Degrees)	Wind speed (m/s)	Gust (m/s)	Temperature (C)	Cloud below the Alternate (feet)
0000	20	2.8	4.3	24	
0030	330	2.8	3.8	24.8	
0100	330	2.2	5.3	25.6	
0130	30	3.8	5.3	25.9	
0200	350	3.8	6.0	26.9	
0230	320	3.2	7.0	27.4	
0300	190	2.2	2.8	27.8	
0330	40	3.8	5.3	28.8	
0400	320	2.8	3.8	29	
0430	350	3.2	4.3	29.5	
0500	10	2.8	4.3	29.9	
0530	110	7.0	12.4	29.2	
0533	80	10.8	11.9	27.9	
0600	80	10.3	14.0	27.1	
0630	90	10.3	14.0	24.6	
0700	80	8.6	11.3	23.2	
0730	90	10.3	14.0	21.9	
0800	90	8.6	10.8	20.7	
0829	130	6.5	9.8	20.1	
0830	130	6.5	9.8	20.1	2000
0900	130	4.8	7.0	19.6	2000
0930	130	6.0	8.6	19.4	2000
1000	110	5.3	8.1	19.3	2000
1030	110	4.8	7.6	19.2	2000
1100	110	4.8	7.0	19.1	2000
1130	110	3.8	4.8	19.1	2000
1200	110	3.2	4.8	19.1	2000

1211	90	3.8	6.0	19	2000
1230	110	3.8	4.3	18.9	
1300	110	3.8	4.8	18.8	
1330	100	3.8	4.8	18.5	2100
1333	100	3.8	4.8	18.5	2100
1400	100	4.3	4.8	18.5	2100
1430	80	3.8	5.3	18.3	1900
1500	90	3.8	6.0	18.2	1900
1530	110	3.8	5.3	18	1700
1600	100	3.2	3.8	17.8	1500
1630	100	3.2	3.8	17.9	1500
1700	120	3.2	4.3	17.8	1500
1730	100	3.2	3.8	17.9	1500
1800	90	2.2	3.2	17.8	1500

Table 6: Observations of Easterly Change at Canberra Airport on December 18, 2018

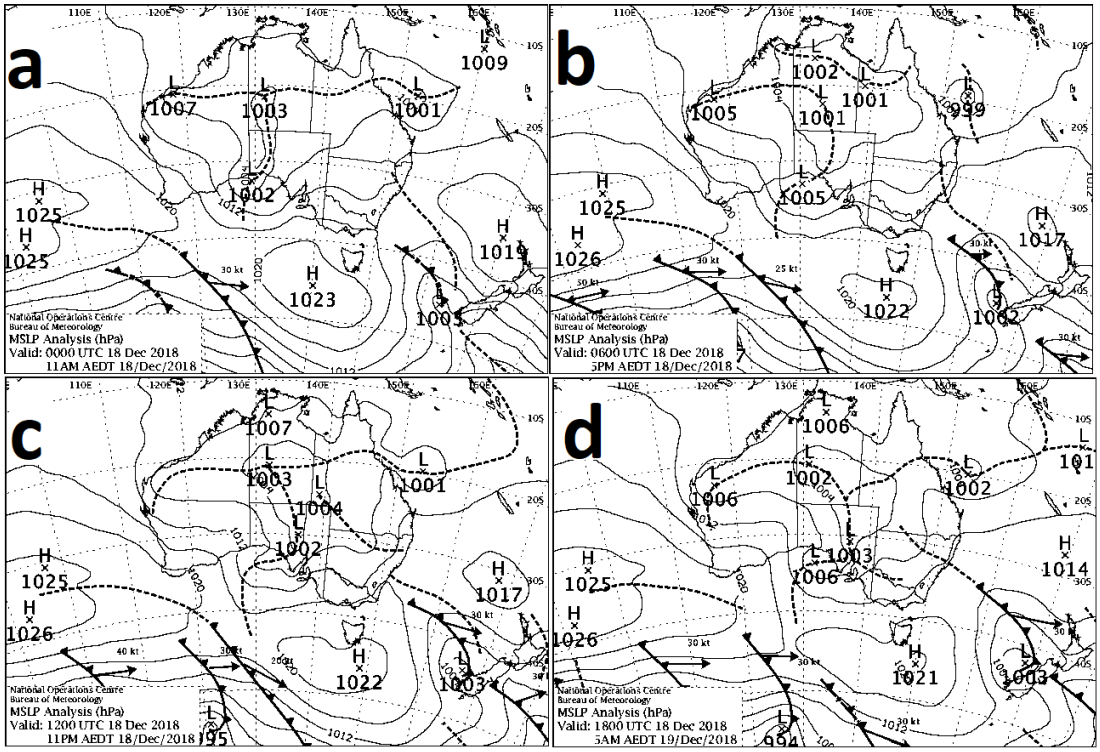

Figure 34: Synoptic weather charts from 0000UTC to 1800UTC December 18, 2018 at Canberra Airport.

a) 0000 UTC December 18, 2018, b) 0600 UTC December 18, 2018, c) 1200 UTC December 18, 2018, d) 1800 UTC December 18, 2018. Shown are contours of Mean Sea Level Pressure

(MSLP) in intervals of 4hPa, local maxima and minima of MSLP, manually analysed cold fronts (solid lines with triangular barbs), and low-pressure troughs (dashed lines). (Obtained from http://www.bom.gov.au/australia/charts/).

The MSLP charts from 0000UTC to 1800UTC December 18, 2018 are shown in Figure 34. In the east, a surface high pressure system was over the Southern Ocean south of Tasmania, extending a weak ridge over south eastern Australia, including northeast of Victoria and southeast of NSW. A low-pressure system located in the west of New Zealand, extending a cold front ahead of the weak ridge. Further west, a low pressure near South Australia, extending an inland as a trough across the central part of Australia. Over 24 hours from 0000UTC to 1800UTC, the synoptic situation did not change too much. This pattern of synoptic situation indicated three forcing mechanisms of the easterly change (Taylor et al., 2005). The first mechanism was the synoptic scale dynamic forcing, as there was a cold front and weak coastal ridging over the south-eastern Australia. In this case, both the fronts and coastal ridging are weak, but the cooler and denser air behind the front makes it possible for the changes to propagate through the Canberra region from the east due to the density current if the temperature in Canberra was high enough. From Table 7, the six stations east of Canberra are consistently easterly winds from 0000 UTC to 0530 UTC on December 18, 2018, the easterly winds are mainly directed by pressure gradient by the weak coastal ridging. The second forcing mechanism is the synoptic thermal forcing, the inland heat; the inland low near South Australia, manifested as an inland trough across central Australia, caused a large dry and hot air-mass on the western side of the dividing ranges. From Table 8, it is noticed that the inland temperatures are up to 33.1°C at YYNG and 29.9°C at Canberra, however, the temperatures over the rest of the stations mentioned in the east are between 18 and 22 °C, which are close to SST under the easterly environment. This extended area of continental heating results in an extensive spatial-scale thermal forcing, that enhances the inland directed flow along the coast, and accelerates

the easterly flow to propagate further inland. The third forcing mechanism is mesoscale thermal forcing over the GDR plateau. In the Australian east-coast cases, the contrast in surface conditions between the moist, forested coastal escarpment and drier tableland (on and the west of GDR) results in an increase in the gradient in sensible heat flux, which should enhance the plateau effect. As the coastal plain is relatively narrow, there can be an interaction between the sea breeze and plateau effect circulation. The solar heating of elevated terrain expands the air column above and results in an increase in the height of any given pressure surface. The horizontal pressure gradient resulting from the slope in these pressure surfaces drives an initial elevated outflow from the plateau. As a result of this mass transfer, a reverse near-surface pressure gradient develops which drives a low-level flow onto the plateau. The mechanism is essentially the same as that which results in a sea-breeze circulation (Whiteman, D.C. 2000; Taylor et al., 2005). At Canberra Airport, easterly usually starts as a coastal sea breeze before moving further inland. However, in this case, the first and the second are the dominant mechanisms forcing of the easterly change at Canberra whereas, the third one, the mesoscale plateau and sea-breeze interaction takes a small effect.

Hours and minutes (UTC)	YSCB	BBDX	UDAX	YSNW	YMER	YMRY
0000	20	110	130	120	100	140
0030	330	90	140	90	120	140
0100	330	80	150	100	130	150
0130	30	110	130	110	130	90
0200	350	100	130	140	130	100
0230	320	110	120	120	130	100
0300	190	100	120	120	130	110
0330	40	110	130	110	130	120
0400	320	120	130	120	130	130
0430	350	130	130	130	130	130
0500	10	120	120	130	140	140
0530	110	120	140	110	130	140

Table 7: Observations of winds directions (in degrees) from 0000 UTC to 0530 UTC on December 18, 2018 at six stations.

The six stations are Canberra (YSCB), Braidwood (BBDX), Ulladulla (UDAX), Nowra (YSNW), Moruya (YMRY) and Merimbula (YMER))

Hours and minutes (UTC)	YSCB	YYNG	BBDX	UDAX	YSNW	YMER	YMRY
0400	29	31.9	20.4	22.6	21.7	19.9	20.4
0430	29.5	32.9	19.6	22.5	21.9	19.5	19.6
0500	29.9	33	17.9	22.6	22	19.7	19.3
0530	29.2	32.7	17.9	22.4	21.8	19.5	19.5
0600	27.1	33	17.6	21.7	22.4	19.8	19.2
0630	24.6	33	17.1	21.7	21.6	19.5	19.1
0700	23.2	32.7	16.9	21.4	21.8	19.6	19
0730	21.9	33.1	16.8	21.2	21.1	19.6	18.9
0800	20.7	31.8	16.8	21.1	20.7	19.2	18.6
0830	20.1	30.8	16.6	21.1	20.7	19.2	18.7
0900	19.6	29.6	16.5	21.1	20.6	18.9	18.2
0930	19.4	28.5	16.4	21	20.4	18.9	18.2
1000	19.3	26.1	16.5	21.1	20.3	18.9	18.1
1030	19.2	26.2	16.3	21	20.3	18.7	18

Table 8: Observations of temperatures (in °C) from 0400 UTC to 1030 UTC on December 18, 2018 at seven stations.

The seven stations are Canberra (YSCB), Braidwood (BBDX), Ulladulla (UDAX), Nowra (YSNW), Moruya (YMRY), Merimbula (YMER) and Young (YYNG).

5.3.4 Density Current Theory Application to Easterly Change

The theory of density currents is in detail in Chapter 2: to verify the density current theory, the easterly change observation data are employed to the equations (1) to (4) in Chapter 2:

In this case, the density current speeds can be estimated using the observation data from Canberra Airport. From Equation (1) and Table 9, for a cool lower layer overlain by a warm upper layer:

$$\rho_{cold} = P_1/RT_1 = 1003.8/ (287.058*293.25) = 0.012021415,$$

$\boldsymbol{\rho_{warm} = P2/RT2}$ = 1010.1/ (287.058*303.05) = 0.011644709.

Hence, $\mathbf{c} = \sqrt{\boldsymbol{g'H}}$, the density current speed

Where $\boldsymbol{g'} = \boldsymbol{g(\rho_{cold} - \rho_{warm}) / \rho_{cold}}$= 0.307095165 (10)

and, *H*, the cold air depth (m) at Canberra, is about (300m), as in Figure 32, the average elevation of the ranges east of the Canberra is 900m, while the elevation at Canberra is 575m.

So, the density current speed:

$$\mathbf{c_{DC}} = \sqrt{\boldsymbol{g'\ H}} = \sqrt{0.307095165 * \mathbf{300}} = \sim 9.6\text{m/s } (\sim 18.7\text{knots}). \quad (11)$$

The percent difference as (predicted – observed)/observed is 0.7% which indicates the predicted speed in (11) is consistent with the observational data from Canberra Airport station observations(see Table 9 and Table 14). This demonstrates the density current theory applies to easterly change at Canberra. However, it is important to note that the calculation of $\mathbf{c_{DC}}$ is highly dependent on the value of ***H,*** so care was taken in selecting the value of H from detailed orographic maps.

	18th December, 2018
Time of change (UTC)	0530
T_{cold}(K)	293.25
T_{warm}(K)	303.05
P_{cold}(hPa)	1013.8
P_{warm}(hPa)	1010.1
ρ_{cold} (kg/m^3)	0.012021415
ρ_{warm}(kg/m^3)	0.011644709
Δρ (kg/m3)	0.00037671
g'(m/s2)	0.307095165
Cdc(ρ)(knots)	18.7
Cdc(ρ)(m/s)	9.60

Observed mean winds (m/s)	9.53

Table 9: Details of the density currents for the easterly change in Canberra on December 18th, 2018.

5.3.5 2018/2019 summer season analysis of easterly wind changes

In total there were 25 easterly changes at Canberra Airport during the 2018/2019 summer season. The maximum is 9 in January, then 5 in February 4 in December and 3 in October and twice in both November and March. For the timing of change, there are 8 times between 0700 UTC to 0800 UTC and 07 times between 0800UTC and 0900 UTC, about 60% of the totally change, however, only once in before 0500 UTC and after 1000UTC. The wind speeds are between 7 to 10.8 m/s and gusts between 9.1 to 15.1 m/s at the time of change.

Month	Day	Time of change	Wind direction (Degrees)	Wind speed (m/s)	Gust (m/s)
10	21	0900	070	7.0	9.1
10	28	0749	070	8.1	11.3
10	31	0814	090	7.6	10.3
11	15	0430	080	8.1	10.8
11	19	0814	070	8.1	10.8
12	18	0530	110	7.0	12.4
12	20	0707	110	10.8	12.9
12	28	0928	070	8.1	10.3
12	29	0700	070	9.1	14.0
01	01	0900	080	7.0	9.8
01	02	0710	070	9.8	15.1
01	05	0600	090	7.6	10.8
01	09	0729	080	7.0	9.1
01	16	0616	150	7.6	9.1
01	17	0855	130	9.1	11.9
01	26	0848	080	10.3	11.3
01	29	0930	080	8.1	11.3
01	31	0812	140	7.0	16.1
02	04	0846	110	8.1	11.9
02	13	1000	070	9.1	11.3
02	19	0715	090	9.1	11.9
02	20	0843	080	8.1	13.6

02	26	0709	110	8.1	14.6
03	09	0700	070	8.6	11.3
03	14	0526	090	8.1	9.1

Table 10: All the easterly changes at Canberra Airport in 2018/2019 summer season.

5.3.6 Discussion and Conclusions

The easterly change mechanisms include mesoscale sea breezes, differential heating at both meso- and continental-scales and coastal ridging. The GDR is located east of the ACT. When an inland trough directs a hot airmass over ACT, whereas a cold airmass can be directed by a surface high pressure system either over south-eastern Australia or over the sea, from the east. The cold airmass will finally cross the GDR, leading to temperature and pressure differences. The density current theory applies to this easterly change. Of the 25 easterly changes during the 2018/2019 summer season; the timing of changes is mostly between 0800 UTC and 0900 UTC.

The wind change always plays an important role for airport operation. The easterly change at Canberra Airport often occurs in the late afternoon and evening in summertime, then propagates farther inland, reaching airports in the west of NSW, such as Young (YYNG), in the late evening. The easterly change lasts from unstable daytime to stable night. The boundary layer and a low-level nocturnal jet are not considered in this study. The speed of the easterly change propagating to the west, and how far west could reach is a possible future research topic.

5.4 ANALYSIS OF TWO STRONG SOUTHERLY BUSTERS

5.4.1 Introduction

In this study, two strong southerly buster events of November 20, 1973 and January 31, 2019 are examined along the New South Wales coast. Sydney Airport Half hourly METAR and SPECI aviation observation data and synoptic charts were obtained for both days. The

similarity and difference between the two SSBs events are analysed for the observations and synoptics in this chapter. The simplified density current model produced speeds are matching well with the observational southerly buster data for both the SSB events at Sydney airports. For January 31, 2019, it takes advantage of the recently available Himawari-8 high-resolution temporal and spatial satellite visible, inferred, and RGB night microphysical data, operational model outputs, Sydney wind profiler data, radar data and other observational data. The data analyses support the widespread view that the southerly buster is a density current, coastally trapped by the Great Dividing Ranges (Figure 34).

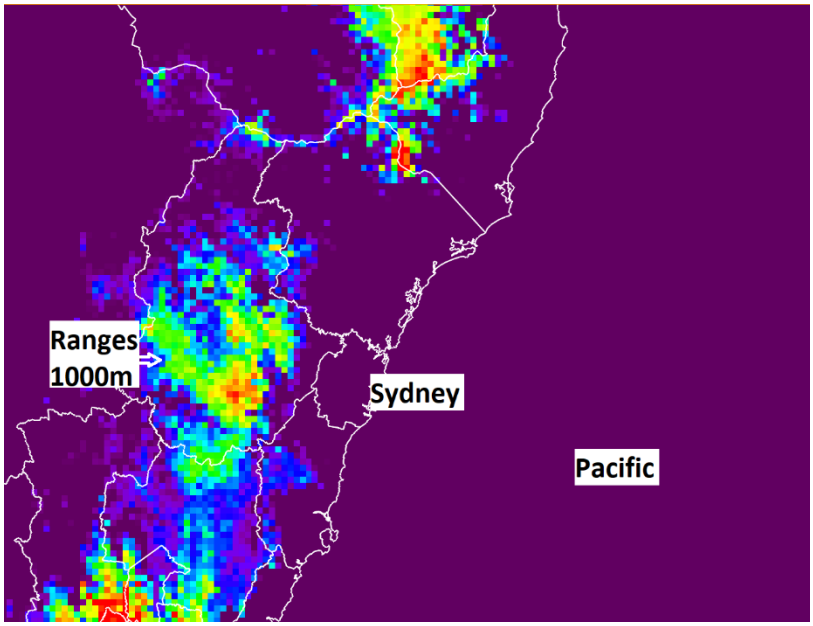

Figure 35: Topography of New South Wales Pacific Ocean coast with the Great Dividing Range west of Sydney in metres (m).

The map includes the regional district boundaries and the elevation bands are in metres. The heights west of Sydney Airport (YSSY) are ~1000m.

5.4.2 Station observations

On November 20, 1973 at Sydney Airport (YSSY), the wind directions were consistent north-westerly between 310 and 330 degrees, the wind speeds were fresh to strong from 8.2 to 14.9

m/s and gusts 10.3 to 20.1 m/s from 0000UTC to 0605UTC before the SSB due to the synoptic winds ahead of the trough(Figure 35(a)). At 0605UTC, the SSB arrived at YSSY with southerly wind speeds of 15.4m/s, gusting to 26.8m/s (maximum gust of the event), then the fresh to strong southerly winds last for the rest of the day. The wind gusts reached 26.8m/s which were well above the criterion for YSSY warning. Meanwhile, a key signature was a sudden Mean Sea Level Pressure (MSLP)rise of 6hPa (from 1001hPa to 1007hPa) and a sharp temperature drop of 16°C (from 35°C to 19°C) within three hours after the SSB. Three hours after the SSB, the MSLP kept rising (up to 1016hPa) and the temperatures maintained stable (17 to 19°C) (Figure 35 (b)). On January 31, 2019 at the Sydney Airport (YSSY), the wind directions were north-westerly to north-easterly between 310 to 050 degrees, the wind speeds were moderate to fresh from 3.1 to 8.7 m/s and gusts 4.1 to 10.3 m/s from 0000UTC to 0640UTC before the SSB due to the synoptic winds ahead of the trough (Figure 36 (a)). At 0640UTC, the SB arrived at YSSY with southerly wind speeds of 11.8m/s, gusting to 14.9m/s, three minutes later at 0644UTC, the SB became SSB that the wind gusts reached 26.8m/s which were well above the criterion for YSSY warning, then maintained the SSB to 1000UTC with maximum gusts of 25.2m/s at 0830UTC, then the fresh to strong southerly winds last for the rest of the day. Meanwhile, a key signature was a sudden MSLP rise of 8.3hPa (from 1005.8hPa to 1014.1hPa) and a sharp temperature drop of 15.2 °C (from 36.8°C to 21.6°C) within three hours after the SSB. Three hours after the SSB, the MSLP kept rising (up to 1021.8hPa) and the temperatures maintained stable (18.5 to 21.7°C) (Figure 36 (b)).

The similar observations of the two events (See Table 11):

- Wind directions both shifted from northerly to southerly (180 degrees at the changing time).
- The changing times were both in the late afternoon after the maximum temperatures occurred during the day

- Wind speeds both were in excess of 15m/s.
- The maximum gusts after the change were both above 21m/s which met the criteria of SSBs for issuing warning for winds.
- The both occurred sharp decreasing of temperatures and sudden increasing of MSLP
- The magnitudes of temperatures change within three hours after the change were close (16°C and 15.2°C).
- The magnitudes of MSLP change within three hours after the change were both above 5hPa (6hPa and 8.3hPa).

The difference between the two events' observations are shown in Table 11.

The wind directions before the change were consistently north-westerly on November 20, 1973 while were from north-westerly to north-easterly, there were more northerly components and the sea breeze presented ahead of the SB on January 31, 2019.

- The wind directions after the change were between 160-180 degrees on November 20, 1973 while were from 180 to 210 degrees on January 31, 2019.
- The wind speeds before the change were fresh to strong (8.2-14.9m/s) on November 20, 1973 while were moderate to fresh (3.1-8.7 m/s) on January 31, 2019.
- Maximum temperature before the change was 37 °C on November 20, 1973 while was 39.8 °C on January 31, 2019.

		November 20, 1973	January 31, 2019
Changing Time (UTC)		0605	0640
Wind directions	Before the change	310-330	310-050

(degrees)	After the change	160-180	180-210
Wind speeds (m/s)	Before the change	8.2-14.9	3.1-8.7
	After the change	5.1-15.4	7.7-20.1
Wind gusts (m/s)	Before the change	10.3-20.1	4.1-10.3
	After the change	6.7-26.8	9.8-25.2
Temperatures change within three hours after the change (°C)		16	15.2
Temperature (°C)	Maximum before the change	37	39.8
	Minimum after the change	17	18.5
MSLP change within three hours after the change (hPa)		6	8.3
MSLP (hPa)	Minimum before the change	1001	1005.6
	Maximum within 15 hours after the change	1015	1021.2
SB periods (hours)		3	7
SSB periods (hours)		<= 0.5	>3

- Minimum temperature after the change was 17 °C on November 20, 1973 while was 18.5 °C on January 31, 2019.
- MSLP change within three hours after the change was 6hPa on November 20, 1973 while was 8.3hPa on January 31, 2019.
- Both minimum MSLP before the change and maximum MSLP within 15 hours after the change were higher on November 20, 1973 than those on January 31, 2019.
- SBs last for 3 hours and SSBs last for less than 0.5 hours on November 20, 1973 while last for 7 hours and more than 3 hours respectively on January 31, 2019.
- Maximum before the change and minimum after the change are both higher on November 20, 1973, however, the temperature differences are similar.

Table 11: Information in details on the two SSBs on November 20, 1973 and January 31, 2019.

This pressure rise had become noticeably steeper, starting at Mt Gambier and reached a maximum amplitude and steepness from Nowra to YSSY. The rapid pressure rises associated with the coastal ridging occur behind the SB are a signature feature of the main CTD (Holland and Leslie, 1986).

Figure 36: Observations from 0025UTC to 2355UTC on November 20, 1973 at Sydney (YSSY).

(a) Wind speed, gust and direction change. (b) Pressure and Temperature Changes during the SSB. Time in UTC for horizontal axis in both (a) and (b), the black arrow under the horizontal

axis indicates the wind change time. In (a), Wind speed, gust and direction change wind speed gusts in m/s for primary vertical axis (left), wind directions in degrees for secondary vertical axis (right). Wind speeds (blue clustered columns, m/s), Wind gusts (grey clustered columns, m/s), Wind directions (orange lines, degrees). In (b), MSLP in hPa for primary vertical axis (left), temperatures in Celsius degrees for secondary vertical axis (right). MSLP (green lines, hPa), Temperatures (red lines, Celsius degrees).

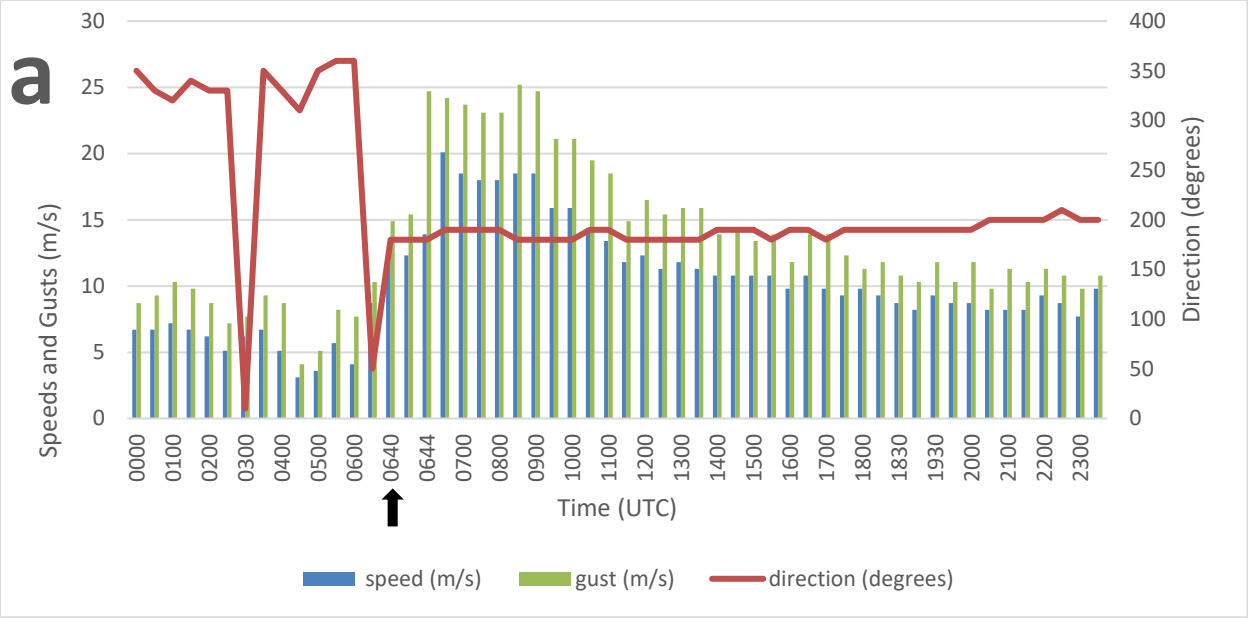

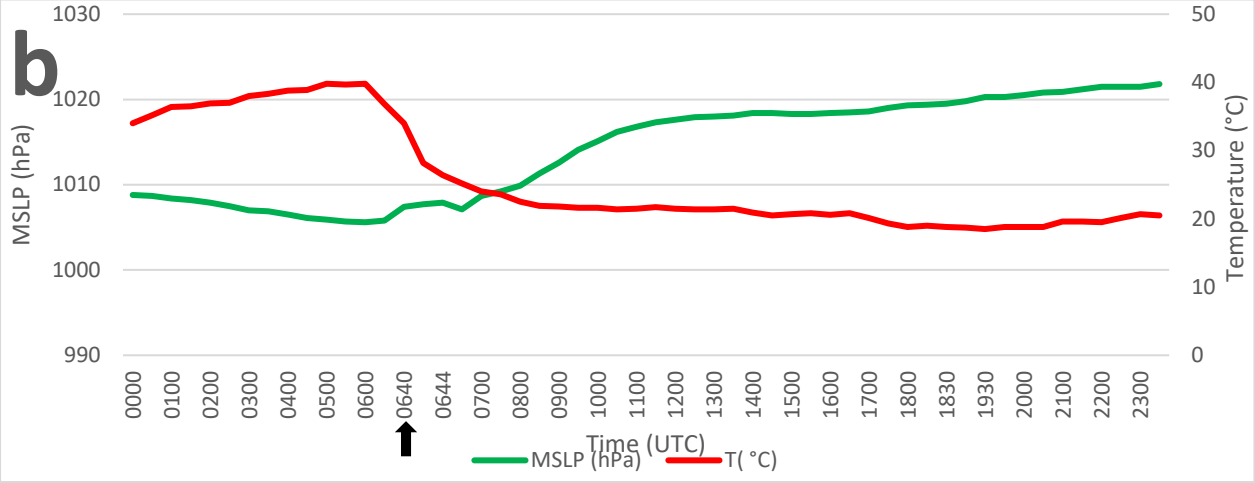

Figure 37: As Figure 36, except from 0005 to 2330UTC on January 31, 2019 at Sydney Airport

5.4.3 Synoptic Overview

The synoptic situation is obtained from archived mean surface level pressure (MSLP) charts. The two southerly buster events of November 20, 1973 and January 31, 2019 propagated along the southeast coast of Australia. A southerly buster is generated when a cold front is blocked and experiences anti-cyclonic deformation near the Great Dividing Range (McInnes 1993). The surge of air propagates northward as a coastally trapped orographic jet up the east coast of Australia, the duration of which is generally less than 24 h, from the time the cold front reaches the Great Dividing Range in southern NSW to its dissipation on the north coast or southern coast of Queensland (Baines 1980; Howells and Kuo 1988; McInnes et al. 1994). The pressure ridge associated with the southerly buster is induced by the southerly flow up the southern parts of the Great Dividing Range resulting in anti-cyclonic vorticity that creates a region of high pressure ahead of the main high-pressure cell behind the frontal system (Helen Reid, 1999)

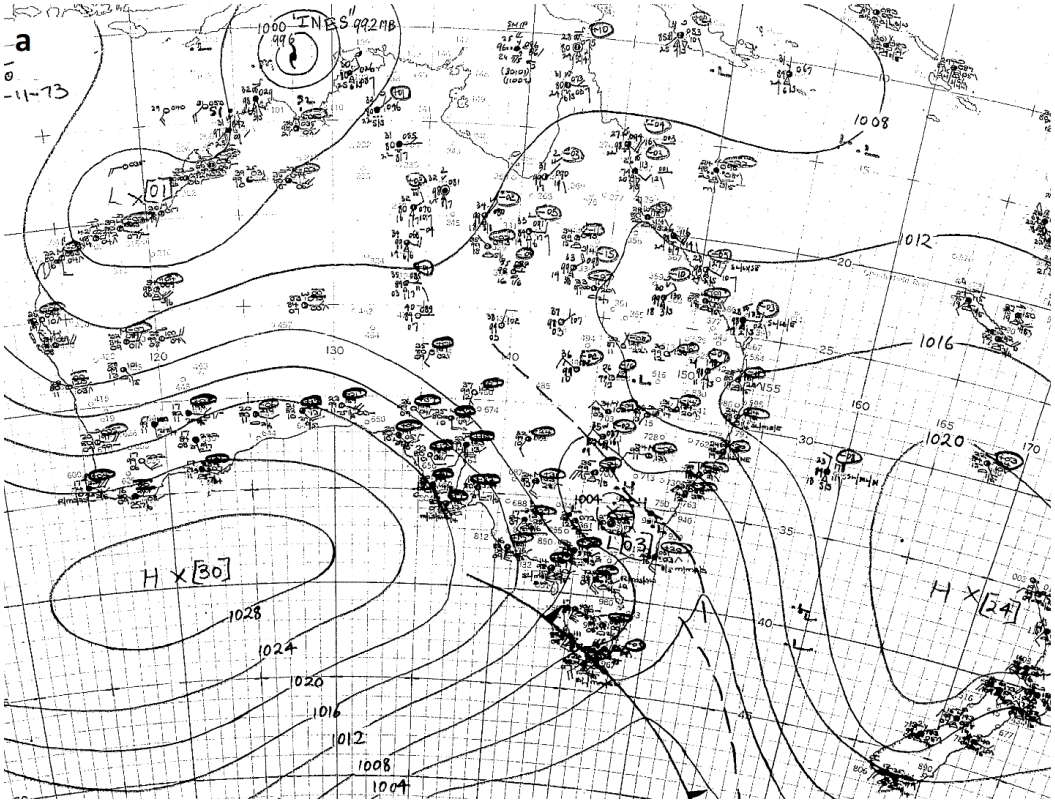
a
INES
1000
996
992 MB
1008
1012
1016
1020
1004
L [03]
H X [30]
1028
1024
1020
1016
1012
1008
1004
H X [24]

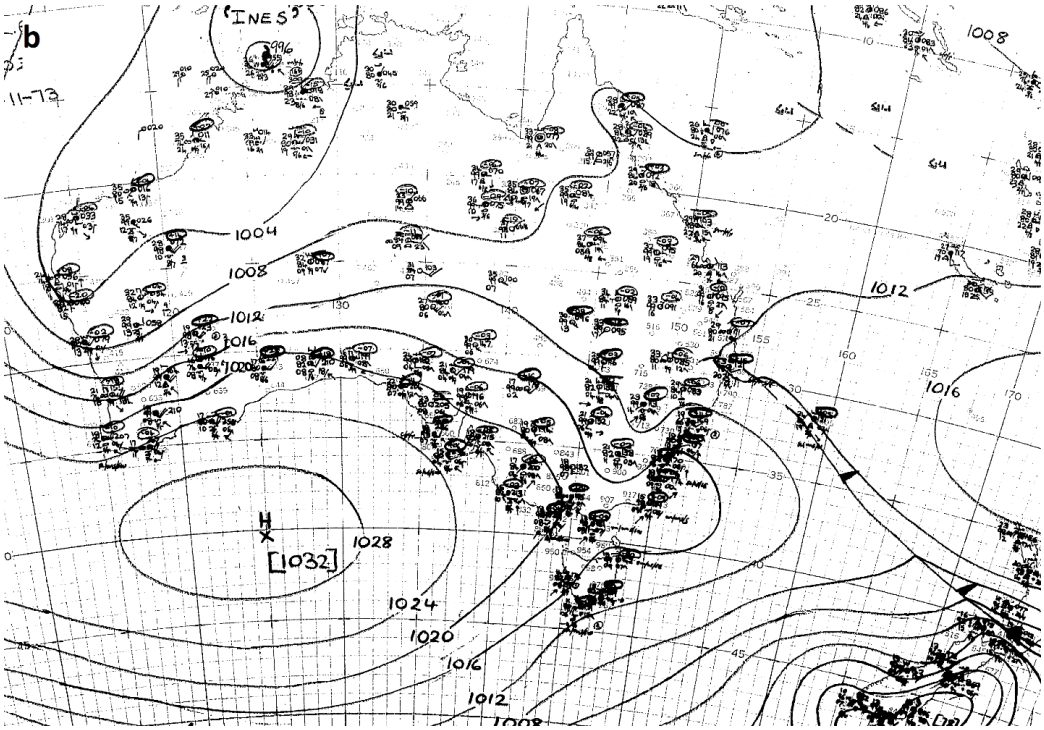
b
INES
996
1008
1004
1008
1012
1016
1020
1012
1016
H
[1032]
1028
1024
1020
1016
1012

Figure 38: Synoptic weather charts for 0200UTC November 20(a) and November 21 (b), 1973. Shown are manually analysed contours of Mean Sea Level Pressure (MSLP) in intervals of 4hPa, local maxima and minima of MSLP, cold fronts (solid lines with triangular barbs), and low-pressure troughs (dashed lines).

A phenomenon well-known to Australian meteorologists is the rapid establishment of a strong coastal ridge, which occurs when a Southern Ocean anticyclone approaches south-eastern Australia. This ridging is initiated by a high-pressure surge which begins off the coast of southern Victoria, then moves rapidly along the NSW coast, and often travels along most the entire east coast of Australia, in a distance for 2000-3000km. In contrast, the parent anticyclone moves only several hundred kilometres (Holland and Leslie, 1986). The MSLP chart on 0200UTC November 20, 1973 (Figure 38 (a) displayed the synoptic pattern four hours before the SSB arrived Sydney at 0605Z. From the MSLP chart, a high pressure system with centred value 1024hPa ((located between 160-165 E and 35 – 40 S) was over the southern Tasman Sea, extending a ridge from the east over north NSW into the east part of south Queensland, a second stronger high pressure system with centred value 1030hpa (located around 115-125 E and 37-43 S) was over the broad Southern Ocean, extending a ridge from the west over the south of Western Australia, South Australia, Victoria and south of NSW. Between the two surface high pressure systems, there was a prefrontal trough across a low which lied between the border of Victoria and NSW, followed by a cold front ahead of the stronger surface high pressure system. The MSLP chart was a classical southerly buster pattern. Unfortunately, the archived MSLP charts can only be obtained once a day. The MSLP chart on 0200UTC November 21, 1973 (Figure 38 (b) displayed the synoptic pattern 20 hours after the SSB arrived Sydney. It was noticeable that the high pressure system over the Tasman Sea moved toward the northeast (the centre located the east of 170E and 30 – 35S), weakening with the ridge only extending to the coastal fringe of south Queensland, the second stronger high pressure system

over Southern Ocean strengthened with centred value 1032hpa (located around 118-128 E and 37-43 S), extending a ridge from the west over the south of Western Australia, South Australia, Victoria and south of NSW. Between the two surface high pressure systems, there was a prefrontal trough across a low which lied between the border of Victoria and NSW, followed by a cold front ahead of the stronger surface high pressure system.

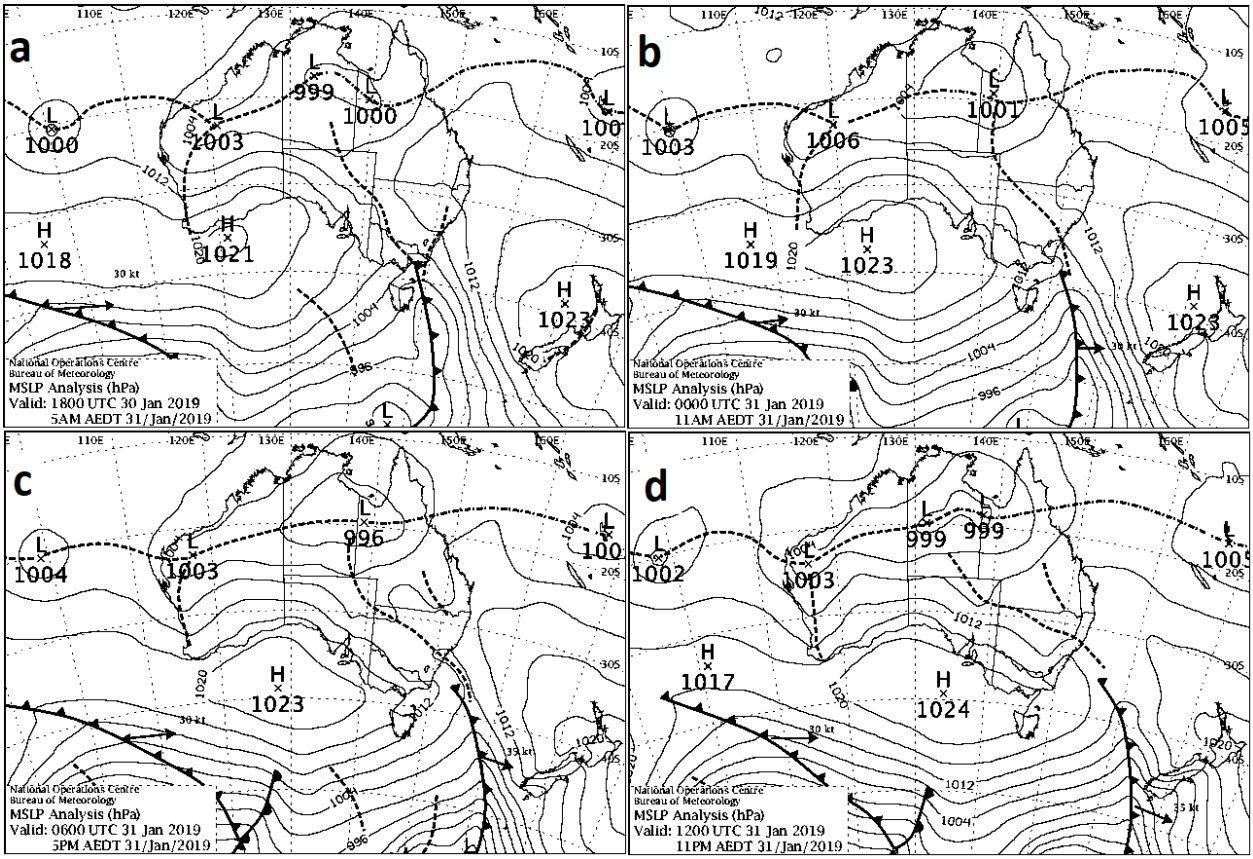

Figure 39: Synoptic weather charts from 1800UTC January 30 to 1200UTC January 31, 2019. a) 1800 UTC January 30, 2019, b) 0000 UTC January 31, 2019, c) 0600 UTC January 31, 2019, d) 1200 UTC January 31, 2019. Shown are contours of Mean Sea Level Pressure (MSLP) in intervals of 4hPa, local maxima and minima of MSLP, manually analysed cold fronts (solid lines with triangular barbs), and low-pressure troughs (dashed lines). (From http://www.bom.gov.au/australia/charts/).

The MSLP charts from 1800UTC January 30 to 1200UTC January 31, 2019 are shown in Figure 39. At 1800UTC January 30, coastal ridging was initiated at the south-western extremity of the Great Dividing Range, between Mt Gambier and Cape Otway, associated with the northward movement of cold air behind a nearly zonal Southern Ocean front. East of Mt Gambier the cold flow was blocked by the southern slopes of the Great Dividing Range, thereby driving the ducted disturbance eastwards along the Victorian coast. At 0000 UTC January 31, the coastal ridging had propagated around the southeast corner of Australia and was located on the NSW coast, north of Gabo Island and Merimbula. At 0600 UTC January 31, a strong high-pressure centre (1023hPa) was situated in the Great Australian Bight, with an inland trough west of the ranges and a frontal zone off eastern Australia, further extending the coastal ridge along the southeast NSW coast. At 0600 UTC January 31, the cold front had continued moving northeast while the high-pressure centre increased to 1024hPa, strengthening the ridge over southeast NSW. By 1200UTC January 31, the coastal ridge propagated further north, with the high centre remaining over the Southern Ocean, and the second surface high pressure centre moving to the south of the Tasman Sea. Between the two surface high pressure systems, there was a prefrontal trough across a low which lied between the border of Victoria and NSW, followed by a cold front ahead of the stronger surface high pressure system.

We notice that the two SSBs both occurred on the synoptic situation when a prefrontal trough was crossing a low which lied between the border of Victoria and NSW, followed by a cold front ahead of the stronger surface high pressure system between the two surface high pressure systems, the type of MSLP chart was a classical southerly buster pattern.

5.4.4 Satellite Imagery

The satellite images are not presented on November 20, 1973 in the paper, however, the Himawari-8 high-resolution temporal and spatial satellite images are shown on January 31,

2019, reveals a roll cloud accompanying the SB offshore near Williamtown, extending to the southeast over the Tasman Sea. Ahead of the cold front cloud band, shallow solitary waves are moving with the cold front cloud band. Clarke (1961) determined the mesoscale structure of the dry cold fronts using serial pilot balloon flights, radiosonde, and aircraft data. He found closed circulations (roll vortices) in the velocity field behind several fronts; in two cases, double circulations with the roll vortices were inferred (Clarke, 1961).

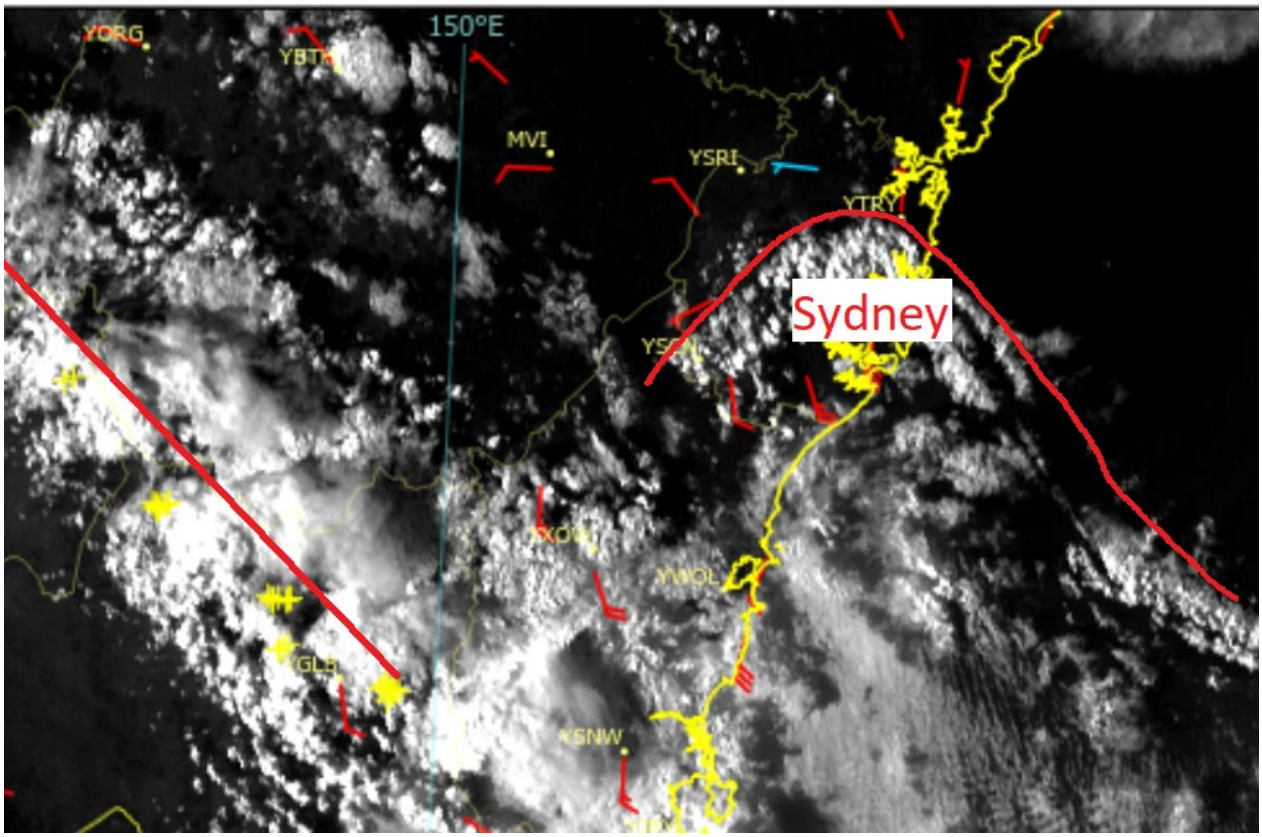

Figure 40: Himawari-8 satellite visible image at 0700UTC on January 31, 2019 over New South Wales coast.

Image shown with the permission of the Australian Bureau of Meteorology. The AWS wind barbs show wind direction and speed in m/s (red barbs, short barb=2.5m/s, long barb = 5m/s) the curve north of Sydney indicates the leading edge of the SB accompanied by a roll cloud behind. The inland cloud band (red line) locates the parent cold front to the SB associated with thunderstorms (yellow crosses).

Cloud features associated with the SB also were detected from the Himawari-8 visible imagery (Figure 40) at 0700UTC on January 31, 2019. The red curve indicates the leading edge of the SB accompanied by a roll cloud. The roll cloud is consistent with the schematics of Figure 12 and Figure 13. The inland cloud band (red line) provides the location of the parent cold front to the SB which is consistent with the schematic (Figure 12). The roll cloud can produce wind shear which is sufficiently strong enough to pose a hazard to aircraft operating at low altitudes (typically landing or taking off). It is obvious that the winds behind the red curve are southerly and northerly ahead of the red curve.

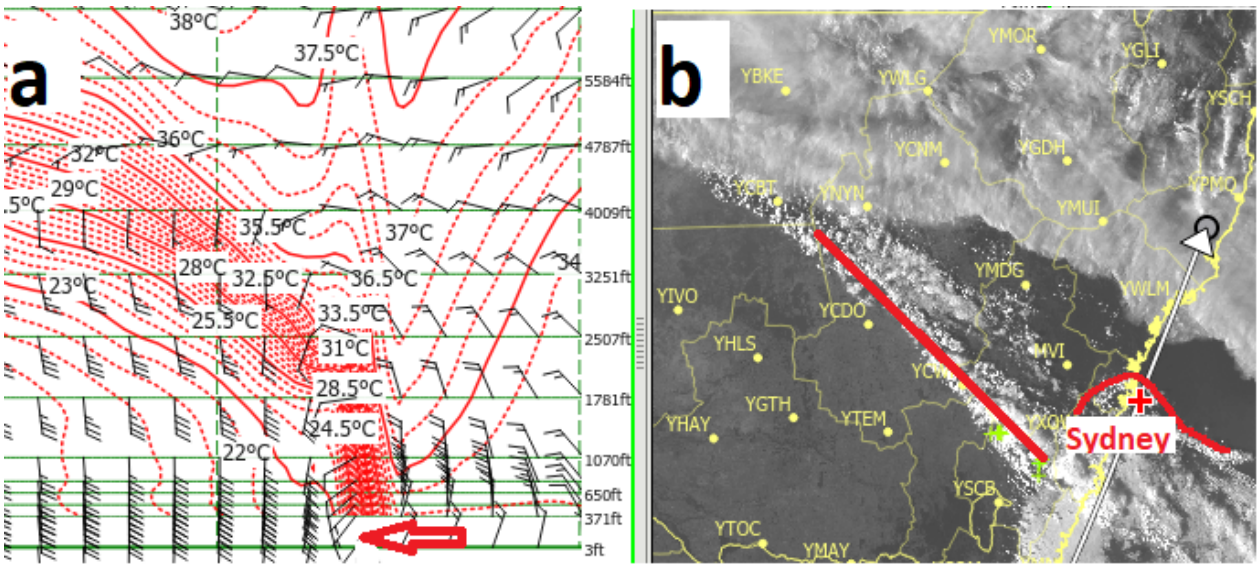

Figure 41: Model cross Section for potential temperatures (°C) and winds below 800hPa (elevation in feet in the right) at 0700UTC on January 31, 2019 along the NSW coast.

(a): Model cross Section for potential temperatures (°C) and winds below 800hPa (elevation in feet in the right) at 0700UTC on January 31, 2019 along the NSW coast (black wind barbs, short bar=2.5m/s, long bar = 5m/s), both the red solid lines with intervals every 2.5°C and dash lines with intervals every 0.5°C are the potential temperatures, the red arrow points at the changing point.

(b): Himawari-8 satellite visible image at the same time in Figure 41 (a) and Figure 40, the curve north of Sydney indicates the leading edge of the SB accompanied by a roll cloud behind. The inland cloud band (red line) locates the parent cold front to the SB associated with thunderstorms (yellow crosses). The cross Section in (a) is for the white arrow line along the NSW coast, the red cross in (b) is corresponded to the red arrow in (a) for wind change point.

From Figure 41, the vertical structure is presented before and after the change at 0700UTC on January 31, 2019 along the NSW coast. The SSB change at Sydney Airport was at 6:40 UTC, the time was just 20 minutes after the change. Figure 41 (a) shows the ACCESS (the Australian Community Climate and Earth-System Simulator) model cross Section for potential temperatures (°C) and winds below 800hPa the potential temperatures, the red arrow points at the changing point which is corresponded to the Red Cross in Figure 41 (b). The wind shear is apparent across the changing point just north of Sydney. The winds are stronger near surface and low levels before and after change. The fresh to strong southerly winds behind the change are mostly below 3000ft, this is consistent with the height of the Great Dividing Rang in the west. This is from model results, and we will further discuss it through observation below in Figure 42. Meanwhile, the potential temperature has a sharp change across the change point and the isothermals are squeezing behind the change.

The cross Section revealed a strong inversion from the surface to 2000ft after the change. Clearly, in this case, the southerly change is shallow with an overlying deep inversion. Fronts with a north-west/south-east orientation can experience blocking by the coastal mountain ranges (Figure 7) of southeast Australia and progressively increase speed of propagation on the eastern side, while continuing to move more slowly on the western side of the ranges. The effect is more pronounced for shallow cold fronts than those with the cold-air layer deeper than the height of the ranges (Coulman, 1985).

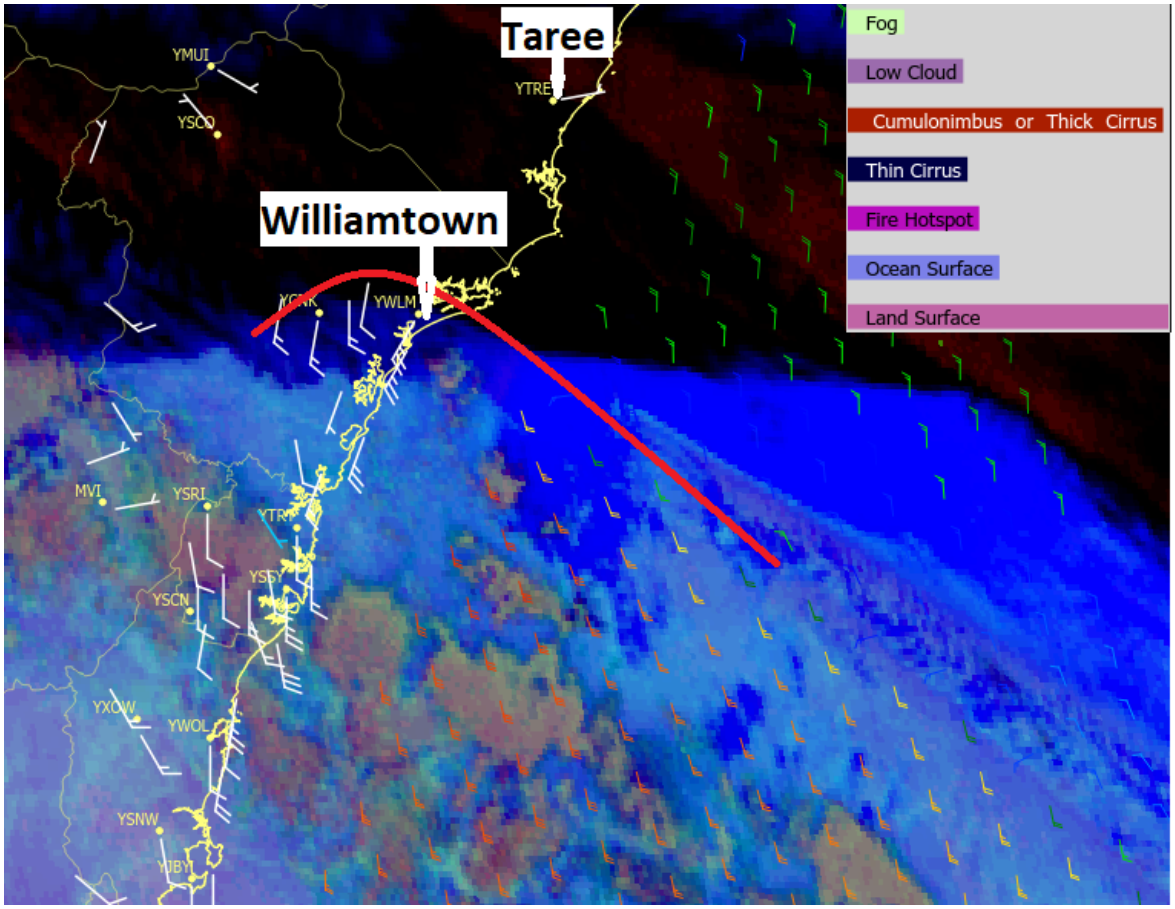

Figure 42: Himawari-8 satellite RGB night microphysical image for low cloud and fog at 1200UTC on January 2019.

Product derived from 10.8μ IR channel, 12.0μ IR channel and 3.9μ NIR channel. Colours based n EUMETSAT standard, interpretation guidance on the up-right corner. The overlain winds are the AWS wind barbs showing wind direction and speed in m/s (white barbs land, short barb=2.5m/s, long barb = 5m/s) and microwave advanced scatterometer (ASCAT) winds (wind barbs sea, short barb=2.5m/s, long barb = 5m/s, data buffer is 22 hours from 20190131). The red curve between Williamtown and Taree indicates the leading edge of the SB.

Similar to Figure 40, the red curve represents the leading edge of the change, Himawari-8 satellite RGB night microphysical image for low cloud and fog at 1200UTC on January 2019 in Figure 42. Product derived from 10.8μ IR channel, 12.0μ IR channel and 3.9μ NIR channel.

Colours based n EUMETSAT standard, interpretation guidance on the up-right corner. The overlain winds are the AWS wind barbs showing wind direction and speed in m/s (white barbs land, short barb=2.5m/s, long barb = 5m/s) and microwave advanced scatter meter (ASCAT) winds (wind barbs sea, short barb=2.5m/s, long barb = 5m/s, data buffer is 22 hours from 20190131). ASCAT are useful for monitoring SBs despite this polar orbiting satellite providing data of relatively limited temporal frequency. Fortunately, in this case, descending data was available. The red curve between Williamtown and Taree indicates the leading edge of the change. We notice that the change at Williamtown was at 0952UTC and at Taree was at 1300UTC. Behind the change, the winds were fresh to strong southerly with at the speed of 10-15m/s over the water and coastal fringe which were responsible for the extensive stratus low clouds east of the ranges and low cloud and fog near the coastal fringe and sea. Winds weakening further inland east of the ranges, becoming variable light winds over the ranges at Mount Victoria (MVI in Table 12); Ahead of the change, the winds were light variable over land and 7-10m/s northerly winds over the water. Low cloud and fog was only far offshore near the front zone, while some cumulonimbus or thick cirrus occurred both over the land and water.

5.4.5 Sydney Airport Wind Profiler Data

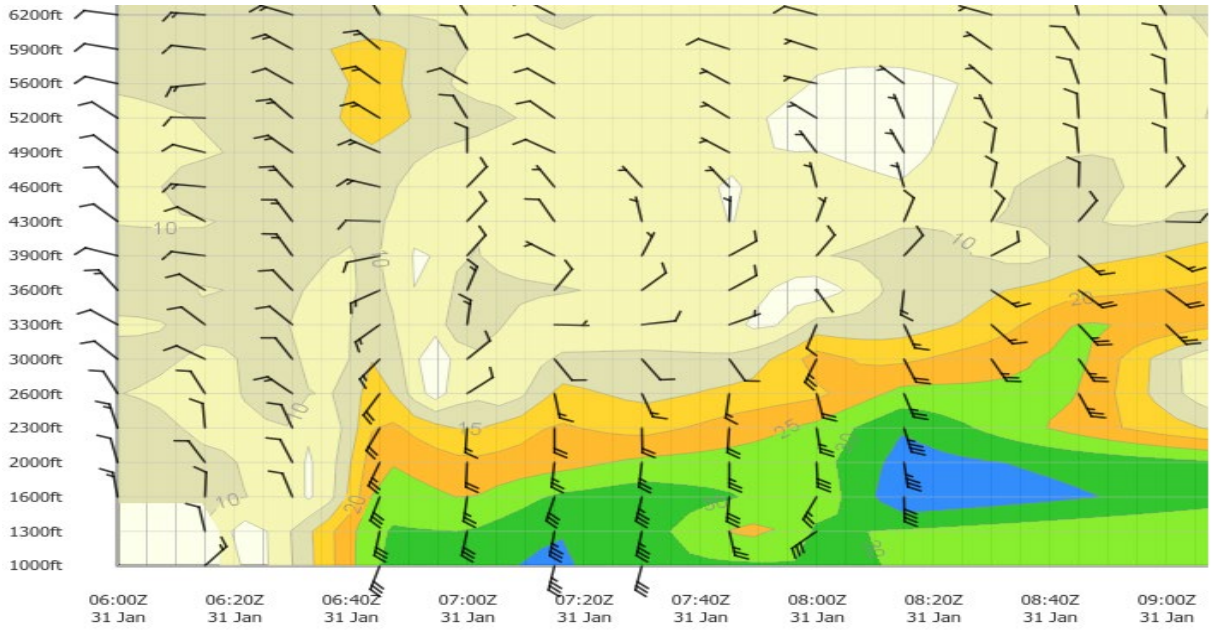

Figure 43: Sydney Wind Profiler from 0600UTC to 0900UTC on January 31, 2019.

The wind barbs show wind direction and speed in m/s (short bar=2.5m/s, long bar = 5m/s).

The Sydney Airport wind profiler data can be obtained on January 31, 2019, but it is not available on November 20, 1973. The data from the profiler are at every 15 minutes. Before the change (06:40UTC), the north to north-westerly winds were dominant below 6200ft. Sea breeze occurred after 0600UTC, from Figure 37(b) and Table 14, the winds at 0630 were 050 degrees at the speed of 17m/s with gust 20m/s. We can also see the sea breeze occurred at 0300UTC were 010 degrees at the speed of 12m/s with gust 15m/s from Table 14. At 0640UTC, the winds sharply changed to 180 degrees at the speed of 23m/s with gust 29m/s. The southerly winds were only below 4000ft, this demonstrated that the SSBs are trapped by the GDR (Great dividing Ranges) as we know the elevation of Mount Boyce is 3700ft. Another feature was that the southerly winds were much stronger near the surface and in the low level, decreasing with the height.

5.4.6 Discussion of observations from January 30th to 31st from along the NSW

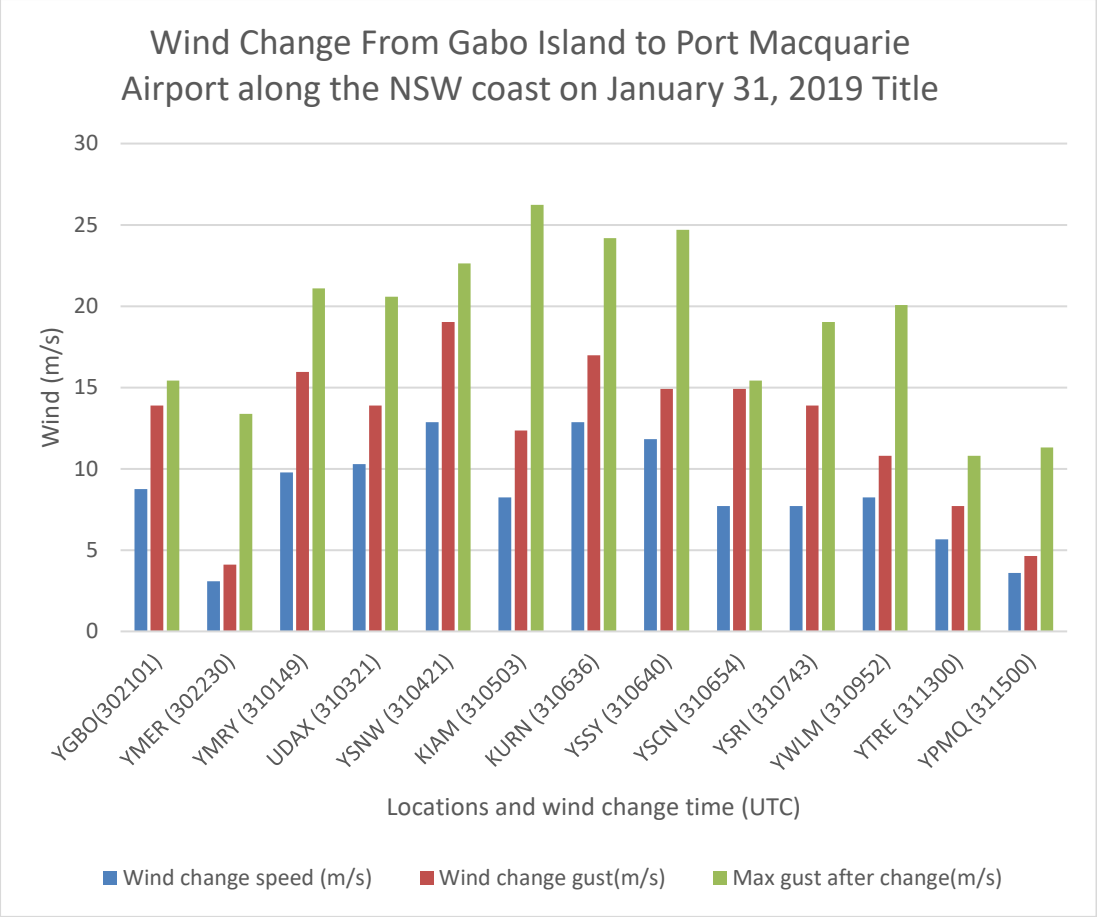

Figure 44 Observations of wind change from January 30th to 31st from along the NSW coast from Gabo Island to Port Macquarie.

The Aviation IDs are used in the Table 12. Locations with Changing date and time in the brackets in UTC (e.g. 302101 means at 21:01 on 30th) for horizontal axis, wind speed gusts in m/s for vertical axis. Wind change speeds (blue clustered columns, m/s), Wind change gusts (orange clustered columns, m/s.), Max gusts after change (grey clustered columns, m/s.).

From the observations (Figure 44 and Table 13), the wind change speeds, wind change gusts and maximum gusts after change, it is noticeable that southerly wind change was strong at Gabo Island (YGBO), where the CTD was initiated, at 21:01 (UTC) on 30th January, 2019,

the maximum wind gust was 15.4m/s after the change, attained the criteria of southerly buster (SB) (>=15m/s). When the winds went through Merimbula (YMER), the winds were weakening, the maximum wind was 13.4m/s which was below the southerly buster, then the winds speeded up again at Moruya(YMRY), with the maximum gust of 21.1 m/s which met the criteria of a strong southerly buster (SSB) (>=20.5 m/s). when the SSB propagated northward, via Ulladulla (UDAX), Nowra (YSNW), Kiama (KIAM), Kurnell (KURN), Sydney (YSSY), Williamtown (YWLM), the maximum gusts were all attained to SSBs. The two locations Camden (YSCN) and Richmond (YSRI) were less than SSBs, but were still SBs, which was because the two locations are further inland, the winds were weakening when propagating to these two locations. However, when the winds moved across Williamtown (YWLM) to Taree (YTRE) and Port Macquarie (YPMQ), the winds dropped to below SBs, the maximum gusts were only around 11 m/s.

We notice that the maximum winds meet the SSB criteria were from YMRY to YWLM which are above 20.5m/s, after YWLM, the winds dropped quickly. This can be explained by two reasons. The first one is that due to the diurnal reason. When the southerly change propagated to the YMRY, the temperature inland start to increasing, and the difference of the two types of airmass are becoming higher. This keeps increasing till the evening the southerly change arrives to YWLM, the temperatures ahead of the change are decreasing due to the radiation cooling. The other main reason is that the topography contribution. NSW is divided into four main geographical zones considering the climatology: The Coastal Stripe, the Tablelands, the Western Slopes and Palins, and the Far West. The coastal stripe lies between the Pacific Ocean and Tablelands to the west. Mostly very narrow, about 60 to 100kmin width. The Hunter Valley, is one of the largest river valleys on the NSW coast, ranging from approximately 120 km to 310 km north of Sydney about 190km of width.

The coastally trapped disturbances (CTD) are propagating in the Coastal Stripe region, the Tablelands are the barriers and the Hunter Valley is a gap. The researches on CTD dynamics to barrier height and topographic variability shows that average propagation speeds increased (decreased) by 15%– 20% with the increased (decreased) a topographic multiplication factor (Sensitivity of Coastally Trapped Disturbance Dynamics to Barrier Height and Topographic Variability in a Numerical Model.) From YMRY to YSSY, the narrow Coastal Stripes are adjacent to the high ranges and tablelands in the west, therefore the winds picking up and getting their maximum from YMRY to YSSY. The average propagation speed of the leading coastal trough was proportional to barrier height and not barrier slope. The influence on the propagation of CTD of large gaps of which the width is of order 25–50% of the Rossby radius. In this case, we get Rossby radius is 274km (see 5.4.8. and Table 14) and the gap is 190km which is above 50%. It is found that the gaps influence CTD propagation by effectively stalling the propagation at their mouth for a period and subsequently weakening the gravity current-like features (vertical extent, strength and abruptness of the wind and stratification changes at the leading edge). Consistent with the findings of (Reason et al. 2006), the wind gusts changed decrease after passing YWLM, indicating the dynamical influence of large valleys on the propagation of coastally trapped disturbances. This is the reason why winds drop off after YWLM. The most intense part of the wind surge crossed the coast during the evening near the Hunter Valley (a significant gap in the east coast mountain barrier). This led to flow splitting inland up the Hunter Valley and northward along the east coast. The coastal component developed into a CTD in the form of a wind surge that accelerated ahead of the region of onshore forcing until it encountered a reduced mountain barrier farther north, and the flow spilled inland signalling the end of the event.

Name	Aviation ID.
Gabo Island	YGBO
Merimbula Airport (AP) Automatic Weather Station (AWS)	YMER
Moruya AP AWS	YMRY
Ulladulla AWS	UDAX
Nowra AWS	YSNW
Kiama AWS	KIAM
Kurnell AWS	KURN
Camden AP	YSCN
Sydney AP	YSSY
Richmond AP	YSRI
Williamtown	YWLM
Taree AP AWS	YTRE
Port Macquarie AP AWS	YPMQ
Mount Victoria	MVI

Table 12: Locations and Aviation IDs

Aviation ID and Timing of change	Wind direction (Degrees)	Wind change speed (m/s)	Wind change gust(m/s)	Max gust after change(m/s)
YGBO (302101)	240	8.7	13.9	15.4
YMER (302230)	140	3.1	4.1	13.4
YMRY (310149)	160	9.8	15.9	21.1
UDAX (310321)	210	10.3	13.9	20.6
YSNW (310421)	190	12.9	19.0	22.6
KIAM (310503)	210	8.2	12.3	26.2
KURN (310636)	220	12.9	17.0	24.2
YSSY (310640)	180	11.8	14.9	24.7
YSCN (310654)	200	7.7	14.9	15.4
YSRI (310743)	130	7.7	13.9	19.0
YWLM (310952)	200	8.2	10.8	20.1
YTRE (311300)	190	5.7	7.7	10.8
YPMQ (311500)	190	3.6	4.6	11.3

Table 13: Observations of wind change from January 30th to 31st.

Along the NSW coast from Gabo Island to Port Macquarie.

5.4.7 Radar Images

Southerly busters can be detected on radar images. In the study, three Doppler radar data are used. The three Doppler radars are located at Sydney Terry hills (Meteor 1500 S-band Doppler), Wollongong (Appin) (DWSR 8502S 2° S-band) and Kurnell (DWSR 8502S 2° S-band). All the radar images in the case study are using the 0.5-degree elevation, the reason behind is that the southerly change is shallow, and the depth is usually below 1km. The change in Sydney basin can be well recorded by Sydney Terry hills radar (Figure 45b), also by Kurnell radar and Wollongong radar (Figure 46 to Figure 48).

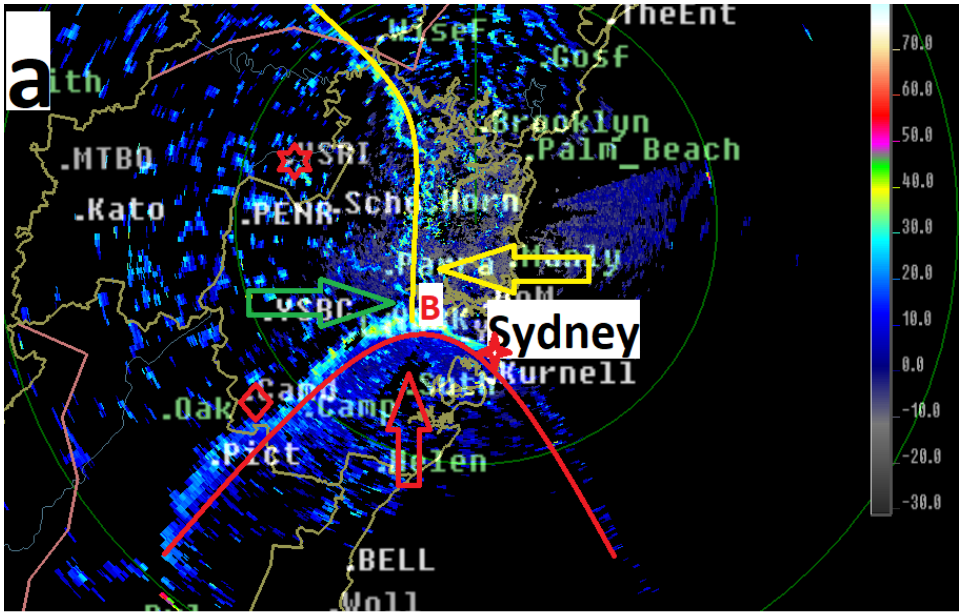
a
Sydney
B
.MTBO
.Kato
.PENR
.YSBK
.Oak
.Pict
.BELL
.Gosf
.Brooklyn
.Palm_Beach
.Kurnell
.Helen
70.0
60.0
50.0
40.0
30.0
20.0
10.0
0.0
-10.0
-20.0
-30.0

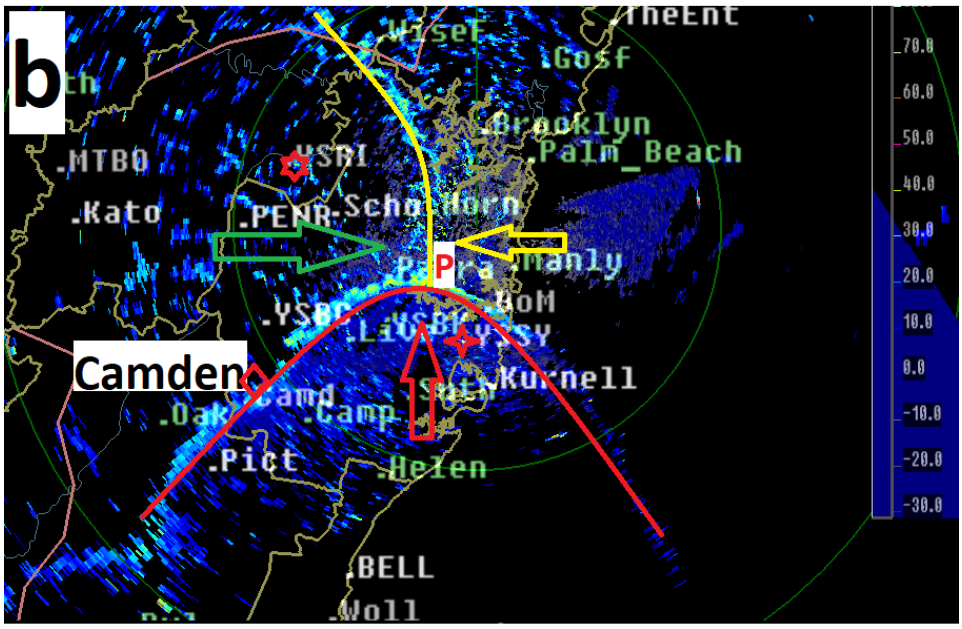
b
Camden
P
.MTBO
.Kato
.PENR
.YSBK
.Oak
.Pict
.BELL
.Gosf
.Brooklyn
.Palm_Beach
.Manly
.BoM
.Kurnell
.Helen
70.0
60.0
50.0
40.0
30.0
20.0
10.0
0.0
-10.0
-20.0
-30.0

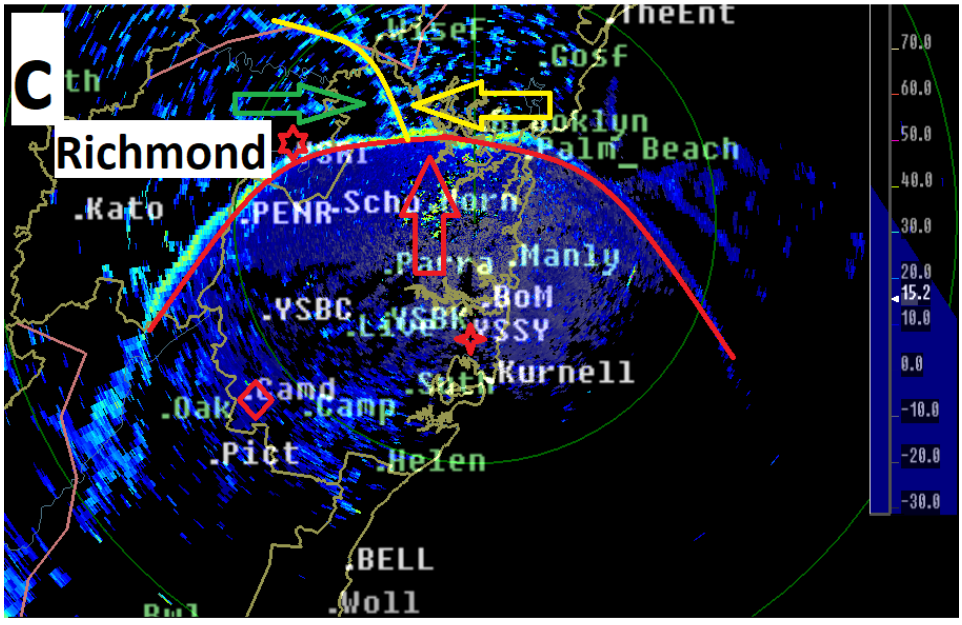
c
Richmond
.Kato
.PENR
.YSBG
.Oak
.Pict
.BELL
.Gosf
.Palm_Beach
.Manly
.BoM
.Kurnell
.Helen
70.0
60.0
50.0
40.0
30.0
20.0
15.2
10.0
0.0
-10.0
-20.0
-30.0

Figure 45: 0.5-degree elevation reflectivity, radar scans from Terry Hill radar for three locations in Sydney region.

a): 0640 UTC SSB at Sydney Airport (four-point star), the capital letter B in (a) represents the place name of Bankstown. b): 0654UTC SSB at Camden Airport (diamond), the capital letter P in (b) represents the place name of Parramatta. c): 0743 UTC SSB at Richmond Airport (six-point star). The red up arrow represents the southerly airmass, the green right arrow represents the prefrontal hot and dry north westerly flow, and the yellow left arrow represents the sea breeze airmass. The yellow line is the boundary between north westerly flow and sea breeze, the red line is the boundaries between southerly airmass and northerly flows (including prefrontal hot and dry north westerly flow and north easterly sea breeze). Range rings are at 50km and 100km from the radar.

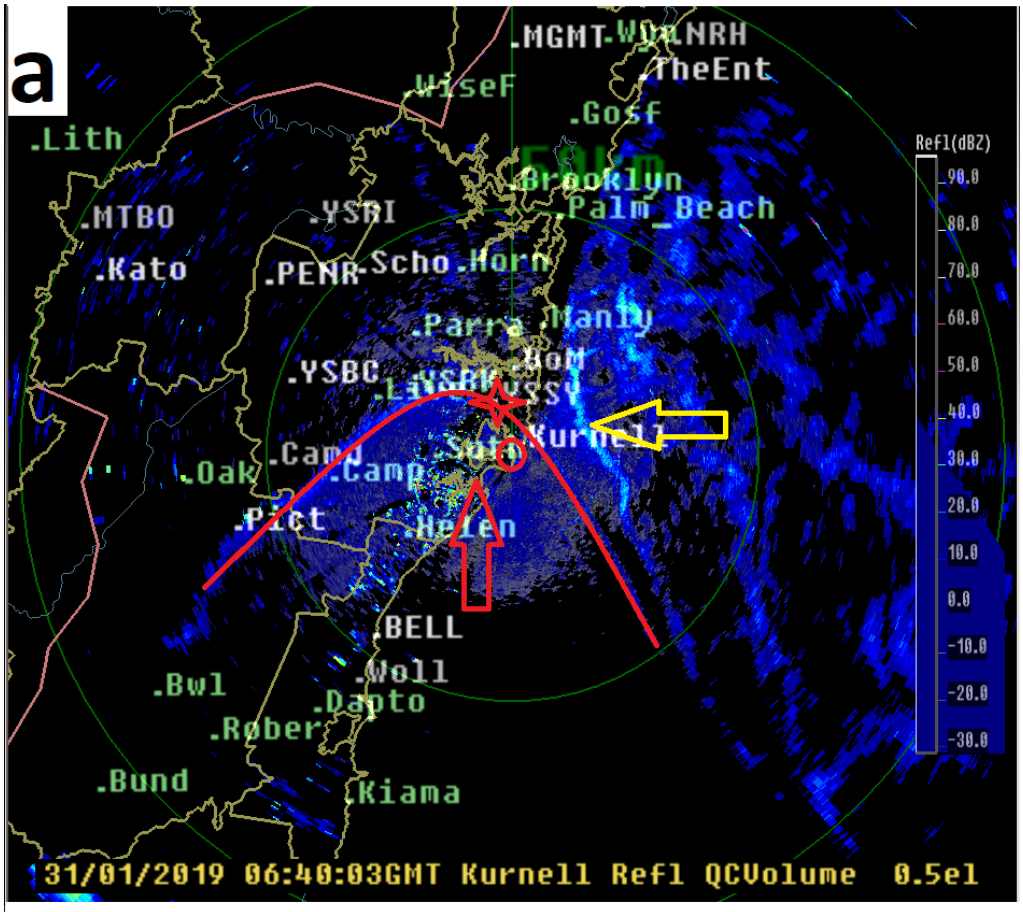
a
.MGMT
.WilNRH
.TheEnt
.WiseF
.Gosf
.Lith
.Brooklyn
.Palm_Beach
.MTBO
.YSRI
.Kato
.PENR
.Scho
.Horn
.Parra
.Manly
.YSBC
.BoM
.Kurnell
.Oak
.Camd
.Camp
.Pict
.Helen
.BELL
.Woll
.Bwl
.Dapto
.Rober
.Bund
.Kiama
Refl(dBZ)
90.0
80.0
70.0
60.0
50.0
40.0
30.0
20.0
10.0
0.0
-10.0
-20.0
-30.0
31/01/2019 06:40:03GMT Kurnell Refl QCVolume 0.5el

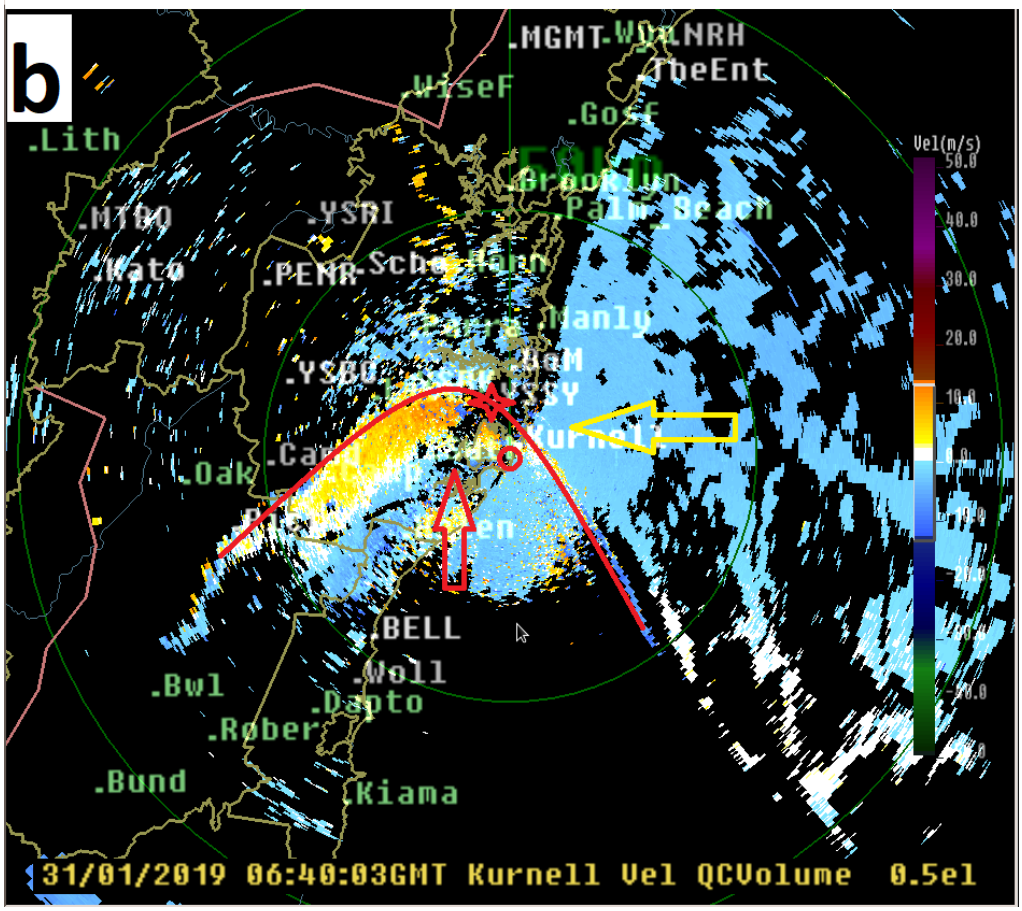
b
.MGMT
.WilNRH
.TheEnt
.WiseF
.Gosf
.Lith
.Brooklyn
.Palm_Beach
.MTBO
.YSRI
.Kato
.PENR
.Scho
.Manly
.YSBC
.BoM
.Kurnell
.Oak
.BELL
.Woll
.Bwl
.Dapto
.Rober
.Bund
.Kiama
Vel(m/s)
50.0
40.0
30.0
20.0
31/01/2019 06:40:03GMT Kurnell Vel QCVolume 0.5el

Figure 46: 0.5-degree elevation reflectivity and velocity radar scans from Kurnell radar at 0640 UTC SSB at Sydney Airport.

a): reflectivity radar scan. b): velocity radar scan. Sydney Airport is at the four-point star and Kurnell radar location is at the red circle. The red up arrow represents the southerly airmass and the yellow left arrow represents the sea breeze airmass. The red line is the boundary between southerly airmass and northerly flows (including prefrontal hot and dry north westerly flow and north easterly sea breeze). Range rings are at 50km and 100km from the radar.

From the Kurnell radar scans at 0640 UTC when the SSB occurred at Sydney Airport in Figure 46, the distinctive narrow line can be seen from both reflectivity (a) and velocity (b) scans, the line is highlighted in red which represents the boundary between southerly airmass and northerly flows (including prefrontal hot dry north westerly flow and north easterly sea breeze). The Kurnell radar is in the south of the Sydney Airport. The winds in red up arrow area behind the red line are southerly flows but in two colours, this can be explained that when the SSB passed Kurnell toward north, the winds between Kurnell radar and Sydney Airport are moving away from the radar in yellow echoes from velocity scan image, the winds south of the Kurnell radar are moving towards the radar in blue echoes. The winds ahead of the changing line (red line) are north easterly sea breeze in blue in the left yellow arrow area, which are moving towards the Kurnell radar. The hot and dry prefrontal north westerly flow are not clear from the Kurnell Radar (Figure 46 b). Note that triple point added the possibility of convection.

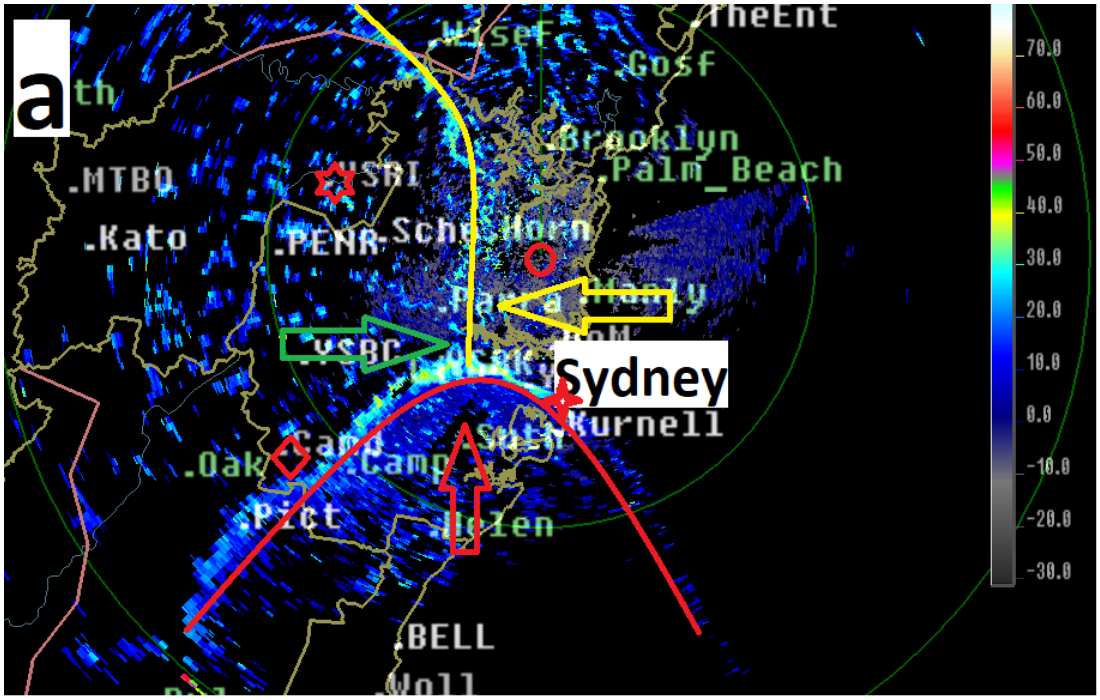
a
.TheEnt
.Gosf
.Brooklyn
.Palm_Beach
.MTBD
.Kato
.PENR
.Sydney
.Kurnell
.BELL
70.0
60.0
50.0
40.0
30.0
20.0
10.0
0.0
-10.0
-20.0
-30.0

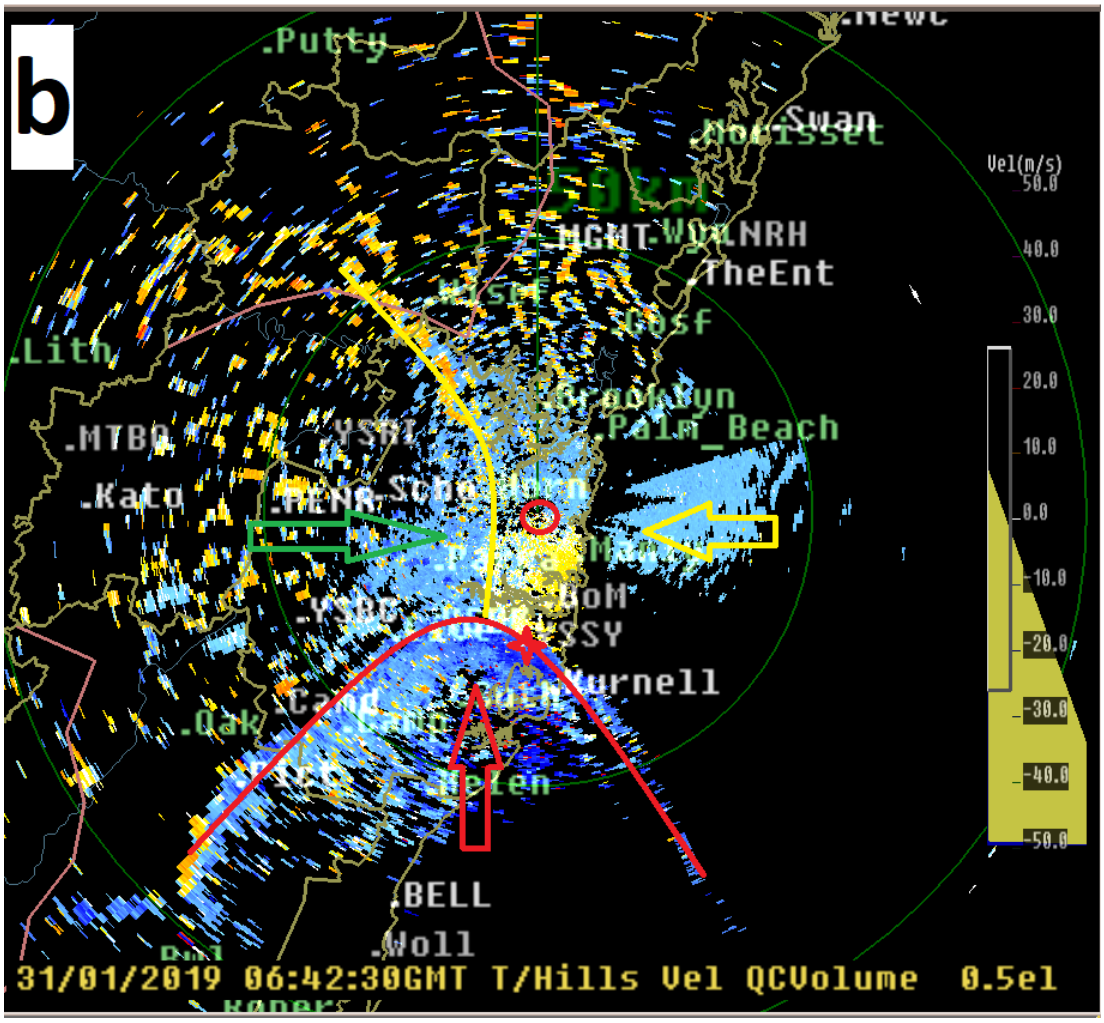
b
.Putty
.Swan
.TheEnt
.Gosf
.Brooklyn
.Palm_Beach
.MTBD
.Kato
.Kurnell
.BELL
Vel(m/s)
50.0
40.0
30.0
20.0
10.0
0.0
-10.0
-20.0
-30.0
-40.0
-50.0
31/01/2019 06:42:30GMT T/Hills Vel QCVolume 0.5el

Figure 47: 0.5-degree elevation reflectivity and velocity radar scans from Terry Hills radar at 0640 UTC SSB at Sydney Airport.

a): reflectivity radar scan. b): velocity radar scan. Sydney Airport is at the four-point star and Terry Hills radar location is at the red circle. The red up arrow represents the southerly airmass, the right green right arrow represents the hot and dry prefrontal north westerly flow and the yellow left arrow represents the sea breeze airmass. The red line is the boundary between southerly airmass and northerly flows (including prefrontal hot and dry north westerly flow and north easterly sea breeze). Range rings are at 50km and 100km from the radar.

From the Terry Hills radar scans at 0642 UTC two minutes after the SSB occurred at Sydney Airport in Figure 47 the distinctive narrow line can be seen from both reflectivity(a) and velocity(b) scans, the line is highlighted in red which represents the boundary between southerly airmass and northerly flows(including prefrontal hot dry north westerly flow in right green arrow area and north easterly sea breeze in left yellow arrow area). The Terry Hills radar is in the north of the Sydney Airport. The winds in red up arrow area behind the red line are southerly flows in blue, this can be explained that winds are moving towards the Terry Hill radar which is different from Figure 46 b in two colours due to the radar location. The winds ahead of the changing line (ahead of red line in left yellow arrow area) are north-easterly sea breeze in blue over north and east part of radar which means winds are moving towards the radar, but in yellow over the south part which means the winds are moving away from the Terry Hills radar. The hot and dry prefrontal north westerly flow (ahead of red line in right green arrow area) are in blue which means the winds are moving towards the Terry Hills Radar (Figure 46 b)

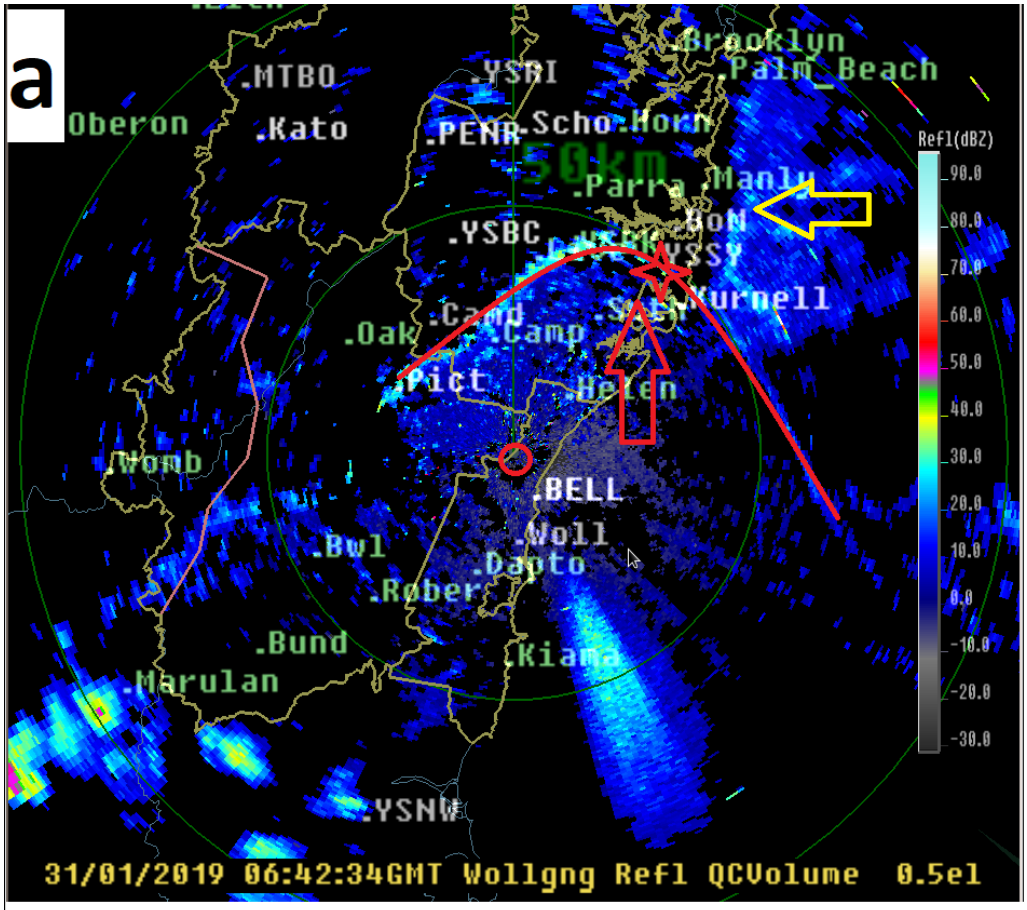
a
.MTBO
YSRI
Brooklyn
Palm_Beach
Oberon
.Kato
.PENR
Scho.Horn
50km
.Parra
Manly
.YSBC
BoM
YSSY
Wurnell
.Oak
.Camp
Pict
Helen
.Womb
.BELL
.Woll
.Bwl
.Dapto
.Rober
.Bund
.Kiama
.Marulan
.YSNW
Refl(dBZ)
90.0
80.0
70.0
60.0
50.0
40.0
30.0
20.0
10.0
0.0
-10.0
-20.0
-30.0
31/01/2019 06:42:34GMT Wollgng Refl QCVolume 0.5el

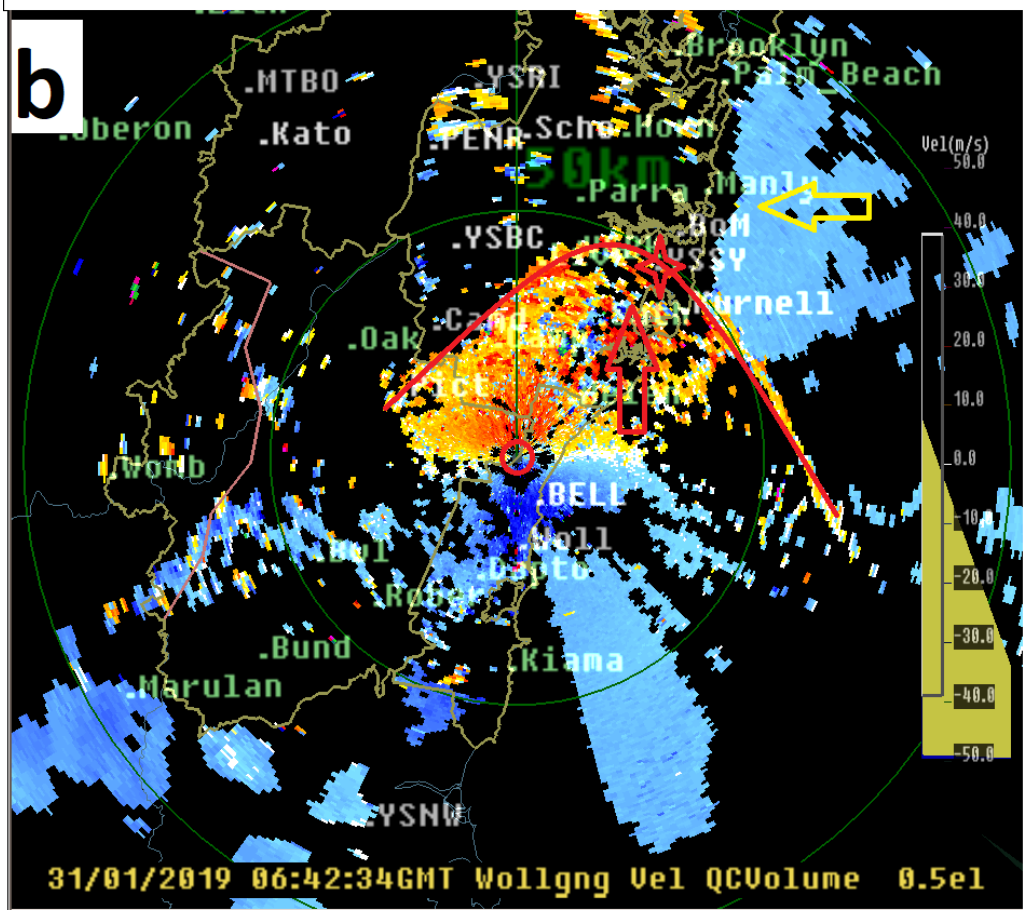
b
.MTBO
YSRI
Brooklyn
Palm_Beach
.Kato
.PENR
50km
.Parra
Manly
.YSBC
BoM
YSSY
Wurnell
.Oak
.Womb
.BELL
.Woll
.Bund
.Kiama
.Marulan
.YSNW
Vel(m/s)
50.0
40.0
30.0
20.0
10.0
0.0
-10.0
-20.0
-30.0
-40.0
-50.0
31/01/2019 06:42:34GMT Wollgng Vel QCVolume 0.5el

Figure 48: 0.5-degree elevation reflectivity and velocity radar scans from Wollongong radar at 0640 UTC SSB at Sydney Airport.

a): reflectivity radar scan. b): velocity radar scan. Sydney Airport is at the four-point star and Wollongong radar location is at the red circle. The red up arrow represents the southerly airmass and the yellow left arrow represents the sea breeze airmass. The red line is the boundary between southerly airmass and northerly flows (including prefrontal hot and dry north westerly flow and north easterly sea breeze). Range rings are at 50km and 100km from the radar.

From the Wollongong radar scans at 0642 UTC two minutes after the SSB occurred at Sydney Airport in Figure 48 the distinctive narrow line can be seen from both reflectivity (a) and velocity (b) scans, the line is highlighted in red which represents the boundary between southerly air mass and northerly flows (including prefrontal hot dry north westerly flow which is not shown in the radar images and north easterly sea breeze in left yellow arrow area). The Wollongong radar is in the south of the Sydney Airport. The winds in red up arrow area behind the red line are southerly flows but in two colours which is the same as the Kurnell radar but different from the Terry Hills radar, this can be explained that when the SSB passes the radar toward north, the winds between the Wollongong radar and Sydney Airport are moving away from the radar in yellow echoes from velocity scan image, the winds south of the Wollongong radar are moving towards the radar in blue echoes. The winds ahead of the changing line (red line) are north easterly sea breeze in blue in the left yellow arrow area, which are moving towards the Wollongong radar. The hot and dry prefrontal north westerly flow are not clear from the Wollongong radar (Figure 48 b).

In summary, the southerly change can be detected by low level radar scan images both at reflectivity scans and velocity scans. The Kurnell radar, Terry Hills radar and Wollongong Radar can all present the boundary of the southerly winds and northerly winds in Sydney Basin.

However, the Terry Hill radar well presents the sea breeze line, so it will present prefrontal dry and hot north-westerly flow, cooler sea breeze and cold strong southerly winds and detect the point where the three types of air mass meet. The point of the three types of airmass where is the maximum density difference between the southerly airmass and the northerly airmass is the leading edge point of the southerly change, this can explain why the leading edge point of the southerly change isn't at the coast but at some point in land near the coast (such as Bankstown and Parramatta) and not further inland (such as Camden). Another reason behind could be Coriolis force, not to be discussed in detail for Coriolis force in the thesis.

5.4.8 Density Current Theory: Application to two SSBs.

The theory of density currents is in detail in Chapter 2: the model cross Section for potential temperatures (°C) and winds below 800hPa (elevation in feet in the right) at 0700UTC on January 31, 2019 along the NSW coast Figure 41 are indicative of a density current. To verify the density current theory, the two SSBs observation data are employed to the equations (1) to (4) in Chapter 2:

$$\rho = P/RT\,, \qquad (1)$$

$$c = \sqrt{gH}. \qquad (2)$$

$$c_{DC} = \sqrt{g'H}\,, \qquad (3)$$

$$\boldsymbol{g}\,(\rho 1\text{-}\rho 2)/\rho 1\,, \qquad (4)$$

For the two SSBs, the density current speeds can be estimated using the observation data from the Sydney Airport.

From Equation (1) and Table 14, for a cool lower layer overlain by a warm upper layer on 20th November 1973:

$$\boldsymbol{\rho_{cold}} = \boldsymbol{P_1/RT_1} = 1007/\ (287.058*292.15) = 0.011985741,$$

$$\boldsymbol{\rho_{warm}} = \boldsymbol{P2/RT2} = 1001/\ (287.058*308.15) = 0.011319478.$$

Hence, $\mathbf{c} = \sqrt{\boldsymbol{g'H}}$, the density current speed

Where $\boldsymbol{g'} = \boldsymbol{g}(\boldsymbol{\rho_{cold}} - \boldsymbol{\rho_{warm}}) \ / \ \boldsymbol{\rho_{cold}} = 0.544762408$ (12)

and, H, the cold air depth (m) at Sydney, is about (1000m), from Figure 35

So, the density current speed:

$$\mathbf{c_{DC}} = \sqrt{\boldsymbol{g'\ H}} = \sqrt{0.544762408 * \mathbf{1000}} = \sim 23.3\text{m/s (}\sim 45.4\text{knots).}$$

(13)

The same way, the density current speeds can be obtained on 31st January 2019:

$$\mathbf{c_{DC}} = \sqrt{\boldsymbol{g'\ H}} = \sqrt{0.524732393 * \mathbf{1000}} = \sim 22.9\text{m/s (}\sim 44.5\text{knots)} \qquad (14)$$

The estimated speed in (18) and (19) are consistent with the observational data from both days at Sydney Airport station observations (see Table 14) which demonstrates the density current theory applies to strong southerly busters.

	20th November, 1973	31st January, 2019
Changing time (UTC)	0605	0630
T_{cold}(K)	292.15	294.75
T_{warm}(K)	308.15	309.95
P_{cold}(hPa)	1007	1014.1
P_{warm}(hPa)	1001	1005.8
ρ_{cold} (kg/m^3)	0.011985741	0.011963776
ρ_{warm}(kg/m^3)	0.011319478	0.011323187
Δρ (kg/m3)	0.000666263	0.00064059
g'(m/s^2)	0.544762408	0.524732393

$C_{dc(\rho)}$(knots)	45.4	44.5
$C_{dc(\rho)}$(m/s)	23.3	22.9
Observed winds (m/s)	15-27	15-25
Rossby L (km)	280	274

Table 14: Details of the density currents for the two SSB

5.4.9 Discussion and Conclusions

The two strong southerly buster events of November 20, 1973 and January 31, 2019 are some in similarity in timing of changing, maximum wind speed, and difference in temperatures and pressure before and after change by Sydney Airport Half hourly METAR and SPECI aviation observation data.

The temperatures before and after change are both lower on November 20, 1973 than on January 31, 2019 which indicates that the temperatures are getting higher compared to 46 years ago, but the difference of the temperatures before and after change are not changing.

The two SSBs both occurred on the synoptic situation when a prefrontal trough was crossing a low which lied between the border of Victoria and NSW, followed by a cold front ahead of the stronger surface high pressure system between the two surface high pressure systems, the type of MSLP chart was a classical southerly buster pattern.

The satellite images and the model guidance show the characteristics of the SSBs which is consistent with the schematic structure.

The Sydney Airport wind profiler data suggests that the depth of SSBs at Sydney is around 1000m which is consistent with the height of the west ranges.

The observation of SSB changing along the NSW coastal stripe shows the maximum winds after change are from YMRY to YWLM, after YWLM which can be explained by the temperature diurnal change and topography in NSW.

The SSB can be detected by low level radar scan images both at reflectivity scans and velocity scans from the Kurnell radar, Terry Hills radar and Wollongong Radar in Sydney region.

The simplified density current model applies to the two SSBs and the results are close to the observation.

5.5 OTHER DENSITY CURRENTS

Other density currents in NSW such as Illawarra downslope winds which often occurs overnight near Illawarra coast when a cold front is passing through. The mean winds over mean winds up to over 30 knots and the gusts in excess of 41 knots are observed Wollongong and Nowra Airport which is a potential hazardous weather phenomenon for aviation. The downslope winds are typical density currents. In pots frontal condition, the cold air over the ranges west of Illawarra coast drops directly from the escarpment to the airport, forming a density current. Aerodrome warning for damaging winds should be issued when downslope winds develop.

Trapped lee wave and large amplitude waves over the Great Dividing Range (GDR) and east of the GDR, from the Snowy Mountains, Brindabella Ranges and other smaller ranges in the south eastern quarter of NSW, via central tablelands Blue Mountains area to the north over the northern Tablelands. SIGMET should be issued for the severe mountain waves.

Figure 48 shows the atmospheric gravity waves in the low level over ahead of a southerly change Tasman Sea. The low level solitary wave train can only be seen in the visible satellite image, but can't be seen from the infrared satellite image. The atmospheric gravity waves are generated in a stable low level boundary layer by the intrusion of colder, denser north-easterly surface air into a warmer northwest upper level atmosphere ahead of the change. The wave train may cause turbulence, wind shear and visibility drop which is potential hazards for low level flights and activities over the water.

In the future work, both Illawarra downslope winds, mountain waves over eastern NSW and gravity waves over the water of NSW are interesting topics which can provide better service for aviation when the forecast is improved.

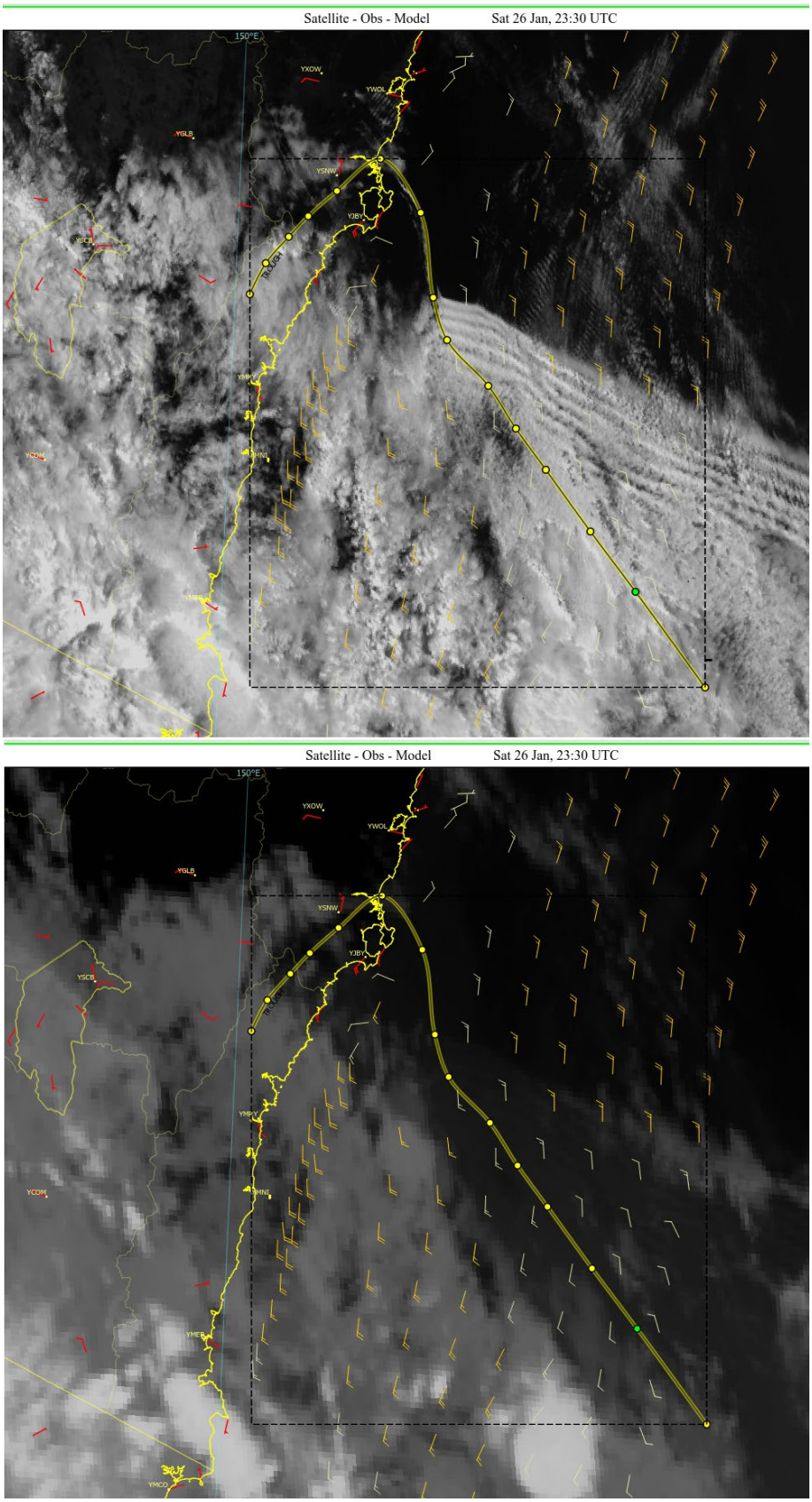

Figure 49: Himawari-8 satellite image at 2330UTC on 26th, January 2019.

Product derived from 10.8μ IR channel, 12.0μ IR channel and 3.9μ NIR channel. Colors based n EUMETSAT standard, interpretation guidance on the up-right corner. The overlain winds are the AWS wind barbs showing wind direction and speed in m/s (white barbs land, short barb=2.5m/s, long barb = 5m/s) and microwave advanced scatterometer (ASCAT) winds (wind barbs sea, short barb=2.5m/s, long barb = 5m/s, data buffer is 22 hours from 20190126).

Chapter 6: Climate Analysis for Southerly Busters

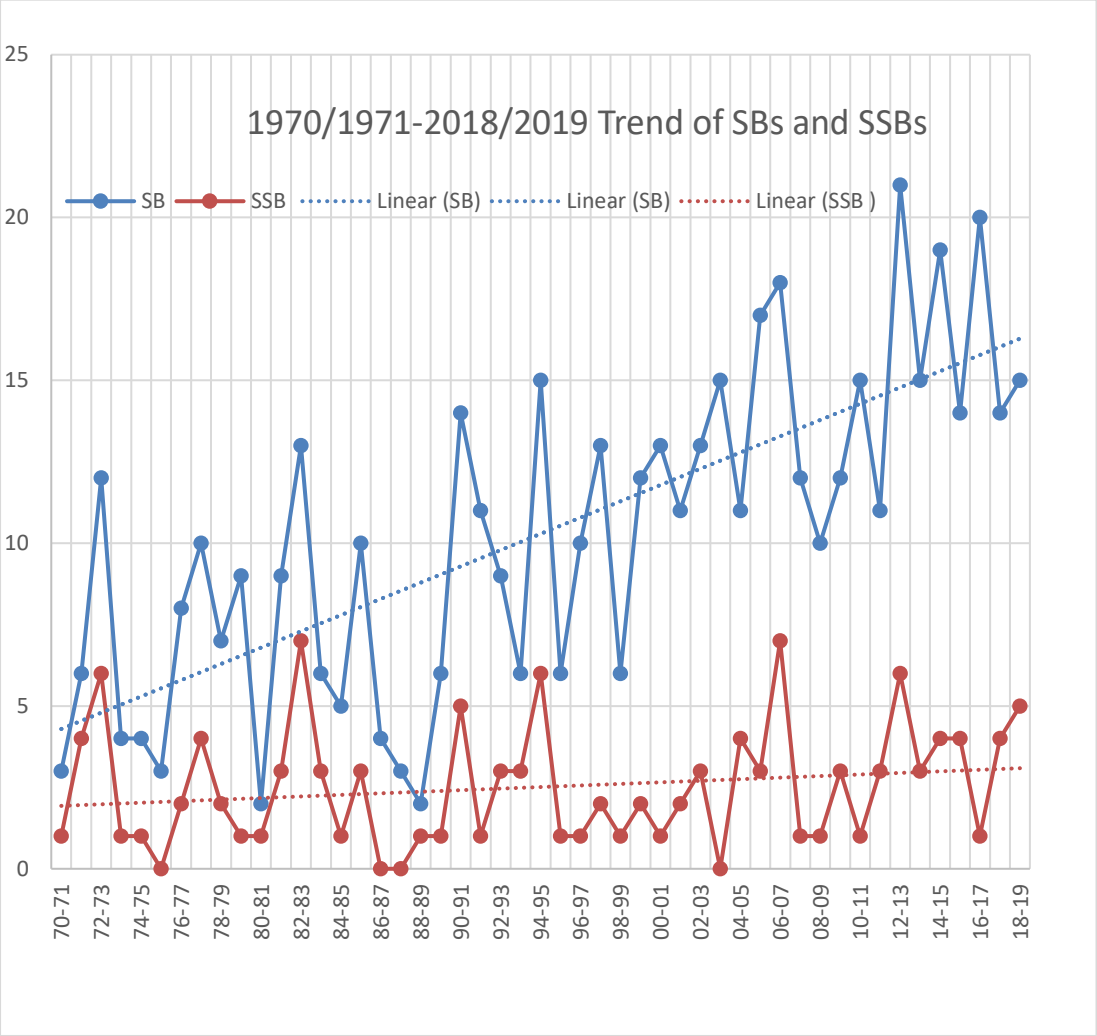

Figure 50: Number of SBs and SSBs trend over Warm Season from 1970/1971 to 2018/2019 at Sydney Airport

Warm season in year for horizontal axis, number of SBs and SSBs for vertical axis. SBs (blue solid line overlain the dot points), SSBs (red solid line overlain the dot points.), SBs linear trend line (blue dash line, m/s), SSBs linear trend line (red dash line, m/s).

Following the data selection criteria, there have been 504 SBs and 123 SSBs over the last 49 years from 1970/1971 to 2018/2019 at Sydney Airport. Figure 49 shows the time series of SBs and SSBs, and their trend lines. The SBs are increasing year by year which is consistent with

the linear trend line. However, the SSBs are not increasing over time, which can be explained using the theory in Section 5.4, the warm air temperatures before the change and the cooler air temperatures after the change are both warming in recent years, but the maximum temperature difference does not increase significantly.

The 504 SBs and 123 SSBs are classified into two groups with 25 years in each period, and with each year overlapped (e.g., 1994-1995) (see Table 15). Permutation testing results for SSB (Figure 51) p-value is 0.708 indicates no significant difference between the time periods 1970-1994 and 1995-2018, however, for SB (Figure 52) the p-value is 0.000, indicating a statistically significant difference between the time periods 1970-1994 and 1995-2018. These results are consistent with Figure 50.

Periods (25years each periods)	SB	SSB
1970-1971 to 1994-1995	181	60
1994-1995 to 2018-2019	338	69

Table 15: Two Periods SBs and SSBs (25 years for each period)

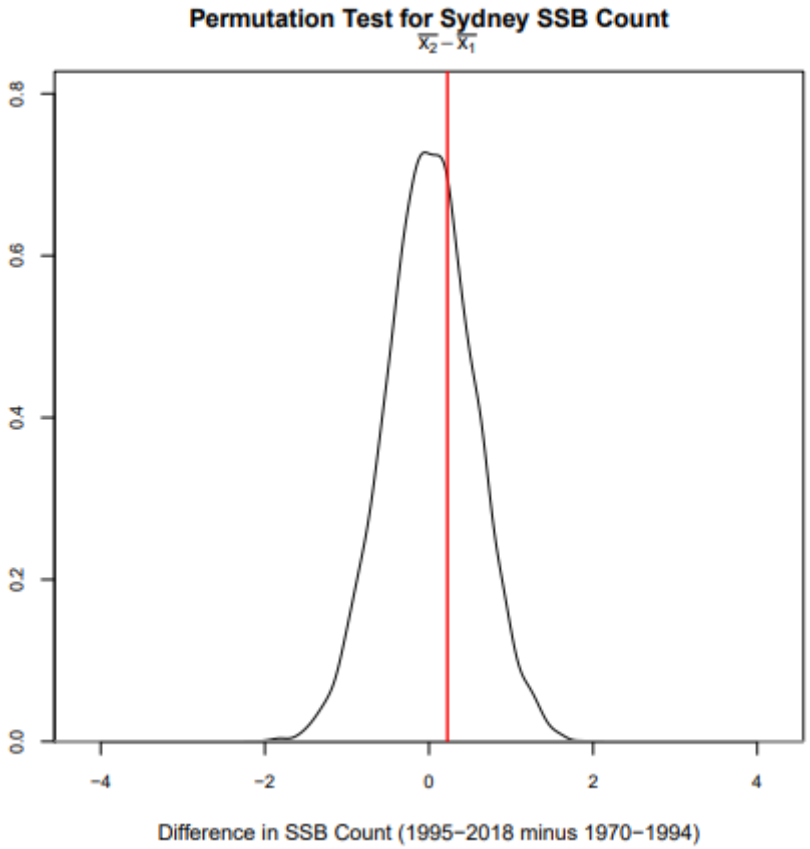

Figure 51: Difference in SSB Count (1995-2018 minus 1970-1994)

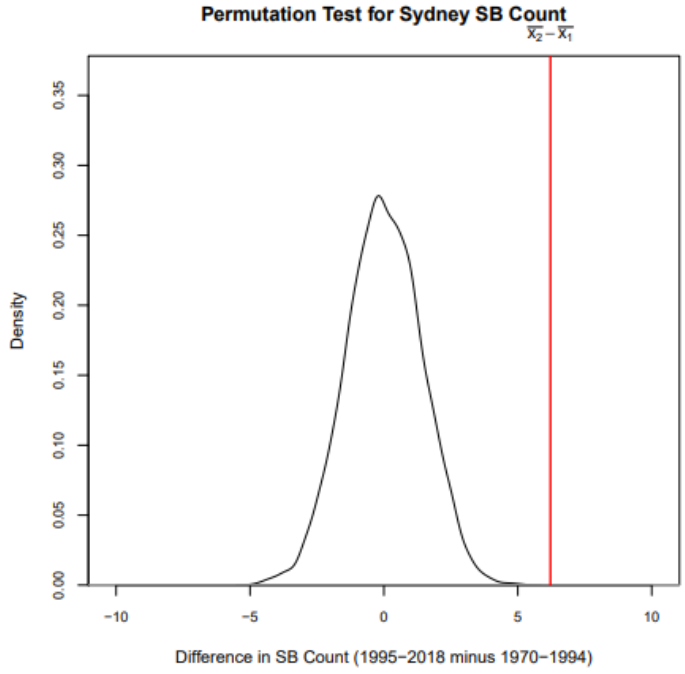

Figure 52: Difference in SB Count (1995-2018 minus 1970-1994)

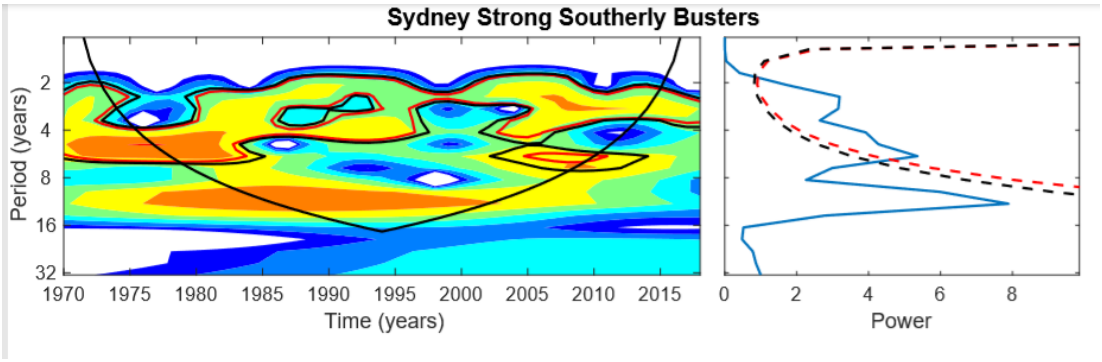

Figure 53: Wavelets for SSB (1970-1994 and 1995-2018).

Meteorological time series such as SBs and SSBs, clearly are nonstationary. Wavelet analysis first de-trends the time series, then reveals the periodic signals (if any) in the time series (Lau and Weng, 1995). Wavelet analysis for total SSBs at Sydney Airport. Low values (blue) in the wavelet power spectrum (left) indicate low variability while high values (red) indicate high variability. Peaks in the global power spectrum (right) on the right panel indicate high variability. The dashed/solid red line indicates the 95% confidence level, while the dashed/solid black line indicates the 90% confidence level in each plot.

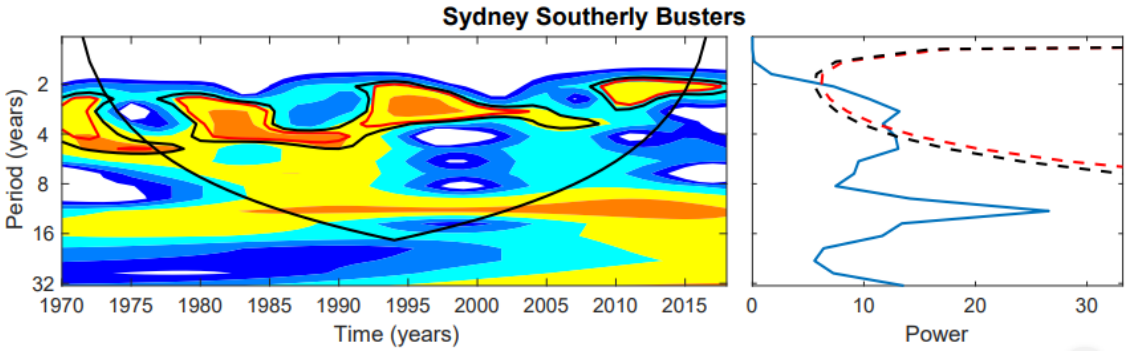

Figure 54: Wavelets for SB (1970-1994 and 1995-2018).

As Figure 53 except for SB.

Figure 53 and Figure 54 display the results for wavelet analysis for total SSBs and SBs at Sydney Airport. The wavelets identify the periodicities and their temporal distribution. Note

the presence of 2-7-year periods (e.g. ENSO and others) and a (statistically not significant) decadal signature as well. The data set is not long, just 49 years, so multi-decadal signals will not appear.

Permutation tests were made with a larger number of permutations; p-values less than 0.05 were obtained.The analysis above shows that the frequency of SBs has increased significantly over the period 1970-2018, but the frequency of SSBs has not changed significantly over the same period. Given that SBs are often associated with hazardous weather, the currently warming climate is generating an increasing number of SBs, and therefore poses an increasing risk to public safety.

Chapter 7: Conclusions

The topic of this thesis is Atmospheric Density Currents: Impacts on Aviation over NSW and ACT. The study focusses on density currents which have significant influence on aviation over NSW. Five experiments have been conducted and a climatological study on the southerly busters at Sydney Airports has been carried out. The results have been achieved are shown below:

In Section 5.1, a Trapped Southerly Buster and Associated Solitary Waves on October 6-7, 2015 shows that the data analyses support the widespread view that the southerly buster is a density current, coastally trapped by the GDR. In addition, it appears that solitary waves develop in this event because the prefrontal boundary layer is shallow and stable. A simplified density current model produced speeds matching well with observational southerly buster data, at both Nowra and Sydney airports. Extending the density current theory, to include inertia-gravity effects, suggests that the solitary waves travel at speeds approximately 20% faster than the density current. This speed difference is consistent with the high-resolution satellite data, which shows the solitary waves moving increasingly ahead of the leading edge of the density current.

In Section 5.2, a short gusty wind event associated with a squall line, presents a detailed analysis of a short-lived gusty wind event associated with a long-lived squall line on the northwest of New South Wales (NSW) on 13th December 2019. The damaging winds were generated by density current propagation and downward transfer of horizontal momentum from the thunderstorm downdrafts of a squall line. The low-pressure system and the prefrontal trough provided a synoptic environment for a squall line development. Observations of the six

stations over the northwest region of NSW showed that the winds caused by a squall line are extremely strong and the duration was from 2 minutes to 12 minutes which indicated a quall line caused a large-scale downburst including macroburts and microburst of this event. The satellite images disclosed the damaging winds were associated with the GPATS over last 10 minutes, further confirmed the damaging winds were caused by the thunderstorms. The sounding data from Moree airport showed a deep dry adiabatic layer below the cloud base, a deep layer moisture, a dry slot in the middle level, strong westerly steering winds and large value of CAPE which are all the favourite conditions for causing damaging winds.24 hours forward trajectories for air parcels display the time of the maximum wind gusts were consistent with the maximum mix depth. The convective parameters and indices showed some of the parameters and indices were met the threshold of the operational guidance for thunderstorm damaging winds, but some of them were not met the criteria, this induced a good reason to nudge the operational guidance.

In Section 5.3, density current event over NSW and ACT, discloses that the easterly change mechanisms include mesoscale sea breezes, differential heating at both meso and continental scales and coastal ridging. All the mechanisms lead to temperature difference and pressure difference. The density current theory applies to the easterly change. There are totally 25 times easterly changes during the 2018/2019 summer season, the timing of change is mostly between 0800 UTC and 0900 UTC. The wind change always plays an important role for airport operation. The easterly change at Canberra Airport often occurs in the late afternoon and evening in summertime, then propagates to the further inland airports such as Wagga Wagga, Temora, and Young in the late evening. The easterly change experiences from unstable daytime to stable night, the boundary layer and a low-level nocturnal jet is not considered in this study. The speed of easterly change propagating to the west and how west is a possible future extension of this research.

In Section 5.4, the two strong southerly buster events of November 20, 1973 and January 31, 2019 have some similarity in timing of changing, maximum wind speed, and difference in temperatures and pressure before and after change by Sydney Airport half hourly METAR and SPECI aviation observation data. The temperatures before and after change are both lower on November 20, 1973 than on January 31, 2019 which indicates that the temperatures are getting higher compared to 46 years ago, but the difference of the temperatures before and after change are not changing. The two SSBs both occurred in a synoptic situation when a prefrontal trough was crossing a low which lied between the border of Victoria and NSW, followed by a cold front ahead of the stronger surface high pressure system between the two surface high pressure systems. The MSLP chart showed a classical southerly buster pattern. The satellite images and the model guidance show the characteristics of the SSBs which is consistent with the schematic structure. The Sydney Airport wind profiler data suggests that the depth of SSBs at Sydney is around 1000m which is consistent with the height of the west ranges. The observation of SSB changing along the NSW coastal stripe shows the maximum winds after change are from YMRY to YWLM, after YWLM which can be explained by the temperature diurnal change and topography in NSW. The SSB can be detected by low level radar scan images both at reflectivity scans and velocity scans from the Kurnell radar, Terry hills radar and Wollongong Radar in Sydney region. The simplified density current model applies to the two SSBs and the results are close to the observation.

In Section 5.5, other density currents over NSW and ACT such as Illawarra downslope winds, mountain waves and prefrontal low level solitary waves are to be studied in the future.

In Chapter 6, a climate analysis of southerly busters found a significant increase in number of SBs over last 49 years; however, the SSBs had no trend in frequency of occurrence.

The study has employed data sets using different sensing platforms to identify the features of density currents. The results of this study could provide a good reference for aviation

forecasters as well as for aviation customers such as pilots, airlines and air traffic control. For aviation forecasters, they can provide more timely and accurate forecasts; for aviation customers, they can make better decision and get better operational managements.

Bibliography

Allen, J., Karoly, D.J., Mills, G. A., 2011: A severe Thunderstorm Climatology for Australia and Associated thunderstorms environments. Australian Meteorological and Oceanographic Journal. 61:143-158

"Australian Demographic Statistics, Jun 2019". 19 December 2019. Retrieved 19 December 2019. Estimated Resident Population – 1 June 2019

Baines, P. G., 1980: The dynamics of the southerly buster. Australian Meteorological. Magazine, 28, 175–200.

Bender, F. A. M., V. Ramanathan, and G. Tselioudis, 2012: Changes in extratropical storm track cloudiness 1983–2008: Observational support for a poleward shift. Climate Dyn., 38, 2037–2053,doi:https://doi.org/10.1007/s00382-011-1065-6.

Bluestein HB, Jain MH. 1985. Formation of mesoscale lines of precipitation: Severe squall lines in Oklahoma during the spring. Journal of the Atmospheric Sciences 42: 1711–1732.

Bureau of Meteorology, 2020. http://www.bom.gov.au/marine/knowledge-centre/hazards.shtml

Callum Shakespeare Spontaneous generation of internal waves: Physics Today: Vol 72, No 6, 34 (2019); https://doi.org/10.1063/PT.3.4225

Christie, D.R., 1983. Solitary waves as aviation hazard, Eos Trans. AGU.

Clarke, R.H., 1961. MESOSTRUCTURE OF DRY COLD FRONTS OVER FEATURELESS TERRAIN. Journal of Meteorology, 18(6): 715-735.

Colquhoun, J.R., Shepherd, D.J., Coulman, C.E., Smith, R.K. and McInnes, K., 1985. The Southerly Burster of South Eastern Australia: An Orographically Forced Cold Front. Monthly Weather Review, 113(12): 2090-2107.

Coniglio, M.C., Brooks, H.E., Weiss, S.J. and Corfidi, S.F. (2007). Forecasting the Maintenance of Quasi-Linear Mesoscale Convective Systems. Wea. Forecasting, 22, 556–570.

Coulman, C., 1985. Orographically forced cold fronts: mean structure and motion, Boundary-Layer Meteorology, Dordrecht, Holland, pp. 57-83.

"Domestic aviation activity" (PDF). Bureau of Infrastructure, Transport and Regional Economics. Retrieved 4 January 2020.

Draxler, R.R. and Hess, G.D. (1998). An Overview of the HYSPLIT_4 Modelling System for Trajectories, Dispersion on and Deposition. Australian Meteorological Magazine, 47, 295-308.

Egger, J., and K. P. Hoinka, 1992. Fronts and orography. Meteorology and Atmosheric Physics, 48, 3–36.

Evans, J.S. and C.A. Doswell (2001). Examination of derecho environments using proximity soundings. Weather Forecasting, 16, 329-342.

Fu, Q., C. M. Johanson, J. M. Wallace, and T. Reitchler, 2006: Enhanced mid-latitude tropospheric warming in satellite measurements. Science, 312, 1179, doi:https://doi.org/10.1126/science.1125566.

Fyfe, J. C., N. P. Gillett, and G. J. Marshall, 2012: Human influence on extratropical Southern Hemisphere summer precipitation. Geophys. Res. Lett., 39, L23711, doi:https://doi.org/10.1029/2012GL054199.

Garratt J.R. 1988 "Summertime Cold Fronts in Southeast Australia - Behaviour and Low- Level Structure of Main Frontal Types" Monthly Weather Review Vol 116, pp.636-649

Garratt, J., 1986. Boundary-layer effects on cold fronts at a coastline, Boundary-Layer Meteorol, pp. 101-105.

Garratt, J.R., 1994. Review: the atmospheric boundary layer, Earth Science Reviews, pp. 89-134.

Geerts, B., 2001. Estimating Downburst-Related Maximum Surface Wind Speeds by Means of Proximity Soundings in New South Wales, Australia, Weather and Forecasting, pp. 261-269.

Gillett, N. P., J. C. Fyfe, and D. E. Parker, 2013: Attribution of observed sea level pressure trends to greenhouse gas, aerosol, and ozone changes. Geophys. Res. Lett., 40, 2302–2306, doi:https://doi.org/10.1002/grl.50500.

Gentilli, J., 1969. SOME REGIONAL ASPECTS OF SOUTHERLY BUSTER PHENOMENA. Weather, 24(5): 173-184.

Gill, A.E., 1977. Coastally trapped waves in the atmosphere, Q.J.R. Meteorol. Soc., pp. 431-440.
Gill, A.E. 1982. Atmosphere-Ocean Dynamics. Academic Press. London. Chapter 8.
Holland, G.J. and Leslie, L.M. 1986. Ducted coastal ridging over S.E. Australia, Quarterly Journal of the Royal Meteorological Society., 731-748.
Gillett, N.P. and Thompson, D.W.J., 2003. Simulation of recent southern hemisphere climate change, Science (New York, N.Y.), pp. 273-275.
Grise, K.M. and Polvani, L.M., 2014. Is climate sensitivity related to dynamical sensitivity? A Southern Hemisphere perspective, Geophys. Res. Lett., pp. 534-540.
Grundstein, A., Shepherd, M. and Miller, P., 2017. The Role of Mesoscale-Convective Processes in Explaining the 21 November 2016 Epidemic Thunderstorm Asthma Event in Melbourne, Australia.(Report)(Author abstract), Journal of Applied Meteorology and Climatology, pp. 1337-1343.
Hjelmfelt, M.R., 2007. Plant Disturbance Ecology, Plant Disturbance Ecology, pp. 59-101.
Holland, G.J. and Leslie, L.M., 1986. Ducted coastal ridging over S.E. Australia, Q.J.R.
Meteorol. Soc., pp. 731-748. http://www.airservicesaustralia.com/wp-content/uploads/12-139FAC_NCIS-Runway-selection_P2.pdf (runway selection)
http://www.eumetrain.org, Shallow Cold Fronts. In: http://www.eumetrain.org (Editor), http://www.eumetrain.org/satmanu/CMs/ShCF/navmenu.php?page=2.0.0.
http://www.nssl.noaa.gov/users/mcon/public_html/2005_summer_exp_plan.pdf
https://www.sydneyairport.com.au/corporate/sustainability/community/aviation-enthusiasts (Sydney Airport runway)
ICAO, 2016. Annex 3 to the Convention on International Civil Aviation,International Standards and Recommended Practices, Meteorological Service for International Air Navigation.
J.Hartigan et al., 2018: Trends in Precipitation and Temperature in Canberra
Liu, C.-H., and M. W. Moncrieff, 1996: A numerical study of the effects of ambient flow and shear on density currents. Monthly Weather Review.,124, 2282–2303.
Klimowski BA, Bunkers MJ, Hjelmfelt MR, Covert JN. 2003. Severe convective windstorms over the northern high Plains of the United States. Weather and Forecasting 18: 502–519.
Kraus, H., Ewenz, C.M., Kremer, M. and Hacker, J.M., 2000. The Multi-Scale Structure of the Australian Cool Changes, Meteorol Atmos Phys, pp. 157-175.
Lau, K. and H. Weng, 1995: Climate Signal Detection Using Wavelet Transform: How to Make a Time Series Sing. Bull. Amer. Meteor. Soc., 76, 2391–2402.
Mass, C. E., and M. D. Albright, 1987: Coastal southerlies and alongshore surges of the west coast of North America: Evidence of mesoscale topographically trapped response to synoptic forcing. Monthly Weather Review.,115, 1707–1738.
McInnes, K.L. and McBride, J.L., 1993. Australian Southerly Busters. Part I. Analysis of a Numerically Simulated Case Study. Monthly Weather Review, 121(7): 1904-1920.
McInnes, K. L., 1993b: Australian southerly busters. Part III: The physical mechanism and synoptic conditions contributing to development. Monthly Weather Review.,121, 3261–3281.
Miles, J. W. 1980. Solitary waves. Annu. Rev. Fluid Mech.. 12. 11–43.
NASA Langley Air Force Base. Making the Skies Safer From Windshear. Retrieved on 29 March 2010.
Orlanski, I., 2013: What controls recent changes in the circulation of the Southern Hemisphere: Polar stratospheric or equatorial surface temperatures? Atmos. Climate Sci., 3, 497–509, doi:https://doi.org/10.4236/acs.2013.34052.
Whiteman,C.D. 2000. Mountain Meteorology: Fundamentals and Applications, Oxford University Press.
Reason, C., 1994. Orographically trapped disturbances in the lower atmosphere: Scale analysis and simple models, Meteorology and Atmosheric Physics., 53, 131-136.
Pryor, K.L., 2015. Progress and Developments of Downburst Prediction Applications of GOES. Weather and Forecasting, 30(5): 1182-1200.
Rasuly, A.A., Cheung, K.K.W. and Mcburney, B., 2015. Hail events across the Greater Metropolitan Severe Thunderstorm Warning Area, Natural Hazards and Earth System Sciences, pp. 973-984.
Reason, C., 1994. Orographically trapped disturbances in the lower atmosphere: Scale analysis and simple models, Meteorl. Atmos. Phys., pp. 131-136.
Reason, C.J.C. and Steyn, D.G., 1990. Coastally trapped disturbances in the lower atmosphere: dynamic commonalities and geographic diversity, Progress in Physical Geography, pp. 178-198.
Reason, C.J.C. and Steyn, D.G., 1992. Dynamics of Coastally Trapped Mesoscale Ridges in the Lower Atmosphere. American Meteorological Society.

Reason, C.J.C., Tory, K.J. and Jackson, P.L., 1999. Evolution of a Southeast Australian Coastally Trapped Disturbance, Meteorol Atmos Phys, pp. 141-165.
Reid, H. and Leslie, L., 1999. Modeling coastally trapped wind surges over southeastern Australia. Part I: Timing and speed of propagation, Weather and Forecasting, Boston, MA, pp. 53-66.
Ripa, P. 1982. Nonlinear wave-wave interactions in a one-layer reduced-gravity model on the equatorial beta-plane. Journal of Physical Oceanography., 12, 97–111
^ "SOUTHERLY BUSTER". Wellington Times. NSW: National Library of Australia. 23 December 1901. p. 2. Retrieved 27 March 2015.
Solman, S. A., and I. Orlanski, 2014: Poleward shift and change of frontal activity in the Southern Hemisphere over the last 40 years. J. Atmos. Sci., 71, 539–552, doi:https://doi.org/10.1175/JAS-D-13-0105.1.
Speer, M. and Geerts, B., 1994. A synoptic mesoalpha-scale climatology of flash floods in the Sydney Metropolitan area. Aust. Meteor. Mag., 43: 87-103.
Speer, M.S. and Leslie, L.M., 1997. A climatology of coastal ridging over south‐eastern Australia, Int. J. Climatol., pp. 831-845.
Taylor, J. R., M. Kossmann, D. J. Low, and P. Zawar-Reza, 2005: Summertime easterly surges in southeastern Australia: A case study of thermally forced flow. Aust. Meteor. Mag., 54(3): 213-223.
Torrence, C. and G. Compo (1998). A Practical Guide to Wavelet Analysis. Bulletin of the American Meteorological Society 79, 61–78.
Thompson, D.W.J. and Solomon, S., 2002. Interpretation of recent Southern Hemisphere climate change, Science (New York, N.Y.), pp. 895-899.
United States, F.A.A., 1975. Aviation weather for pilots and flight operations personnel. Washington: Federal Aviation Administration.

Appendices

Appendix 1: ICAO ID of Airports mention in the Thesis

ICAO ID.	Name
YGBO	Gabo Island
YMER	Merimbula AP AWS
YMRY	Moruya AP AWS
UDAX	Ulladulla AWS
YSNW	Nowra AWS
KIAM	Kiama AWS
KURN	Kurnell AWS
YSCN	Camden AP
YSSY	Sydney AP
YSRI	Richmond AP
YWLM	Williamtown
YTRE	Taree AP AWS
YPMQ	Port Macquarie AP AWS
MVI	Mount Victoria
YBKE	Bourke
YWLG	Walgett

YCNM	Coonamble
YNBR	Narrabri
YMOR	Moree
YGDH	Gunnedah

Appendix 2: The Observation of SSB at Sydney Airport on January 31, 2019

Time	Wnd dir	Wnd spd	Max Wnd Gust	Air Tp	Dew Pt	QNH Pres	Vis	Cloud	Cloud_1
1900	190	16	20	18.7	18	1019.8	9000	2St600	5St1400
1830	190	17	21	18.8	18.1	1019.5	7000	2St700	5St1400
1825	190	18	23	19	18.3	1019.4	6000	3St800	5St1400
1800	190	19	22	18.8	18	1019.3	6000	3St800	4St1500
1730	190	18	24	19.3	17.8	1019	6000	2St1000	7Sc2000
1700	180	19	27	20.1	17.5	1018.6	9000	2St2000	7Sc3000
1630	190	21	27	20.8	17.2	1018.5	10000	1St2000	8Sc3200
1600	190	19	23	20.6	17	1018.4	10000	1St2000	8Sc3200
1530	180	21	27	20.8	17	1018.3	10000	1St1800	7Sc2500
1500	190	21	26	20.7	17.7	1018.3	10000	1St1800	7Sc2500
1430	190	21	28	20.5	17.9	1018.4	10000	2St1800	7Sc2800
1400	190	21	27	20.9	16.9	1018.4	10000	1St2000	7Sc2700
1330	180	22	31	21.5	17.3	1018.1	10000	1St1800	8Sc2400
1300	180	23	31	21.4	17.4	1018	10000	Sc2400	
1230	180	22	30	21.4	17.6	1017.9	10000	Sc2600	
1200	180	24	32	21.5	17.5	1017.6	10000	Sc2500	
1130	180	23	29	21.7	17.9	1017.3	10000	1St1800	7Sc2400
1100	190	26	36	21.5	17.5	1016.8	10000	3St2200	7Sc3000
1030	190	28	38	21.4	17.6	1016.2	10000	2St1800	7Sc2300
1000	180	31	41	21.6	18.4	1015.1	10000	1St1400	8Sc2500
0930	180	31	41	21.6	19.3	1014.1	8000	1St1200	7Sc2000
0900	180	36	48	21.8	19.2	1012.6	8000	1St1500	7St1900
0830	180	36	49	21.9	18.9	1011.3	7000	7St1500	
0800	190	35	45	22.5	19.7	1009.9	6000	5St1500	
0730	190	35	45	23.6	20.1	1009.2	7000	1St1400	Ac10000
0700	190	36	46	24	19.7	1008.7	7000	1St1400	Ac10000
0646	190	39	47	25.2	18.2	1007.1	6000	1St1500	Ac10000
0644	180	27	48	26.4	17.5	1007.9	6000	1St1500	Ac10000
0641	180	24	30	28.2	15.1	1007.7	10000	1St1800	Ac10000
0640	180	23	29	34	16.8	1007.4	10000	1St1800	Ac10000
0630	50	17	20	36.8	16.4	1005.8	10000	3 11500	
0600	360	8	15	39.8	14.1	1005.6	10000		

0530	360	11	16	39.7	14.7	1005.7	10000		
0500	350	7	10	39.8	13.4	1005.9	10000		
0430	310	6	8	38.9	14.7	1006.1	10000	1Cu4000	
0400	330	10	17	38.8	15.8	1006.5	10000	1Cu4000	
0330	350	13	18	38.3	15.4	1006.9	10000	1Cu3000	
0300	10	12	15	38	15.7	1007	10000	1St2000	
0230	330	10	14	37	14.9	1007.5	10000		
0200	330	12	17	36.9	15.4	1007.9	10000		
0130	340	13	19	36.5	15	1008.2	10000		
0100	320	14	20	36.4	15.5	1008.4	10000		
0030	330	13	18	35.2	15	1008.7	10000		
0000	350	13	17	34	15.5	1008.8	10000		

Appendix 3: Days of SBs and SSBs at Sydney Airport over last 49 years

Year (Oct-Mar)	SB (Day)	SSB (Day)
1970-71	3	1
1971-72	6	4
1972-73	12	6
1973-74	4	1
1974-75	4	1
1975-76	3	0
1976-77	8	2
1977-78	10	4
1978-79	7	2
1979-80	9	1
1980-81	2	1
1981-82	9	3
1982-83	13	7
1983-84	6	3
1984-85	5	1
1985-86	10	3
1986-87	4	0
1987-88	3	0
1988-89	2	1
1989-90	6	1
1990-91	14	5
1991-92	11	1
1992-93	9	3
1993-94	6	3
1994-95	15	6
1995-96	6	1
1996-97	10	1
1997-98	13	2

1998-99	6	1
1999-2000	12	2
2000-01	13	1
2001-02	11	2
2002-03	13	3
2003-04	15	0
2004-05	11	4
2005-06	17	3
2006-07	18	7
2007-08	12	1
2008-09	10	1
2009-10	12	3
2010-11	15	1
2011-12	11	3
2012-13	21	6
2013-14	15	3
2014-15	19	4
2015-16	14	4
2016-17	20	1
2017-18	14	4
2018-19	15	5
Total	504	123

Appendix 4: Details of SSBs for the 49 year period (1971-2019)

Year	Month	Day	Hours (UTC)	direction	speed (m/s)	gust (m/s)
1971	1	20	0125	180	13.4	20.6
1971	10	31	0555	200	16.5	21.1
1971	12	4	0855	190	13.4	20.6
1971	12	14	0755	180	15.4	21.6
1972	1	12	2125	180	14.4	20.6
1972	12	2	1205	190	14.9	26.2
1972	12	11	0740	210	16.5	21.1
1972	12	22	0820	180	16.5	22.6
1972	12	30	0925	200	13.9	21.1
1973	1	3	1255	160	15.4	22.6
1973	2	6	0910	170	17	23.7
1973	11	20	0605	180	15.4	26.8
1974	11	12	0335	180	12.9	20.6
1977	2	1	0510	180	15.4	22.1
1977	2	18	1100	200	15.4	22.6
1977	10	29	0600	190	17	24.2
1977	11	14	0832	180	11.3	20.6

1977	12	27	0730	190	15.4	23.7
1978	1	10	1302	190	15.4	25.2
1979	1	7	1230	200	15.4	20.6
1979	2	13	0930	190	11.3	23.2
1980	1	15	0630	200	12.3	21.1
1980	10	23	2000	190	13.9	21.6
1981	12	3	0730	190	13.4	21.1
1982	2	9	0700	180	14.9	23.2
1982	3	8	1400	190	15.4	22.6
1982	10	4	0730	190	13.4	21.1
1982	11	7	0930	200	14.9	21.1
1982	11	16	0816	190	13.4	21.6
1982	11	25	0530	210	14.4	22.1
1982	12	1	0630	200	13.4	20.6
1983	1	23	1300	190	14.4	20.6
1983	2	17	0001	200	15.4	25.2
1983	12	25	0445	190	13.4	22.1
1984	1	26	0415	190	12.9	20.6
1984	3	27	0700	200	12.3	20.6
1985	1	15	0930	180	13.4	21.1
1985	10	24	2330	170	12.3	21.6
1986	1	2	0930	190	12.3	21.1
1986	2	2	0830	170	12.3	21.6
1989	2	19	0330	180	12.3	20.6
1989	12	20	0625	190	15.4	23.7
1990	11	1	1030	180	12.9	20.6
1990	12	18	0900	170	14.4	25.7
1990	12	23	0600	180	14.4	20.6
1991	2	14	0930	170	11.8	23.7
1991	2	16	0300	180	13.9	20.6
1991	10	6	1010	180	12.9	21.1
1993	1	3	1230	180	14.4	22.1
1993	1	21	0700	190	15.4	24.7
1993	1	25	0300	180	12.9	21.6
1993	2	4	0830	190	14.9	22.6
1994	1	17	0544	200	12.9	20.6
1994	2	27	2000	180	14.4	23.1
1994	10	17	1026	190	15.9	21.6
1994	10	20	1530	200	14.9	21.6
1994	12	21	1010	200	14.9	21.1
1994	12	28	1545	190	17	26.2
1995	2	3	1127	190	14.9	21.1
1995	3	12	0813	200	11.3	21.6
1995	10	19	2315	180	14.4	21.1
1996	12	26	0451	170	15.9	22.6

1998	2	27	0433	180	16.5	22.1
1998	3	24	0340	170	15.4	21.6
1998	12	15	0746	180	9.8	22.1
1999	12	11	1200	180	15.4	21.1
2000	2	5	1427	180	15.9	21.1
2001	1	15	0759	160	21.6	27.8
2001	11	18	0619	180	15.4	22.6
2002	2	11	0258	200	14.9	21.6
2003	1	8	0544	180	17.5	26.2
2003	1	18	0917	180	15.9	21.1
2003	1	26	1530	180	15.4	20.6
2004	11	28	0752	200	14.9	21.6
2004	12	1	0523	180	19	23.1
2004	12	19	0930	190	16.5	20.6
2004	12	27	0600	200	17	22.1
2005	11	15	0122	190	15.4	21.1
2006	1	1	1004	200	18.5	21.6
2006	2	6	1100	190	15.4	21.1
2006	10	8	0202	210	14.9	20.6
2006	10	20	1200	190	14.4	20.6
2006	11	16	0130	200	15.9	21.6
2006	11	22	0630	190	17.5	20.6
2006	11	29	0541	170	14.4	20.6
2006	12	11	0839	190	19	21.6
2007	3	24	0720	200	14.9	22.6
2007	10	19	1300	190	14.9	20.6
2009	1	15	0509	180	13.9	22.6
2009	11	22	1331	180	17.5	22.1
2010	1	23	0418	190	16.5	23.1
2010	3	21	1012	200	17	21.6
2010	11	18	1610	200	15.4	20.6
2011	2	6	0244	190	15.4	20.6
2011	10	30	0930	180	15.9	20.6
2011	11	14	1030	190	15.4	20.6
2012	3	21	1430	190	15.4	21.1
2012	10	22	0136	180	15.9	21.1
2012	11	21	1330	180	14.9	20.6
2012	12	9	0030	190	16.5	22.6
2012	12	16	1100	200	17	21.6
2013	1	18	0900	190	18	23.7
2013	2	1	0330	180	16.5	21.6
2013	10	10	1200	190	16.5	22.1
2013	11	3	0510	170	15.9	21.1
2013	12	28	1853	180	17	22.1
2014	10	19	1900	190	17	21.1

2014	11	14	0948	200	19	21.1
2015	3	1	0434	190	20.1	26.7
2015	10	6	1830	190	15.9	21.1
2015	10	26	0930	190	15.4	20.6
2016	1	14	0422	210	22.6	31.4
2016	2	25	1900	190	14.9	20.6
2016	12	17	1100	180	15.4	20.6
2017	10	30	0600	190	15.4	22.6
2017	12	20	0430	180	15.9	21.1
2018	1	9	0802	200	15.9	22.6
2018	2	14	1100	180	15.4	20.6
2018	10	23	1444	190	15.4	21.1
2018	12	2	0639	180	15.4	20.6
2018	12	21	1730	200	15.9	21.1
2019	1	23	0400	190	16.5	22.1
2019	1	31	0644	180	13.9	24.7

Appendix 5: Details of SBs for the 49 year period (1971-2019): separated by green colour for each year

Year	Month	Day	Hours	direction	speed (m/s)	gust (m/s)
1970	10	20	0555	190	15.4	0
1970	12	5	0355	180	15.4	0
1971	1	9	1155	190	15.4	0
1971	10	31	0507	180	17	0
1971	11	25	0125	170	13.4	18
1971	11	29	0215	180	11.3	16.5
1971	12	4	0725	190	9.3	15.4
1971	12	14	0755	180	15.4	21.6
1972	1	12	2125	180	14.4	20.6
1972	11	2	1555	200	11.3	16.5
1972	11	6	1325	190	12.9	18
1972	12	2	1205	190	14.9	26.2
1972	12	11	0740	210	16.5	21.1
1972	12	22	0820	180	16.5	22.6
1972	12	23	1102	180	12.3	15.4
1972	12	30	0925	200	13.9	21.1
1973	1	3	1255	160	15.4	22.6
1973	1	31	0920	200	10.3	18.5
1973	2	6	0910	170	17	23.7
1973	3	18	2100	200	10.3	17.5
1973	3	28	1300	180	10.3	18.5
1973	11	20	0605	180	15.4	26.8
1973	12	6	2255	180	10.3	16.5

1974	2	2	0635	170	4.1	15.9
1974	2	6	0325	180	13.4	18
1974	10	12	1730	180	11.3	17.5
1974	11	12	0335	180	12.9	20.6
1974	12	6	2000	190	13.4	18
1975	1	18	0100	180	12.9	16.5
1975	11	25	1140	160	10.3	15.4
1975	12	12	1930	190	11.8	16.5
1976	1	14	2330	190	11.3	15.4
1976	11	26	0405	180	11.3	15.4
1976	12	7	0635	180	10.3	17.5
1976	12	26	1105	190	9.3	15.4
1977	1	16	0702	210	12.9	19
1977	1	30	0700	190	11.8	16.5
1977	2	1	0510	180	15.4	22.1
1977	2	6	0230	180	10.3	16.5
1977	2	18	0945	180	12.9	18.5
1977	10	14	0700	190	10.3	18.5
1977	10	29	0538	190	13.4	20.1
1977	11	14	0832	180	11.3	20.6
1977	12	10	0430	190	11.3	18
1977	12	16	0830	180	12.3	17.5
1977	12	27	0715	190	13.9	20.1
1978	1	10	1302	190	15.4	25.2
1978	2	9	1045	180	12.9	18
1978	2	21	1040	200	12.9	17.5
1978	2	25	0600	180	10.3	15.9
1978	10	27	2359	200	11.3	16.5
1978	10	31	1900	180	11.3	16.5
1978	11	1	0030	180	12.3	18
1979	1	7	1230	200	15.4	20.6
1979	1	10	0710	180	14.4	19.5
1979	2	13	0930	190	11.3	23.2
1979	3	27	2100	200	11.8	18
1979	10	27	0425	210	7.7	16.5
1979	11	1	0700	180	10.3	15.9
1979	12	10	1232	190	11.8	19.5
1979	12	13	0300	180	11.8	15.9
1979	12	23	0830	200	10.3	16.5
1980	1	15	0609	210	10.3	17
1980	2	8	0930	190	8.7	15.4
1980	2	21	1230	190	9.3	15.9
1980	2	24	0845	200	12.9	18
1980	10	23	2000	190	13.9	21.6
1981	1	28	2200	180	9.3	15.4

1981	12	3	0702	190	11.3	16.5
1981	12	5	0813	170	11.3	18.5
1981	12	19	0712	180	9.8	15.4
1982	1	1	1000	170	10.3	16.5
1982	1	7	0610	190	9.3	15.9
1982	2	9	0522	180	9.8	15.9
1982	2	20	2300	190	9.8	15.4
1982	2	23	1905	170	9.8	15.4
1982	3	8	1300	190	9.8	15.9
1982	10	4	0700	200	11.3	17.5
1982	10	8	0822	190	11.3	17.5
1982	10	27	1700	190	8.2	15.4
1982	11	7	0830	200	9.3	16.5
1982	11	10	0700	190	8.7	15.4
1982	11	16	0816	190	13.4	21.6
1982	11	25	0500	200	13.4	19
1982	12	1	0600	190	10.3	17
1982	12	24	1130	190	10.3	15.4
1983	1	23	1200	190	12.3	18.5
1983	2	2	0330	190	10.3	15.9
1983	2	17	0001	200	15.4	25.2
1983	3	9	0622	210	11.3	19.5
1983	12	21	0905	190	10.3	15.4
1983	12	25	0445	190	13.4	22.1
1984	2	23	1600	200	11.3	17.5
1984	2	28	0430	200	14.4	19.5
1984	3	7	1338	190	8.2	15.4
1984	3	27	0650	200	10.3	16.5
1984	12	18	1300	180	11.3	18
1985	1	9	0830	190	11.3	17.5
1985	1	15	0905	190	10.8	17
1985	2	16	0630	180	12.3	18.5
1985	3	4	0850	170	11.3	17.5
1985	10	24	1630	180	9.8	18
1985	11	18	1100	170	9.8	15.4
1985	12	31	0325	180	8.2	19.5
1986	1	2	0930	190	12.3	21.1
1986	1	8	1100	180	10.3	15.9
1986	2	2	0730	170	10.3	18.5
1986	2	9	0700	180	10.3	17.5
1986	3	7	1650	170	9.8	15.9
1986	3	9	1400	180	11.3	19.5
1986	3	15	1030	170	9.3	15.9
1986	12	14	1200	170	9.8	15.4
1987	1	18	1630	160	9.3	15.9

1987	1	21	0830	200	8.7	15.4
1987	2	28	1000	170	4.1	15.9
1987	12	6	0955	180	10.3	15.4
1987	12	16	1830	170	9.3	15.4
1988	2	19	0245	170	7.7	15.4
1988	10	12	0955	160	11.3	20.1
1988	11	3	0930	160	9.3	15.9
1989	10	15	2155	190	10.3	17.5
1989	10	18	2230	190	10.8	17
1989	11	30	1430	180	10.3	15.9
1989	12	20	0625	190	15.4	23.7
1990	1	1	0800	170	10.3	15.9
1990	1	3	1400	180	11.3	18.5
1990	10	5	2100	190	10.3	15.9
1990	10	10	0001	170	11.8	17
1990	10	30	1130	190	10.3	16.5
1990	11	1	1030	180	12.9	20.6
1990	11	29	1030	180	9.3	15.4
1990	12	18	0815	180	12.3	19
1990	12	23	0547	170	10.3	17
1991	2	5	0930	180	9.3	15.4
1991	2	14	0930	170	11.8	23.7
1991	2	16	0135	180	12.3	18
1991	2	26	0333	170	11.8	18
1991	3	9	1630	180	11.3	16.5
1991	3	11	1230	180	12.3	18
1991	3	23	0155	180	10.3	15.4
1991	10	1	2120	190	9.8	19
1991	10	6	1010	180	12.9	21.1
1991	10	10	0945	170	10.3	17.5
1991	10	31	0430	180	10.8	18
1991	11	19	1900	170	10.3	16.5
1991	11	29	0855	200	11.3	18
1991	12	10	0800	170	10.3	15.4
1991	12	28	0001	180	10.3	15.4
1992	1	13	2345	180	10.3	17
1992	1	23	0751	180	11.3	18.5
1992	3	15	1225	190	10.8	16.5
1992	10	25	0600	170	10.3	18
1993	1	3	1230	180	14.4	22.1
1993	1	18	0150	170	11.3	18
1993	1	21	0645	170	12.3	20.1
1993	1	24	2325	170	10.3	17
1993	2	1	1410	180	10.8	18.5
1993	2	4	0750	170	10.3	15.9

1993	2	8	0100	170	10.3	15.9
1993	2	11	2300	190	12.9	19.5
1993	10	10	1030	180	10.8	15.9
1993	10	26	0552	180	10.3	15.4
1993	11	27	1230	180	9.3	168.7
1993	12	1	2130	180	9.3	15.4
1994	1	17	0544	200	12.9	20.6
1994	2	27	1425	190	10.3	16.5
1994	10	8	0735	200	12.3	18
1994	10	17	0946	180	13.4	18.5
1994	10	20	1500	200	13.9	19
1994	11	11	1612	190	10.8	18.5
1994	11	27	1556	200	12.9	18
1994	12	7	1911	190	13.4	17
1994	12	13	1723	180	14.4	18.5
1994	12	21	1000	190	11.8	18.5
1994	12	23	1404	190	11.8	17
1994	12	28	1540	170	10.3	17
1995	1	1	1830	180	12.9	18.5
1995	2	3	1037	190	12.9	19.5
1995	2	10	0006	190	8.2	17.5
1995	3	12	0813	200	11.3	21.6
1995	3	31	0505	180	17	0
1995	10	11	1022	170	10.3	15.9
1995	10	19	2206	190	11.3	18
1995	12	4	1330	180	10.8	16.5
1996	1	20	1817	190	11.3	16.5
1996	1	29	0832	170	10.8	16.5
1996	3	7	0055	180	11.8	17
1996	11	15	1046	190	11.3	16.5
1996	11	18	0028	210	12.3	17.5
1996	12	2	0850	200	8.2	15.9
1996	12	7	0340	190	11.3	16.5
1996	12	9	1000	190	12.3	16.5
1996	12	11	2030	190	11.8	15.9
1996	12	26	0451	170	15.9	22.6
1997	1	7	0427	180	12.3	18.5
1997	1	15	2345	180	10.3	15.9
1997	3	12	2016	180	10.8	15.9
1997	11	11	0900	170	11.3	16.5
1997	11	14	1104	170	15.4	17.5
1997	11	23	1930	160	11.8	15.9
1997	12	2	0840	180	14.9	18.5
1997	12	9	1135	190	10.3	17
1997	12	18	0330	160	12.9	15.9

1997	12	19	0830	180	11.8	15.9
1997	12	26	1027	180	10.3	15.9
1998	1	18	0530	160	12.9	15.9
1998	1	28	1055	160	6.7	15.9
1998	2	12	1700	180	12.3	15.9
1998	2	27	0410	160	14.9	17.5
1998	3	23	1805	170	11.3	16.5
1998	10	7	0646	180	11.3	17
1998	11	15	1830	170	12.3	16.5
1999	1	13	1330	160	12.9	16.5
1999	2	7	0300	160	12.9	16.5
1999	3	7	0000	180	7.7	16.5
1999	3	26	1204	180	7.7	17
1999	10	15	1730	180	11.8	15.9
1999	10	18	0955	180	11.8	17
1999	10	22	0900	180	12.9	17.5
1999	10	31	0732	200	8.2	17.5
1999	12	3	1855	190	11.3	16.5
1999	12	11	1200	180	15.4	21.1
1999	12	19	0330	170	11.3	16.5
2000	1	19	0601	170	10.3	16.5
2000	2	5	1300	170	11.3	16.5
2000	3	4	0034	170	11.3	19
2000	3	18	1534	170	10.3	15.9
2000	3	20	1430	180	12.3	15.9
2000	11	6	0300	180	12.9	15.9
2000	11	30	2358	210	8.2	16.5
2000	12	12	0456	170	8.2	15.9
2001	1	8	0241	180	10.8	15.9
2001	1	13	0108	170	9.8	20.1
2001	1	15	0732	190	17	18.5
2001	1	30	0941	190	10.8	15.9
2001	2	5	0430	180	12.3	17.5
2001	2	10	0407	180	10.3	17.5
2001	2	22	0619	170	9.3	16.5
2001	2	28	0452	170	11.8	15.9
2001	3	12	1117	200	9.3	16.5
2001	3	27	2200	180	11.3	16.5
2001	11	6	2300	200	10.8	15.9
2001	11	13	0450	170	10.8	15.9
2001	11	15	2230	170	12.3	15.9
2001	11	18	0619	180	15.4	22.6
2001	11	26	1157	170	10.8	15.9
2001	12	7	0403	190	10.8	17
2002	1	15	1159	180	9.3	15.9

2002	2	2	2352	170	12.9	17
2002	2	11	0030	210	11.3	15.9
2002	3	7	1400	190	13.4	16.5
2002	3	29	1800	160	12.9	15.4
2002	10	19	0058	170	10.3	16.5
2002	10	25	1200	190	12.9	15.4
2002	11	3	1000	180	12.3	15.4
2002	11	20	0519	160	11.3	16.5
2002	12	9	2117	170	12.9	15.4
2002	12	22	0700	170	12.3	15.9
2002	12	23	0017	180	7.7	16.5
2003	1	8	0544	180	17.5	26.2
2003	1	9	1152	170	9.3	15.4
2003	1	18	0846	190	13.4	17.5
2003	1	26	1353	180	12.3	15.9
2003	1	30	1400	180	13.4	17.5
2003	3	4	2000	170	12.9	15.4
2003	10	3	0029	200	9.8	15.9
2003	11	2	0249	190	8.2	15.9
2003	11	15	2123	190	10.3	15.4
2003	11	22	0500	180	9.8	16.5
2003	11	23	0300	200	12.3	15.9
2003	11	24	0700	180	10.8	16.5
2003	11	25	0525	190	7.7	15.4
2003	12	1	0530	180	12.9	15.4
2003	12	5	0200	180	12.9	15.9
2004	1	5	1200	190	12.9	15.9
2004	1	14	0000	180	13.9	16.5
2004	2	9	0800	190	12.3	16.5
2004	2	29	0317	180	8.2	19
2004	3	9	1226	200	9.8	17
2004	3	20	2000	170	11.8	15.4
2004	11	19	0900	190	12.3	15.9
2004	11	24	0530	180	12.3	15.4
2004	11	28	0711	180	13.4	15.4
2004	12	1	0523	180	19	23.1
2004	12	19	0859	190	14.4	19.5
2004	12	27	0541	210	17.5	20.1
2005	1	16	0030	180	11.3	15.4
2005	2	15	0924	180	12.3	17.5
2005	3	2	0130	190	12.9	16.5
2005	3	15	2330	200	12.3	15.9
2005	3	28	0800	170	12.9	16.5
2005	10	3	1018	190	10.3	15.4
2005	10	11	1110	190	13.9	17

2005	10	14	0007	180	9.8	15.4
2005	11	15	0116	190	14.4	17
2005	11	19	0830	190	11.8	15.4
2005	11	22	1400	200	12.9	17.5
2005	12	10	0617	170	10.8	15.9
2005	12	21	1431	190	9.3	17.5
2006	1	1	0956	190	11.3	18
2006	1	11	0430	170	11.8	15.9
2006	1	23	1800	170	11.8	15.9
2006	2	4	0211	190	8.2	18.5
2006	2	6	1100	190	15.4	21.1
2006	2	26	1040	170	11.3	15.4
2006	3	6	0806	180	8.7	18
2006	3	10	0130	180	12.3	15.9
2006	3	19	1127	170	13.4	16.5
2006	10	5	1100	190	12.9	15.9
2006	10	8	0202	210	14.9	20.6
2006	10	14	0930	210	12.3	17.5
2006	10	20	1153	210	11.3	18.5
2006	10	25	1030	180	14.4	19.5
2006	10	28	0430	180	12.9	15.9
2006	11	13	1000	180	12.9	15.9
2006	11	15	0934	190	14.4	20.1
2006	11	22	0630	190	17.5	20.6
2006	11	28	2200	170	12.9	15.4
2006	12	6	1430	180	12.9	17.5
2006	12	11	0839	190	19	21.6
2006	12	14	1515	190	8.2	16.5
2006	12	19	0000	180	12.3	15.9
2007	1	12	1343	180	10.8	15.9
2007	1	27	0015	200	12.9	18
2007	1	30	1700	190	13.4	16.5
2007	3	24	0720	200	14.9	22.6
2007	10	3	1123	170	13.4	15.9
2007	10	19	1200	180	12.9	16.5
2007	11	4	1900	210	12.9	15.9
2007	11	22	2000	190	12.3	15.4
2007	12	16	0900	180	11.8	15.4
2008	1	17	0430	190	11.3	15.4
2008	1	20	1400	190	11.8	15.4
2008	1	31	1010	190	12.3	17.5
2008	2	7	0543	170	11.8	15.9
2008	2	12	2230	180	11.3	15.4
2008	2	28	0545	180	12.9	15.9
2008	3	20	1004	190	12.3	18

2008	10	4	1530	190	11.8	15.4
2008	10	20	2230	200	11.8	15.4
2008	10	27	1430	190	12.3	16.5
2008	10	31	0710	180	9.3	16.5
2008	12	3	0739	190	8.7	15.9
2008	12	9	2030	190	12.9	15.9
2009	1	1	1018	190	12.3	17
2009	1	15	0509	180	13.9	22.6
2009	1	24	0651	170	9.8	15.4
2009	3	26	1330	190	12.3	15.4
2009	10	25	1315	160	12.3	15.9
2009	11	22	1331	180	17.5	22.1
2009	11	30	0200	190	14.4	17.5
2009	12	3	2130	180	11.8	15.4
2010	1	2	0552	200	7.7	16.5
2010	1	13	0001	180	10.3	15.4
2010	1	23	0411	210	10.8	16.5
2010	1	29	1122	180	10.8	17
2010	2	5	1330	190	12.3	15.4
2010	2	28	1130	180	10.8	16.5
2010	3	10	0440	180	10.3	17.5
2010	3	21	1000	200	14.9	19.5
2010	10	7	0109	180	13.4	16.5
2010	10	23	1750	170	10.8	15.9
2010	11	8	0930	210	8.7	15.4
2010	11	18	1530	200	10.3	15.4
2010	11	28	1800	200	12.3	15.4
2010	12	23	0730	180	12.3	15.9
2010	12	27	0824	160	10.3	15.4
2011	1	2	0430	180	11.8	15.9
2011	1	24	0930	190	13.4	17
2011	2	6	0239	200	13.9	17.5
2011	2	11	2130	200	13.9	19
2011	2	13	0600	180	11.8	15.4
2011	2	20	1508	210	11.3	17
2011	3	14	0344	180	10.8	15.9
2011	3	25	2030	200	12.3	15.9
2011	10	30	0919	170	10.8	20.1
2011	11	14	1009	180	8.7	15.4
2011	11	30	1400	200	11.8	15.4
2011	12	3	2337	180	10.3	15.9
2011	12	27	0414	180	10.3	15.4
2012	1	4	0600	200	13.9	19
2012	1	5	1730	190	12.9	16.5
2012	1	31	1106	170	11.3	16.5

2012	3	6	1917	200	10.8	15.9
2012	3	17	0030	190	10.3	16.5
2012	3	21	1315	190	13.9	16.5
2012	10	20	0336	180	11.8	18
2012	10	21	2300	170	13.4	16.5
2012	11	9	0900	190	12.9	17
2012	11	12	1630	180	12.3	15.4
2012	11	19	0621	200	10.8	15.9
2012	11	21	1250	200	10.8	15.9
2012	12	8	2255	180	12.9	15.9
2012	12	10	0436	170	10.8	15.9
2012	12	16	1031	210	10.8	18.5
2012	12	20	0006	180	10.3	15.4
2012	12	28	0200	180	13.4	15.9
2013	1	1	1500	190	12.3	15.4
2013	1	8	1500	180	11.8	15.4
2013	1	13	1130	180	12.9	17
2013	1	18	0834	190	10.3	17
2013	1	23	0145	190	10.3	15.4
2013	2	1	0000	180	14.9	19
2013	2	10	0330	170	11.8	15.4
2013	2	28	0230	190	10.8	15.4
2013	3	1	0030	160	13.4	17.5
2013	3	16	1930	210	11.8	15.4
2013	10	6	1351	190	9.3	19
2013	10	10	1150	190	12.3	19
2013	11	3	0430	180	13.9	18.5
2013	11	9	1430	170	11.8	15.4
2013	11	11	0130	160	12.9	15.9
2013	11	17	0238	190	7.7	15.4
2013	12	20	1630	190	12.9	15.9
2013	12	23	0412	180	13.9	15.9
2013	12	28	1830	180	14.4	19.5
2014	1	25	0230	170	12.9	15.9
2014	2	4	0130	200	12.3	15.4
2014	2	9	1630	160	12.9	18
2014	3	5	1600	200	12.3	15.4
2014	3	19	0511	180	9.3	17
2014	3	23	1613	190	11.3	16.5
2014	10	5	0830	180	11.8	17
2014	10	19	1852	190	15.4	20.1
2014	10	27	1000	210	10.8	15.9
2014	11	14	0926	200	12.9	16.5
2014	11	21	0641	180	11.8	15.4
2014	12	12	0100	170	11.3	15.4

2014	12	16	1719	180	10.8	16.5
2014	12	18	1652	210	11.3	19
2015	1	12	0053	180	10.3	16.5
2015	1	25	0751	180	12.9	17.5
2015	2	2	0230	170	11.8	15.4
2015	2	4	0447	180	9.8	15.4
2015	2	8	1800	190	11.8	15.4
2015	2	24	0030	190	11.3	15.4
2015	3	1	0434	190	20.1	26.7
2015	3	5	0207	210	9.3	15.4
2015	3	12	1915	190	10.3	16.5
2015	3	15	0000	170	11.8	17
2015	3	20	0200	180	12.9	16.5
2015	10	6	1816	200	14.4	20.1
2015	10	12	0955	180	10.8	15.4
2015	10	22	0332	200	11.3	16.5
2015	10	26	0854	210	10.3	15.4
2015	12	2	0230	180	13.4	16.5
2015	12	11	0830	190	10.3	15.4
2015	12	21	0330	190	10.8	15.9
2015	12	26	1315	190	15.4	18.5
2015	12	27	0600	180	11.8	15.4
2016	1	14	0422	210	22.6	31.4
2016	1	15	0130	200	11.8	15.9
2016	2	3	1500	180	11.8	15.9
2016	2	19	1630	190	12.3	15.4
2016	2	25	1730	190	12.9	16.5
2016	10	7	2100	190	9.8	15.9
2016	10	13	0200	200	12.3	15.4
2016	11	18	1911	180	10.3	15.9
2016	12	2	0921	210	10.3	15.9
2016	12	5	1011	200	10.8	16.5
2016	12	17	1031	200	9.3	18
2016	12	20	1200	180	13.9	17.5
2017	1	1	1830	190	12.9	16.5
2017	1	11	0630	170	11.8	17
2017	1	17	2217	180	9.8	15.4
2017	1	31	0116	170	13.9	17.5
2017	2	2	0121	180	10.3	15.4
2017	2	6	0830	190	12.9	15.9
2017	2	10	0827	180	11.3	15.4
2017	2	12	0400	180	13.4	16.5
2017	2	24	1700	200	11.3	15.9
2017	3	16	1856	170	9.8	15.4
2017	3	22	0630	210	10.8	15.9

2017	3	27	1800	190	13.9	18
2017	3	30	0100	200	11.3	15.4
2017	10	9	1100	180	11.8	15.4
2017	10	19	2358	180	10.8	15.9
2017	10	30	0535	190	12.9	19.5
2017	11	3	1000	180	12.9	15.9
2017	12	20	0226	170	12.3	17.5
2017	12	24	0306	180	11.3	17
2018	1	7	0648	180	11.8	16.5
2018	1	9	0802	200	15.9	22.6
2018	1	30	1130	200	11.8	15.9
2018	2	14	1000	180	14.9	20.1
2018	2	25	0030	180	11.8	15.4
2018	2	28	1600	180	10.8	15.9
2018	3	3	2230	190	13.4	17
2018	3	18	1330	190	11.8	15.4
2018	10	9	2325	180	9.8	15.9
2018	10	23	1413	210	8.7	15.9
2018	10	27	1900	170	11.8	15.4
2018	11	15	0039	180	10.3	15.4
2018	12	2	0636	180	14.9	19.5
2018	12	21	1630	190	10.8	15.9
2018	12	22	0200	190	11.8	15.9
2019	1	5	0107	200	8.2	16.5
2019	1	23	0220	190	13.4	19
2019	1	31	0641	180	12.3	15.4
2019	2	12	1248	200	11.3	19
2019	2	19	0152	180	11.8	17
2019	3	6	0906	180	12.3	18
2019	3	12	1000	170	12.3	17.5
2019	3	15	0000	190	11.8	15.4